University of Liège

Faculty of Applied Sciences

Final project:

Mission analysis of QB50, a nanosatellite intended to study the lower thermosphere

Supervisor: Gaëtan Kerschen

Marc Vila Fernández

Academic year 2010-2011

Acknowledgments

First of all, I would like to thank my coordinator Ludovic Noels and my supervisor Gaëtan Kerschen, for the opportunity they offered by allowing me to participate in this amazing project. Above all Gaëtan Kerschen, who has guided me, solving all my doubts and suggesting me some improvements, during the development of my entire thesis.

My sincere thanks to Gaëtan Kerschen and Amandine Denis for the "Astrodynamique" classes imparted, where I have learnt the theoretical bases of my project, and I have been introduced to STK software.

My special thanks to Pierre Rochus for the subject of "Conception d'expériences spatiales", which has provided me a global vision of the field of aerospace.

Finally I would like to thank my family, above all my mother, and my friends, especially Eduard Lores Garcia and Núria Antillach París, for their continuous support and because without them this project would not have been possible.

Abstract

QB50 is a program intended to study the lower thermosphere (320-90 km) with a network of 50 nanosatellites. QB50 is the second nanosatellite of the University of Liège, Belgium. Before QB50 it was developed OUFTI-1 within the LEODIUM Project.

These satellites will be launched into a circular orbit at about 330 km altitude and an inclination of 79°. Due to the atmospheric drag, the orbit will decay and progressively lower layers of the atmosphere will be explored. The CubeSats will decay from 330 km to 90 km in approximately 98 days.

In this thesis a complete analysis will be made for a double CubeSat (2U) and some results will be compared with the triple CubeSat (3U) ones. A CubeSat is a cubical satellite with a size of 10 x 10 x 10 cm and a weight of 1 kg.

Finally, in this thesis it will be applied the tool STK/SEET to QB50 mission in order to predict, above all, the radiation that the satellite will receive during its lifetime. A tutorial will be made to show how this tool works.

Contents

List of figures

List of tables

Acronyms

ADCS	Attitude Determination and Control System
APEX	Advanced Photovoltaic and Electronic Experiment
BOL	Beginning of Life
CME	Coronal Mass Ejection
COTS	Commercial-Off-The-Shelf
CPU	Central Processing Unit
CREES	Combined Release and Radiation Effects Satellite
EGM96	Earth Gravity Model 1996
EGM2008	Earth Gravity Model 2008
GENSO	Global Educational Network for Satellite Operations
GPS	Global Positioning System
GS	Ground Station
HPOP	High-Precision Orbit Propagator
IGRF	International Geomagnetic Reference Field
IMU	Inertial Measurement Unit
LEO	Low-Earth Orbit
LOP	Long-term Orbit Predictor
ISS	International Space Station
LEODIUM	Lancement En Orbite de Démonstrations Innovantes d'une Université Multidisciplinaire (Launch into Orbit of Innovative Demonstrations of a Multidisciplinary University)
MPPT	Maximum Power Point Tracking
NASA	National Aeronautics and Space Administration

RAAN	Right Ascension of Ascending Node
SAA	South Atlantic Anomaly
SEET	Space Environment and Effects Tool
SEP	Solar Energetic Particles
SGP4	Simplified General Perturbations
SLBM	Submarine Launched Ballistic Missile
PS	Power System
PV	Photovoltaic
SEET	Space Environment and Effects Tool
SRP	Solar Radiation Pressure
SSWG	Sensor Selection Working Group
STK	Satellite Tool Kit
TLE	Two-Line Elements
ODWG	Orbital Dynamics Working Group
UV	Ultraviolet
VKI	Von Karman Institute
WGS84	World Geodetic System 1984

1. Introduction

The field of aerospace has been investigated for millennia, becoming one of the most exciting, diverse, and fast paced fields of today. This field includes artificial satellites, the object of study of this project. Formerly, satellites required several years of design, big infrastructures to build them and enormous budgets. Fortunately, satellites have evolved and nowadays it is possible to manufacture miniaturized satellites. An example of that is the QB50 mission. These advances allow universities, research organizations and smaller nations to participate in space based research.

A miniaturized satellite is an Earth-orbiting device having lower mass and smaller physical dimensions than a conventional satellite, such as a geostationary satellite. Miniaturized satellites have become increasingly common in recent years. They are often placed in low-Earth orbits (LEO) and are launched in groups. This kind of satellites can be classified according to their mass:

- Minisatellite [100-500 Kg]: They are usually simpler but they use the same technology as the larger satellites. Minisatellites are often equipped with propulsion system for orbit and attitude control.

- Microsatellite [10-100 Kg]: The miniaturization process of satellites begins to be important for those satellites, but sometimes they still use some kind of propulsion.

- Nanosatellite [1-10 Kg]: Their small size makes them affordable and opens up the potential for a swarm of satellites. However, every component has to be reduced in terms of mass and volume and no propulsion is usually foreseen. They can be transported on larger launches, avoiding the need for a dedicated launch.

- Picosatellite [0.1-1 Kg]: The miniaturization process has to be maximized and many new technologies have to be used in order to accomplish the requirements. The CubeSat design, with 1 kg maximum mass, is an example of a large picosatellite (or small nanosatellite).

This thesis is focused on a nanosatellite, called QB50. Firstly, it will be introduced the objectives of the project, as well as an explanation of the QB50 mission, including the concepts of CubeSat. Then the different factors related with the mission analysis will be treated with STK software, and finally a tutorial of a STK tool, called SEET (Space Environment and Effects Tool) will be done.

For each factor an analysis is carried out and the results are presented. First of all, it will be done an estimation of the lifetime of QB50. Afterwards, it will be treated the access, sunlight periods, power collected, radiation, vehicle temperature and impact particles.

The Satellite Tool Kit (STK) is a complete software application for modelling, engineering and operations of space. This software is widely used in the field of astrodynamics, because of the great advantages as:

- Intuitive user interfaces for creation of detailed models and simulations.
- Tens of thousands of data output parameters.
- Fully customizable report and graph styles with hundreds of standard reports and graphs included.

2. Objectives of the QB50 mission

QB50 has the scientific objective to study in situ the temporal and spatial variations of a number of key constituents and parameters in the lower thermosphere (90-320 km) with a network of 50 double CubeSats, separated by a few hundred kilometres and carrying identical sensors for in-situ measurements [1]. QB50 will also study the re-entry process by measuring a number of key parameters during re-entry, and by comparing predicted and actual CubeSat trajectories. On all other missions, CubeSats have been a secondary payload and they have had to accept the orbital requirements of the primary payload (usually higher orbital altitudes), which are often not ideal for the CubeSats. On QB50 mission, the CubeSats will be the primary payload.

Space agencies are not pursuing a multi-spacecraft network for in-situ measurements in the lower thermosphere because the cost of a network of 50 satellites built to industrial standards would be extremely high and not justifiable in view of the limited orbital lifetime. No atmospheric network mission for in-situ measurements has been carried out in the past or is planned for the future. A network of satellites for in-situ measurements in the lower thermosphere can only be realized by using very low-cost satellites, and for this purpose, CubeSats are the only realistic option.

The QB50 network will consist of 50 double-unit CubeSats. The satellites come from different countries: 38 CubeSats are envisaged to be provided by universities in 22 European countries, 8 by universities in the US, 2 by universities in Canada and 2 by Japanese universities.

QB50 has basically two units, the science unit and the functional unit. By one hand the science unit contains a set of standardized sensors for lower thermosphere and re-entry research. By the other hand the functional unit provides the usual satellite functions, like power, CPU, telecommunication, IMU and GPS. The universities are free to design the functional unit.

The 50 satellites will be launched together on a single launch vehicle, a Russian Shtil-2.1, into a circular low-Earth orbit (LEO) at about 320-330 km altitude and an inclination of 79°. Due to atmospheric drag, it is predicted the orbits will decay from 320 km to 90 km in 3 months, this is the minimal duration required to performed suitable in-situ measurements. After launch the CubeSats will be deployed sequentially. The separation speed will have an influence on the total network size.

The initial orbital altitude will be selected for each CubeSat in order to the lifetime will be at least three months, but it has to be below 330 km to avoid a possible collision with the International Space Station (ISS), due to its orbit is usually maintained between 335 km (perigee) and 400 km (apogee).

The launch is planned for June 2014. By that time, GENSO, the Global Educational Network for Satellite Operations, will be fully operational [2]. It will comprise more than 100 ground stations in different parts of the world, providing nearly continuous uplink and downlink capability for all the CubeSats.

The selection of the standardized sensors for in-situ measurements will be managed by the Sensor Selection Working Group (SSWG). The Orbital Dynamics Working Group (ODWG) is responsible for the selection of the initial orbital altitude and the initial separation between CubeSats in the network.

2.1. CubeSats

The concept was originally developed by the California Polytechnic State University and by the Stanford University, with Professors J. Puig-Suari and R. Twiggs, and afterward it widely circulates among the academic world. The CubeSat philosophy is different from the larger satellites. To launch a commercial satellite it is needed millions of dollars and lots of time to cover the period between the design and the launch, whereas a CubeSat, with a small budget, can be designed, tested and launched in a few years, allowing student to participate to all the phases of the mission.

Today the CubeSat project is an international collaboration of more than 100 universities, high schools and private firms developing their own designed nanosatellites. Furthermore, thanks to the great success of CubeSat projects [3], some safe interfaces for CubeSats have been developed and the launch providers are definitely favourable to use the free space to set into orbit this kind of nanosatellites.

The CubeSats offer all the standard functions of a normal satellite (attitude determination and control, uplink and downlink telecommunications, power subsystem including a battery and body-mounted solar panels, on-board data handling and storage by a CPU, and either a technology package or a small sensor or camera). It takes about two years to develop a CubeSat (from the provision of funding until the launch).

A CubeSat must respect the CubeSat designs specifications [4]. This will ensure that the satellite is compatible with the launcher's interface and it will not interfere with the other payloads. The key requirements for a CubeSat are summarized below:

- Its dimensions must be 10x10x10 cm.
- It may not exceed 1 Kg mass.
- Its centre of mass must be within 2 cm of its geometric centre.
- The CubeSat must not present any danger to neighbouring CubeSats, to the launch vehicle or to the primary payload: all parts must remain attached during launch, ejection and operation and no pyrotechnics are allowed.

- Whenever possible, the use of NASA or ESA approved material is recommended: it allows a reduction of out-gassing and contamination.

- Rails have to be anodized to prevent cold-welding and provide electrical isolation between the CubeSat and the deployment system. They also have to be smooth and their edges rounded.

- The use of Aluminium 7075 or 6061 is suggested for the main structure. If others materials are used, the thermal expansion must be similar and approved. This prevents the CubeSat to conk out because of an excessive thermal dilatation.

- No electronic device may be active during launch. Rechargeable batteries have to be discharged or the CubeSat must be fully deactivated.

- At least one deployment switch is required.

- All deployable components, such as antennas, booms and solar panels can be deployed 30 minutes after ejection into orbit.

- It has to undergo qualification and acceptance testing according to the specifications of the launcher: at least random vibration testing at a level higher than the published launch vehicle envelope and thermal vacuum testing. Each CubeSat has to survive qualification testing for the specific launcher. Acceptance testing will also be performed after the integration into the deployment system.

These are the fundamental features of a single CubeSat (1U), but there are bigger formats, as the double CubeSats (2U) with the dimensions of 20x10x10 cm, and the triple CubeSats (3U) with the next dimensions: 30x10x10cm. The structure of a double CubeSat is obtained by stacking two basic units, and obviously the structure of a triple CubeSat, stacking three basic units. The skeleton of these structures could be seen in Figure 2.1.

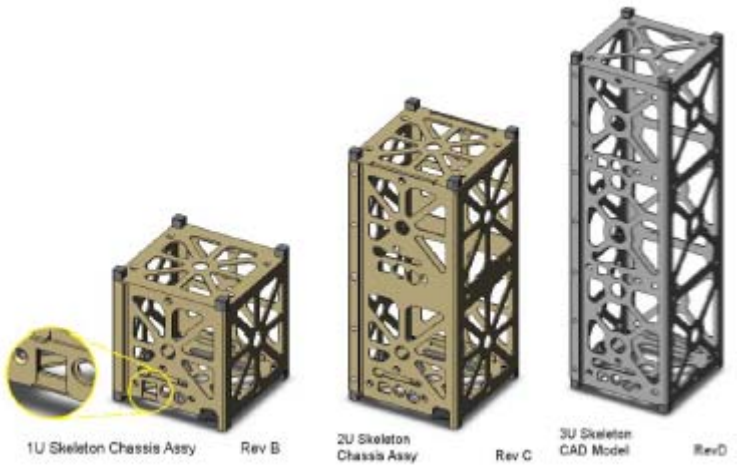

Figure 2.1: Skeleton of a single, double and triple CubeSat

2.2. The lower thermosphere

2.2.1. The atmosphere

The atmosphere of Earth is a layer of gases surrounding the Earth planet by Earth's gravity. The atmosphere protects life on Earth by warming the surface through heat retention (greenhouse effect), reducing temperature extremes between day and night, and filtering the electromagnetic radiations of the Sun. The absorption of the radiations causes local heating, which contributes to the atmospheric structure.

Atmospheric stratification describes the structure of the atmosphere, dividing it into distinct layers, each with specific characteristics such as temperature or composition. The atmosphere has a mass of about 5×10^{18} kg, three quarters of which is within about 11 km of the surface. The atmosphere becomes thinner with increasing altitude, with no definite boundary between the atmosphere and outer space.

In general, air pressure and density decrease in the atmosphere as height increases. However, temperature has a more complicated profile with altitude, but it provides a useful metric to distinguish between atmospheric layers. In this way, Earth's atmosphere can be divided into five main layers:

Exosphere

The exosphere is the outermost layer of Earth's atmosphere. It is mainly composed of hydrogen and helium. The particles are so far apart that they can travel hundreds of kilometres without colliding with one another. Since the particles rarely collide, the atmosphere no longer behaves like a fluid. These free-moving particles follow ballistic trajectories and may migrate into and out of the magnetosphere or the solar wind. This is the area where many satellites orbit the Earth.

Thermosphere

The thermosphere starts just above the mesosphere and extends up to 600 km high. Literally, thermosphere means “heat sphere”. In this layer the temperature rises continually to well beyond 1500°C. The few molecules that are present in the thermosphere receive extraordinary amounts of energy from the Sun, causing the layer to warm to such high temperatures. Within this layer, ultraviolet radiation causes ionization.

Mesosphere

The mesosphere extends from the end of stratosphere to 80–85 km. It is the layer where most meteors burn up upon entering the atmosphere. Temperature decreases with height in the mesosphere. The temperature minimum that marks the top of the mesosphere is the coldest place on Earth and has an average temperature around −85 °C. Due to the cold temperature of the mesosphere, water vapour is frozen, forming ice clouds.

Stratosphere

The stratosphere extends from the troposphere to about 50-55 km. Temperature increases with height due to increased absorption of ultraviolet radiation by the ozone layer, which restricts turbulence and mixing. While the highest temperature may be −60 °C at the troposphere, the top of the stratosphere is much warmer, and may be near freezing.

Troposphere

The troposphere begins at the surface and extends to between 9 km at the poles and 17 km at the equator. This layer is mostly heated by transfer of energy from the surface, so on average the lowest part of the troposphere is warmest and temperature decreases with altitude. The troposphere contains roughly 80% of the mass of the atmosphere, and it is where most weather phenomena like cloud formation take place.

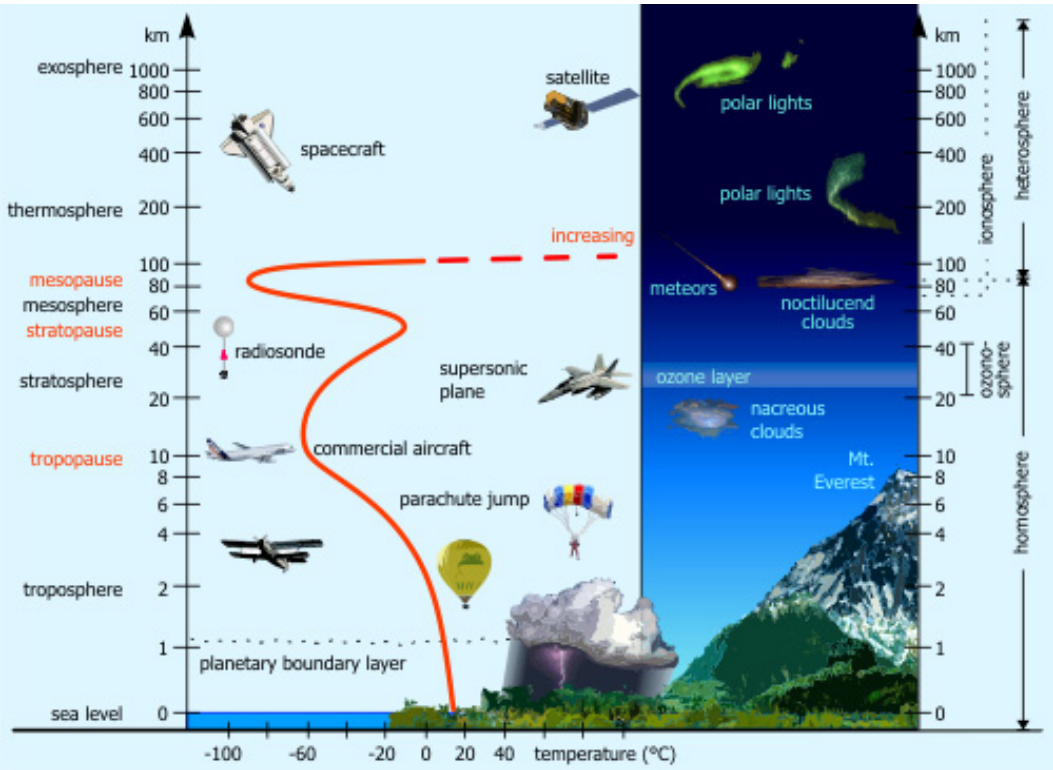

Figure 2.2: Vertical structure of the atmosphere

2.2.2. Why study the lower thermosphere?

The lower thermosphere (90-320 km) is the least explored layer of the atmosphere. The first explorations of this layer were done with highly elliptical orbits. They carried experiments for in-situ measurements but the time they spent in this region was only a few tens of minutes. Nowadays, sounding rocket flights provide the only in-situ measurements, but the time spent in this region is rather short.

Earth observation satellites, which are equipped with powerful remote-sensing instruments, can fly in higher orbits (600-800 km). Although this is an excellent tool for exploring the lower layers, they only observe constituents in the troposphere, the stratosphere and the mesosphere, due to the thermosphere is so rarefied and the return signal is weak. The same happens for remote-sensing observations from the ground with lidars and radars.

With this explanation it is easy to understand why the atmospheric density models do not agree with each other. Some of these models are based on theoretical assumptions concerning key parameters like the exospheric temperature, whereas other models are based upon in-situ data measurements.

The multi-point in-situ measurements of QB50 will be complementary to the remote-sensing observations by the instruments on Earth observation satellites, and the remote-sensing observations from the ground with lidars and radars. The QB50 mission will allow increasing the knowledge of the lower thermosphere and the dynamic phenomena

that take place. All atmospheric models will benefit from the measurements obtained by this mission.

2.2.3. Advantages of low Earth orbit

A network of CubeSats in the lower thermosphere compared to network in higher orbits has the following advantages:

- The lifetime of a CubeSat in a LEO will be three months. This is much less than the 25 years stipulated by international requirements related to space debris.
- A low-Earth orbit allows high data rates because of the short communication distances involved.
- In their low-Earth orbits the CubeSats will be below the Earth's radiation belts, which is very important because CubeSats use low-cost Commercial-Off-The-Shelf (COTS) components.

2.2.4. Study the re-entry process

QB50 mission also offers the occasion to study the re-entry process. The CubeSats, orbiting into a LEO at about 320-330 km, will go down due to the atmospheric drag and they will be able to transmit information during the re-entry phase before being disintegrated in the atmosphere.

The von Karman Institute (VKI) has the intention to provide a double CubeSat with the purpose of performing an atmospheric re-entry flight. To carry out these measurements during the re-entry phase, the VKI CubeSat will be equipped with a thermal protection system. Furthermore, an inertial measurements unit (gyroscopes and accelerometers) will be utilized to perform measurements on the flight trajectory of the CubeSat. Finally, if there are adequate remaining power and data resources available, it is envisaged to carry additional sensors for skin friction and pressure sensors for base flow measurements.

2.3. Launch vehicle

The 50 double CubeSats participating in QB50 will be launched by a Shtil-2.1 rocket from Murmansk in Northern Russia. Shtil[1] family of launch vehicles [5] is based on the 3-stage liquid-propellant R-29RM or RSM-54 SLBM (Submarine Launched Ballistic Missile). The missiles used are withdrawn from active service with the Russian Navy and converted to civilian launch vehicles by removing the warheads and antennas and replacing them by a civilian payload. The launcher has a remarkable track record of

[1] 'Shtil' is a Russian noun, meaning 'calm weather'

several hundred successful launches and only 1 failure. There are four different versions of the Shtil launcher: Shtil-1, Shtil-2.1, Shtil-2R and Shtil-3. But just the first ones are operational: Shtil-1 and Shtil-2.1.

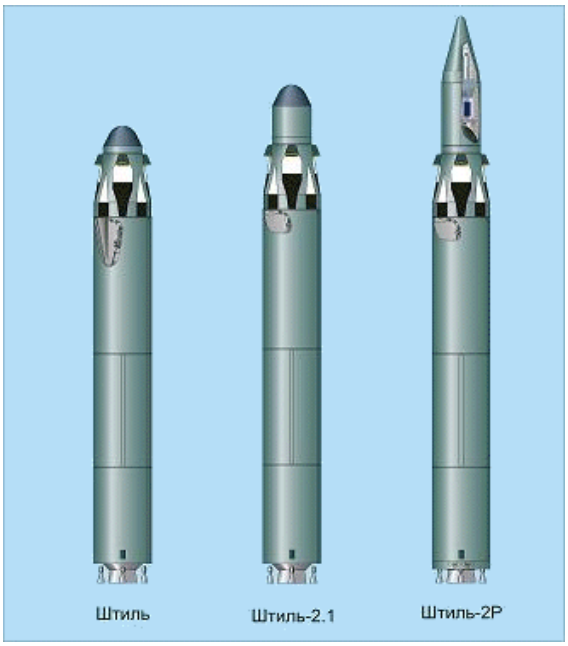

Figure 2.3: Evolution of the Shtil family of launch vehicles

Shtil-1

This is the baseline version of the launch vehicle where the payload is placed inside a special capsule in the space head next to the third stage engine nozzle. It was used to launch on 7th of July 1998, from a submarine in the Barents Sea, two small satellites from the Technical University of Berlin. On 26th of May 2006, it launched the Russian Kompass-2 satellite, also from a submarine in the Barents Sea. The Shtil-1 has a launch capacity of 150 kg into a circular orbit at 300 km altitude (i = 79°) and a payload volume of 0.195 m^3. However, the actual payload mass is reduced by the mass needed for the encapsulation of the payload.

Shtil-2.1

This is an improved version of the Shtil-1 where the payload is accommodated in a special section (max height 1.24 m, max diameter 1 m) on top of the space head. The payload mass that can be launched by a Shtil-2.1 into a circular orbit at 320 km altitude is 230 kg. The Shtil-2.1 was custom designed to accommodate the South African satellite SumbandilaSat (Pathfinder), an 80 kg microsatellite intended for launch in May 2007 into a 500 km circular orbit, but the launch negotiations were not be successfully completed.

Figure 2.4: Distribution of the payload inside Shtil-2.1

2.3.1. The mission profile

The Shtil-2.1 is launched from a submarine at sea surface. The fairing is jettisoned at the time of separation of the third from the second stage. After burnout, the third stage engine is jettisoned from the third stage and falls into the Pacific Ocean. The third stage itself remains in orbit. It has small thrusters for attitude and orbit control for 1200 s. After that time the propellant is exhausted. The third stage also carries a telemetry system and a battery which is sized to provide power for 1200 s. During this time interval, the satellite is separated from the third stage by spring pushers. If requested, the size of the battery can be increased to provide power for a longer time period, allowing a later separation of the payload.

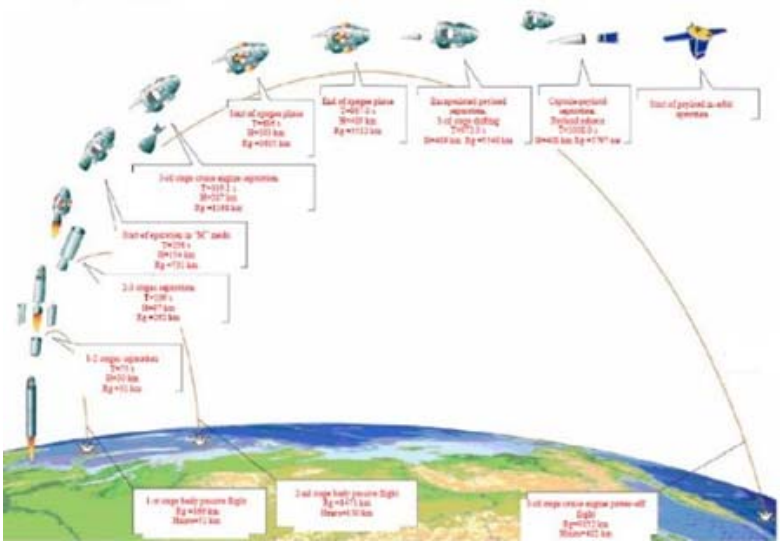

Figure 2.5: Schema of the mission profile

The Shtil-2.1 is fully developed and hardware has been built and tested. As there are currently no other customers it is quite possible that the launch of QB50 in June 2014 will be the first launch of a Shtil-2.1.

3. Orbital mechanics

Orbital mechanics, also called flight mechanics, are the study of the motions of artificial satellites and space vehicles moving under the influence of forces such as gravity, atmospheric drag, thrust, etc. The engineering applications of orbital mechanics also include ascent trajectories, re-entry and landing, and lunar and interplanetary trajectories.

The root of orbital mechanics can be traced back to the 17th century when Isaac Newton (1642-1727) formulated his law of universal gravitation. However, Isaac Newton used Kepler's work as basic information in the formulation of his gravitational theory. The three laws discovered by Johannes Kepler (1571-1630) are:

1. All planets move in elliptical orbits, with the sun at one focus.

2. A line that connects a planet to the sun sweeps out equal areas in equal times.

3. The square of the orbital period of any planet is proportional to the cube of the semi-major axis of its orbit.

These laws can be applied to the motion of the satellites.

3.1. Orbital elements

There are six parameters that have to be defined to characterize the motion of the satellite along its orbit [6]. They are called orbital elements:

Semi-major axis, a

The semi-major axis of an elliptic orbit is its longest distance between the centre of the Earth and the apogee. For the special case of a circular orbit, the semi-major axis is the radius, thus being the apogee and the perigee at the same distance from the centre of the Earth.

Eccentricity, e

The eccentricity is the distance between the foci divided by the length of the major axis. The result is a number between zero and one. An eccentricity of zero indicates a circular orbit.

Inclination, i

The inclination is the angular distance between the orbital plane of a satellite and the equator of its primary. An inclination of 0° indicates that a satellite moves in the same direction to the rotation of its primary. An inclination of 90° indicates a polar orbit. And an inclination of 180° degrees indicates a retrograde equatorial orbit.

Argument of periapsis, ω

The argument of periapsis is the angular distance between the point of periapsis[2] and the ascending node[3]. An argument of periapsis of 0° means that the satellite will be at its closest approach to the central body at the same moment that it crosses the plane of reference from South to North. An argument of periapsis of 90° means that the orbiting body will reach periapsis at its north, most distance from the plane of reference.

Longitude of ascending node or RAAN, Ω

The longitude of the ascending node is the angle from a reference direction, called the origin of longitude, to the direction of the ascending node, measured in a reference plane.

True anomaly, θ

The true anomaly defines the position of a satellite moving along an orbit. It is the angle between the direction of periapsis and the current position of the satellite.

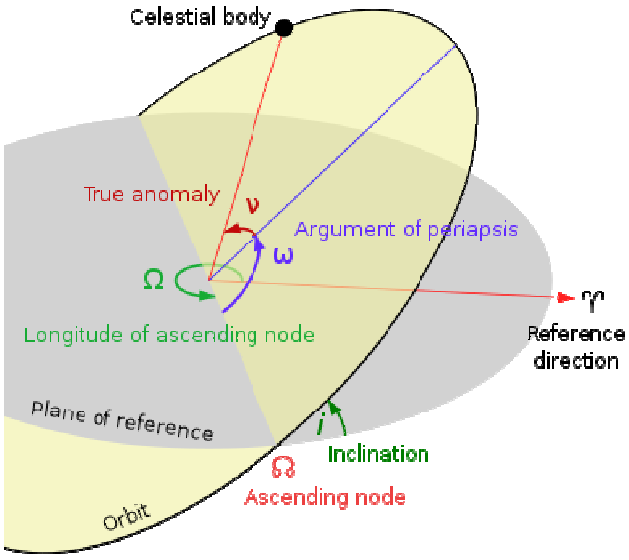

Figure 3.1: Orbital elements

3.2. Orbit perturbations

The orbital elements discussed before provide an excellent reference for describing orbits. However, there are some forces acting on a satellite that perturb it away from the nominal orbit. These perturbations, or variations in the orbital elements, can vary depending on the altitude. QB50 mission is focused on lower thermosphere; hence it has

[2] The point of closest approach to the central body (perigee)

[3] The point where the body crosses the plane of reference from South to North

to be determined the principal perturbations in this layer. As the QB50 nanosatellite will orbit in an initial altitude of 330 km (look at section 5.1), in Figure 3.2 one can observe the main perturbations during its lifetime.

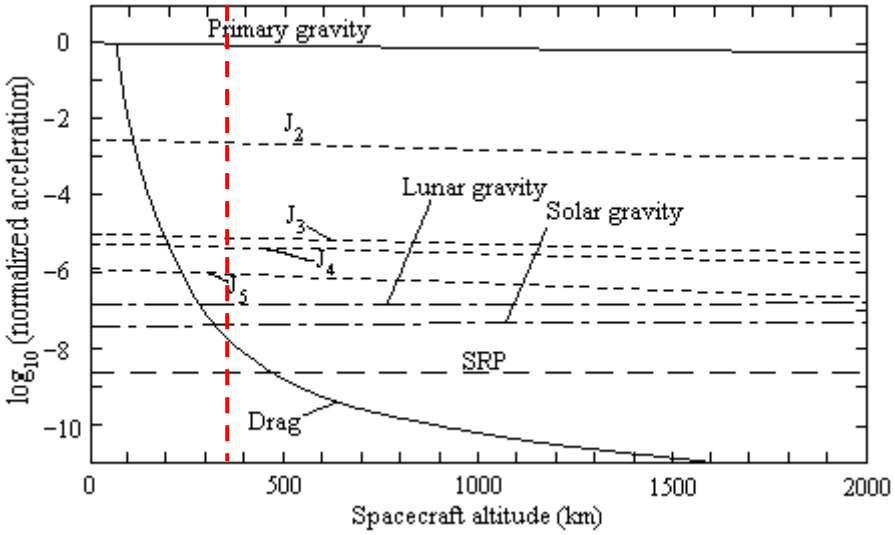

Figure 3.2: Normalized acceleration of perturbations as a function of satellite altitude

Looking at Figure 3.2, it is a fact that the gravity of the Earth is the most important perturbation when the satellite is orbiting. Afterwards, before QB50 descends to approximately 290 km, the third-body perturbation is the second one, whereas during the altitude range of 290-0 km the atmospheric drag gains importance above third-body perturbation. Finally, the last one is the solar radiation pressure (SRP).

3.2.1. Earth's gravity

Earth's gravitational force is often modelled as though the Earth were an inert sphere of uniform density. Unfortunately, the Earth is neither homogeneous nor spherical. This oblateness is caused by the Earth rotation rate[4], but also because its mass is not uniformly distributed and there are slight deviations in both the magnitude and direction of gravity across the surface.

[4] $R_{equator}$ = 6378 km, R_{polar} = 6357 km

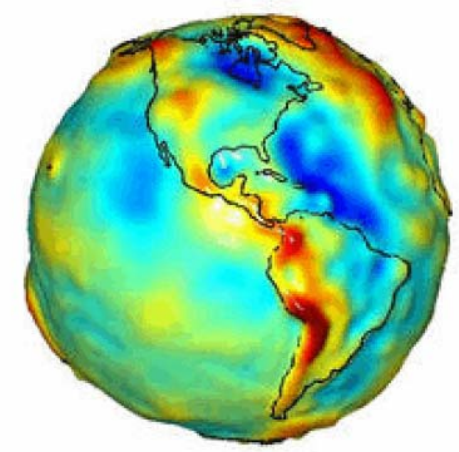

Figure 3.3: The true form of the Earth

To take into account all these aspects, the mathematical expression of the Earth gravitational potential that includes all of them is:

$$V(r,\phi,\lambda)=-\frac{\mu}{r}\left\{1-\sum_{n=2}^{\infty}\left[\left(\frac{R_e}{r}\right)^n J_n P_n \sin(\phi)+\sum_{m=1}^{n}\left(\frac{R_e}{r}\right)^n (C_{nm}\cos(m\lambda)S_{nm}\sin(m\lambda))P_{nm}\sin(\phi)\right]\right\} \quad (3.1)$$

where r is the radial coordinate representing the distance respect the Earth centre, ϕ is the longitude, λ is the latitude, R_e is the equatorial rayon, $P_{nm}sin(\phi)$ are the normalized associated Legendre functions, and C_{nm} and S_{nm} are the normalized gravitational coefficients.

The gravitational potential can be expressed classified into three groups, depending on the value of m and n:

- If $m = 0$, the gravity potential depends only on the latitude. This effect, called zonal harmonics, takes into account the Earth is flattened. Often it is called $C_{n0} = J_n$.

- If $m = n$, the gravity potential depends only on longitude. This effect, called sectorial harmonics, is used to consider the difference in density between the oceans and the continents. They are also called $C_{mm} = J_{mm}$.

- If $m \neq n$ *and* $m \neq 0$, the gravity potential depends both on latitude and longitude. This effect, called tesseral harmonics, is used to take into account great mass concentration.

The main disturbing factor is the J_2 coefficient, due to it is 100 times greater than the other coefficients, as it could be seen in Figure 3.4.

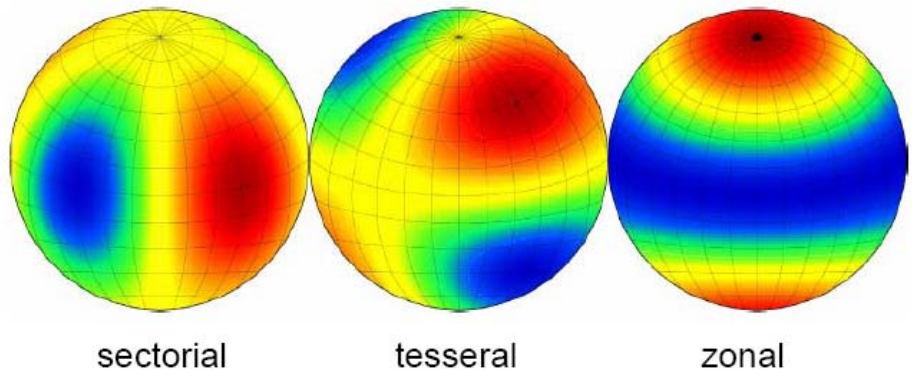

Figure 3.4: The spherical harmonics

3.2.2. Atmospheric drag

Drag is the resistance offered by a gas or liquid to a body moving through it. A spacecraft is subjected to drag forces when moving through a planet's atmosphere. This force is greater during launch and re-entry; however a space vehicle in low-Earth orbit experiences some drag during its motion. The deterioration of a spacecraft's orbit because of the drag is called decay. The drag force F_D on a body acts in the opposite direction of the velocity vector and is given by the equations:

$$F_D = \frac{1}{2}\rho u^2 C_D A \tag{3.2}$$

$$BC = \frac{m}{C_D A} \tag{3.3}$$

where F_D is the drag force, ρ is the atmospheric density, u is the speed of the satellite, A is its cross-sectional area perpendicular to the direction of motion, C_D is the drag coefficient and BC is the ballistic coefficient.

The atmospheric drag affects strongly the orbit lifetime of satellite in LEO. First of all, it has to be known the evolution of the cross-sectional area A, due to it depends on the attitude control and the geometry of the satellite. After that, it has to be defined the drag coefficient C_D, which depends on the geometric form of the satellite. Earth orbiting satellites typically have a coefficient drag in the range of about 2 to 4. The velocity of the satellite u also affects the drag force, but choosing a high precision propagator, the computational errors will be reduced. Finally, the atmospheric density ρ will be treated deeply afterwards.

The ballistic coefficient of a body is a measure of its ability to overcome air resistance in flight. It is inversely proportional to the deceleration; a high number indicates a low deceleration.

3.2.3. Third-body perturbations

Other bodies in the solar system impose additional gravitational forces on spacecraft orbiting the Earth. The proximity and mass of the Moon provides a significant influence, followed by the Sun, as it can be seen in Figure 3.2. The third-body perturbation, basically change the inclination of the orbit with respect to the equator. The effects of these forces acting on the satellite can be expressed as:

$$\ddot{r} = GM\left(\frac{s-r}{|s-r|^3}\right) - \frac{s}{|s|^3} \tag{3.4}$$

where s, M and G are the position, the mass and the gravitational constant of the Moon/Sun respectively, and r is the position of the satellite. Actually, this expression represents the acceleration of the satellite because of the attraction of the Moon/Sun, but also the acceleration of those two bodies on the Earth.

3.2.4. Solar radiation pressure

The SRP is the force exerted by the absorption and reflection of solar photons on the satellite surface. Its curve is effectively independent of the altitude; it is a function of distance from the Sun, rather than from the Earth. Certainly the heliocentric distance of the spacecraft respect the Earth varies, due to the SRP, but the effect on the disturbing acceleration is essentially second order. The other elements influencing on SRP are the solar flux and the reflectivity coefficient. Otherwise this force is not affected by solar wind particles. As it is shown in Figure 3.2, it is the smallest perturbation and compared with the other forces it could be negligible at the altitudes, which the QB50 orbits. This disturbance force [7] is defined as:

$$\vec{F}_{SR} = -P_{SR} \cdot C_R \cdot A_{\odot} \cdot r_{\odot\oplus} \tag{3.5}$$

where P_{SR} is the force per unit area exerted by the solar radiation, C_R is the coefficient of reflectivity of the satellite, A the area of the satellite exposed to the solar radiation and r the radial unit vector between satellite and Sun.

3.3. The orbit of QB50

Before defining the orbit of QB50, there are some restrictions that must be fulfilled:

- The orbit must be circular.
- The initial orbit must be between 330 km (to avoid a possible collision with the ISS) and 320 km.
- The orbit inclination must be about 79°.
- The lifetime must be at least three months.

As the orbit is circular, there are some elements that are common for all circular orbits. The altitude of apogee and perigee is the same. Eccentricity, the element used to describe elongation in an elliptical orbit, is 0. Otherwise argument of perigee, RAAN and true anomaly are still undefined. Taking into account all these aspects, Table 3.1 summarizes the orbital parameters:

Type	LEO
Altitude of apogee/perigee	330-320 Km
Eccentricity	0
Inclination	79°
Argument of perigee	To be determined
RAAN	To be determined
True anomaly	To be determined

Table 3.1: Orbital parameters of QB50

Although there are some parameters defined, the rest of them have to be quantified in order to do the simulation with STK software. The altitude of apogee/perigee depends on the lifetime; hence it will be defined after, in section 5.1. The other three parameters will be arbitraries, but to quantify them it has been taken into account the values from the J. Naviaux' thesis [8]. In this thesis the values are: argument of perigee = 0° and true anomaly = 84°. However, the RAAN value is not defined. Therefore, to quantify it for the simulation, it is considered RAAN = 250°. Table 3.2 includes these values:

Type	LEO
Altitude of apogee/perigee	330-320 Km
Eccentricity	0
Inclination	79°
Argument of perigee	0°
RAAN	250°
True anomaly	84°

Table 3.2: Orbital parameters of QB50 for the simulation

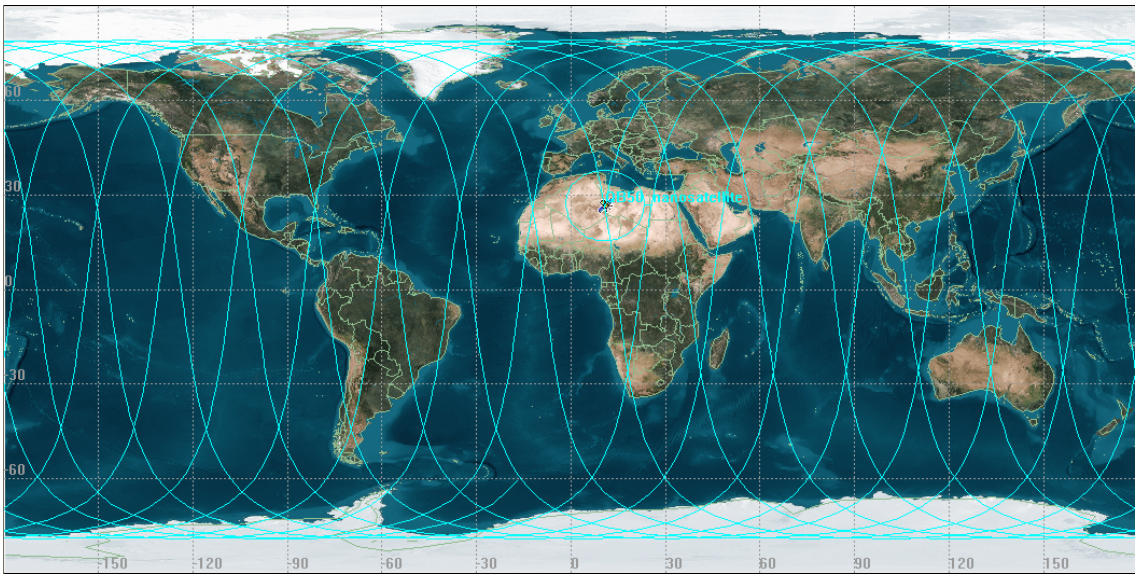

Figure 3.5: QB50's ground track

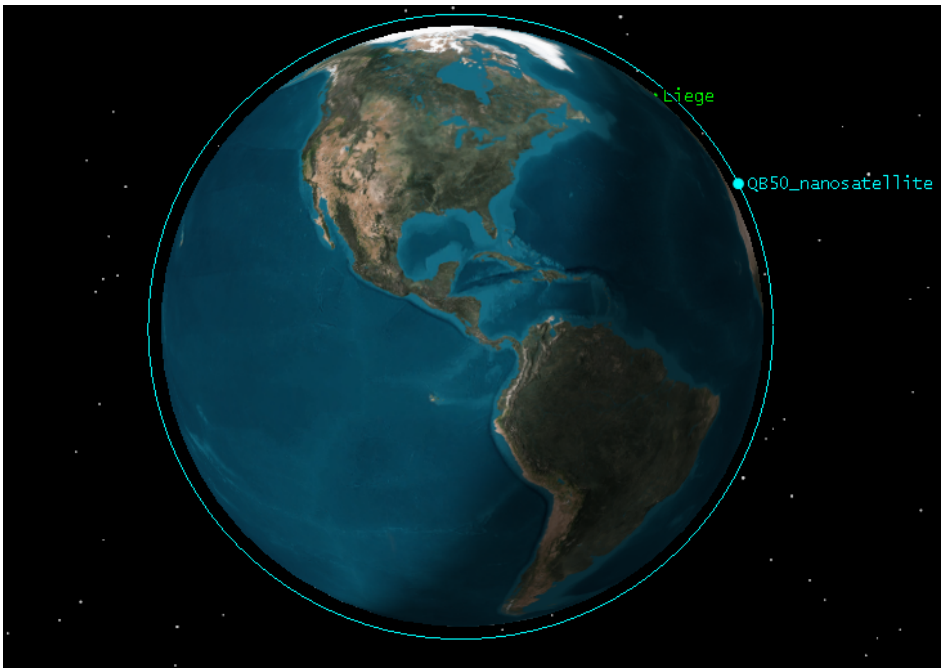

Figure 3.6: QB50's orbit

Figure 3.5 shows a typical ground track of the QB50 orbit over one day, and Figure 3.6 shows a tridimensional view of the orbit.

4. Parameters of QB50

First of all, it is essential to know the characteristics and the parameters influencing the QB50 to obtain accurate results. All necessary parameters for the STK simulation will be analyzed and quantified.

4.1. Mass, *m*

The mass of QB50 is a fixed value, concretely it is equal to 2 kg (see section 2.1), because QB50 is a double CubeSat.

4.2. Dimensions

QB50 is a double CubeSat formed for two single CubeSats (10 x 10 x 10 cm), as it is mentioned previously. Therefore, the QB50 dimensions will be 10 x 10 x 20 cm, as it can be seen in Figure 4.1:

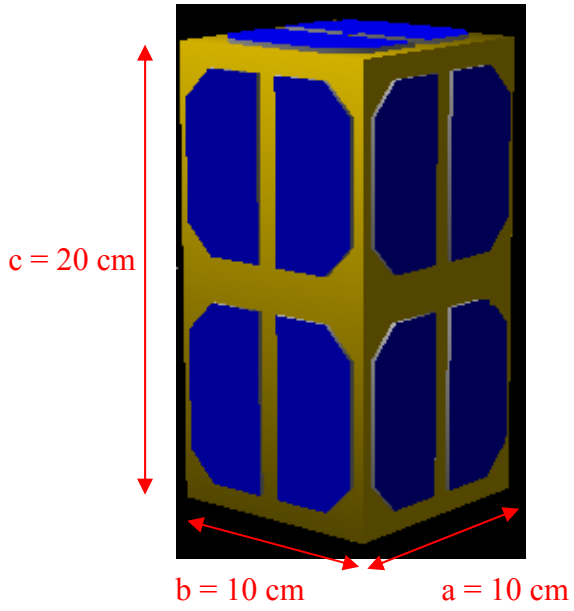

Figure 4.1: Schema of the QB50 dimensions

4.3. Cross-sectional area, *A*

It is the area perpendicular to the direction of motion; however there is no information in terms of attitude control. The drag force depends linearly on *A*, as it can be seen in section 3.2. Taking into account all the geometry requisites exposed in section 2.1 referred to a single CubeSat, the cross-sectional area *A* of a double CubeSat will vary from 0.010 m^2 to 0.028 m^2. Moreover, the double CubeSat has four faces with a surface of 0.020 m^2 and the other two with a surface of 0.010 m^2. Related with the measures of

the faces, G.E. Cook [9] gives a relation based on statistics in order to evaluate the cross-sectional area of a satellite:

$$A = \frac{A_{Tot}}{6} \tag{4.1}$$

where A_{Tot} is all the area surface of the spacecraft. Computing this area, the result leads to $A = 0.01667$ m^2. In this project it has been taken this value for computations, due to it is the best approximation of the cross-sectional area taking into account all the characteristics of QB50.

4.4. Drag coefficient, C_D

As it is shown in Figure 3.2, the atmospheric drag acquires a growing importance when the satellite's altitude decreases. Thereby, as QB50 will orbit in a LEO, this parameter becomes really important for the lifetime of the double CubeSat. In section 3.2.2 there is a detailed explanation of this perturbation. But as a reminder, the drag force F_D depends on, among other parameters, the drag coefficient C_D. As pointed out on the drag equation, the choice of cross-sectional area will affect the numerical value of the drag coefficient. However, the drag coefficient contains not only the complex dependencies of the satellite shape and attitude control, but also the atmospheric composition, the temperature of particles interacting with the satellite's surface and the flow regime. There are other parameters affecting the drag coefficient, but their importance is less than 1%.

Indeed, the drag coefficient is one of the most complex parameters due to the type of flow regime where the motion takes place. The flow regime is the factor most influencing on the drag coefficient. Although at low altitudes the continuum regime is reached, at high altitudes the flow cannot be treated in a continuum way, because of the mean free path of particles. At high altitudes, the atmospheric density is low; leading to relatively infrequent intermolecular collisions. No shock wave is therefore formed around a body moving through the atmosphere at orbit altitudes. This low collision rate produces physical flow phenomena which cannot be predicted accurately using a continuum description. However, it has to be demonstrated that QB50 will be, during the most part of the orbiting time, in free-molecular flow.

It is normal to use 2.2 as the physical drag coefficient of compactly shaped satellites in free molecular flow. This value of C_D is based on studies by G.E. Cook [9]. G.E. Cook provides height-related C_D data adopting the Schamberg's model [10].

To verify the free-molecular flow during the lifetime of the double CubeSat, the Knudsen number K_n will be used. K_n is a dimensionless number defined as the ratio of the molecular mean free path length λ, to a representative physical length scale L:

$$K_n = \frac{\lambda}{L} \tag{4.2}$$

If the Knudsen number is $K_n < 0.1$ it can be assumed continuum flow regime, because the length of the satellite is at least ten times greater than the molecular mean free path. The transition flow regime is reached when $0.1 < K_n > 10$, and finally the free-molecular flow regime occurs when $K_n > 10$.

Montenbruck and Gill [11] proposes an interesting relation between the Knudsen number as a function of the altitude and the object length. This relation is reflected in Figure 4.2:

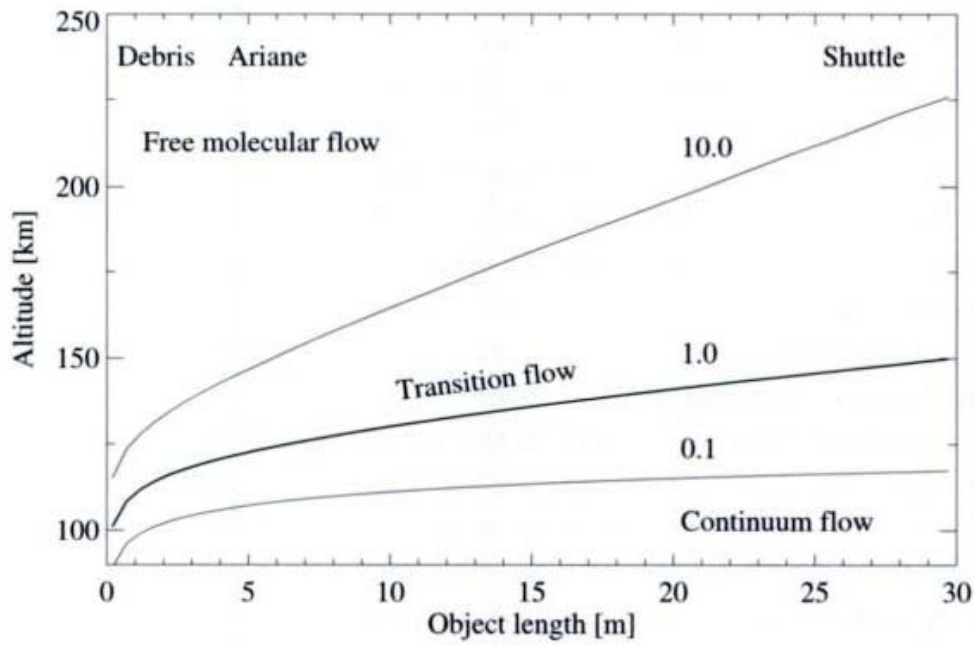

Figure 4.2: K_n as a function of the altitude and the object length

Looking at Figure 4.2 it is easy to see that QB50 will be the most part of the time orbiting through free-molecular flow, due to since the initial altitude until approximately 115 km, the flow regime will be free-molecular. From 115 km of altitude to 90 km the satellite will orbit through transition flow, but this period of time is almost negligible on a time scale of 98 days (look at section 5.2).

Another important aspect that affects C_D is the solar activity (treated in section 4.9). Solar activity also has a significant effect on atmospheric density. High solar activity implies high density. Below 150 km the density is not strongly affected by solar activity; however, at altitudes in the range of 500 to 800 km, the density variations between solar maximum and solar minimum are approximately two orders of magnitude. The large variations imply that satellites will decay more rapidly during periods of solar maxima and much more slowly during solar minima. As QB50 will orbit in the lower thermosphere (outside the range of 500 to 800 km), the effect of solar activity should not exceed 5% of its nominal value [12].

Taking into account all these aspects the value chosen will be 2.2. A value widely used in recent years for the drag coefficient. It is the same value that J. Naviaux proposes on his final year project [8].

4.5. Propagator

The propagator is the tool intended to solve the equations of motion of the satellite in orbit. Therefore, the accuracy of the results will depend on the propagator selected. For this reason, it is important to know the characteristics of each propagator that STK provides in order to choose the best one for the QB50 mission.

The propagator which seems to be the most accurate to forecast the QB50 mission analysis is the **High-Precision Orbit Propagator** (HPOP). It uses numerical integration of the differential equations of motion to generate the position of the satellite. Several different forces modelling the main perturbations are included in the analysis, as a full gravitational field model (based upon spherical harmonics), third-body gravity, atmospheric drag and solar radiation pressure. Also includes some secondary effects as albedo, shadow models, etc. There are available several different numerical integration techniques and formulations of the equations of motion. Hence, because of the many parameter settings available for the user, a precise model of the force model environment for almost any satellite can be specified, thus a highly precise satellite's orbit can be generated.

The other propagators are rejected for different reasons. For example, the **Two-Body**, **J2Perturbation** and **J4Perturbation** propagators do not model the solar radiation pressure, the third-body gravity and the atmospheric drag. The **Simplified General Perturbations** (SGP4) is used with two-line elements (TLE) sets, which includes more environmental forces; however there are more accurate propagators. The **GPS** propagator allows the user to create GPS satellites using element sets form GPS data file. The **Astrogator** propagator is focused on the trajectory design and orbit manoeuvres. The **SPICE** propagator uses ephemeris files created with the SPICE toolkit, an external toolkit of STK. And finally the **Long-term Orbit Predictor** (LOP) provides predictions of the motion of satellites over many months or years, but this propagator uses the same orbital elements as Two-Body, J2Perturbation and J4Perturbation propagators.

4.6. Gravity field models

Earth is not a symmetrical body, as it is mentioned previously (section 3.2.1). This oblateness is caused by its shape, density irregularities and the Earth rotation rate.

STK uses an equipotential ellipsoid surface that approximates the shape of the Earth. The reference ellipsoid is called the **WGS84** (World Geodetic System 1984), which is a

mathematically-defined surface, where the gravity potential is a specific theoretical value (U), and it is the same around the entire surface.

In order to improve the accuracy of this reference ellipsoid, due to it is relatively simply, the WGS84 is used in combination with a more precise model. The two main models are the **EGM96** (Earth Gravity Model 1996) and **EGM2008**. Although both are used to compute the geoid undulation with respect to WGS84 reference ellipsoid, the model chosen is the EGM2008, due to is the most complete and latest model. This model is constructed with combination of GRACE satellite data, topographic data, altimetry on sea, and gravity observations on land areas.

4.7. Atmospheric density models

For a good analysis of QB50 mission, it is necessary to choose an appropriate model to forecast the atmospheric density; above all in a LEO because of, as pointed out before, the drag force plays an important role. Although the simplest way to compute the atmospheric density is the exponential law decreasing with the altitude, it is not enough accurate for a precise analysis, due to the atmospheric density is very complex and it presents spatial and temporal variations. The models intended to predict the atmospheric density have to take into account all the factors such as altitude, solar activity, time of year, time of day, etc. But the principal factors influencing the atmospheric density in the lower thermosphere are: diurnal variations, solar flux variations, geomagnetic variations, semi-annual and seasonal-latitudinal variations and seasonal-latitudinal variations of helium concentration [13].

For the simulation with STK software, there are different models which can be chosen:

- U.S. Standard Atmosphere 1976
- Harris-Priester
- Jacchia 1970
- Jacchia 1971
- Jacchia Lifetime 1971
- Jacchia-Roberts
- CIRA 1972
- MSIS 1986
- MSISE 1990
- NRLMSISE 2000

To choose the correct model for QB50 mission it has to be analyzed all the characteristics and properties of each model, and how they adapt to the density profile of the lower thermosphere.

By one hand, **U.S. Standard Atmosphere 1976** and **Harris-Priester** models are excluded. The first one because it does not take into accounts the phenomenon influencing on the variation of density neither the solar activity. This model only provides accurate results for altitudes lower than 86 km. The second one is also rejected due to it does not take into account all the variations of the solar activity; this model only considers the diurnal density bulge.

By the other hand, the other models belong to the family of Jacchia [14], [15], [16] and [17], or MSIS family [18] and [19], which seem to be equipped with the necessary profile to obtain an accurate forecast for the different factors analyzed.

J. Naviaux [8] has studied the lifetime of the double CubeSat depending on the different models. The results in June 2014 show that **NRLMSISE 2000** [20] predicts the longest lifetime; contrary, **Jacchia 1971** predicts the shorter lifetime. Furthermore, NRLMSISE 2000 is one of the last update models.

The initial altitude will be calculated using both Jacchia 1971 and NRLMSISE 2000, in order to accomplish the minimum lifetime of QB50, three months. It will assure good results. To analyze the other factors ,the model chosen will be NRLMSISE 2000.

4.8. Attitude determination and control system

The attitude of a spacecraft is its orientation and stabilization in space, despite the external disturbing forces acting on it. The Attitude Determination and Control System (ADCS) define directly the motion of the satellite, due to the motion of a spacecraft is specified by its position, velocity, attitude and attitude motion [21]. By one hand, the first two magnitudes describe the translational motion of the centre of mass of the spacecraft. By the other hand, the other two magnitudes describe the rotational motion of the body about the centre of mass.

Attitude analysis may be divided into determination, prediction and control:

- **Attitude determination**: It is the process of computing the orientation of the spacecraft relative to either an inertial reference or some object of interest, such as the Earth. This typically involves several types of sensors on each spacecraft and sophisticated data processing procedures. The accuracy limit is usually determined by a combination of processing procedures and spacecraft hardware.

- **Attitude prediction**: It is the process of forecasting the future orientation of the spacecraft by using dynamical models to extrapolate the attitude history. Here, the limiting features are the knowledge of the applied and environmental torques

and the accuracy of the mathematical model of spacecraft dynamics and hardware.

- **Attitude control**: It is the process of orienting the spacecraft in a predetermined direction. It consists of two areas: attitude stabilization, which is the process of maintaining an existing orientation, and attitude manoeuvre control, which is the process of controlling the reorientation of the spacecraft from one attitude to another. However, the two areas are not totally distinct. The limiting factor for attitude control is typically the performance of the manoeuvre hardware and the control electronics.

Some form of attitude determination and control is required for nearly all spacecraft. Actually an ADCS needs in fact sensors and actuator with the consequent mass and power needed: this is often incompatible with a CubeSat. The problem with a double CubeSat is not only related with the mass requirements, but also with the power collected (see section 8).

4.8.1. The body coordinates system

As it is pointed out before, the goal of attitude determination is to determine the orientation of the spacecraft. Hence, before processing with the estimation of inertia properties, a reference frame linked to the body of the satellite is needed.

The double CubeSat has six faces. Four of them measure 0.002 m^2 and the others 0.001 m^2. Furthermore, all these faces are covered by solar cells, instead of the face which will hold the antenna deployment system. The orthogonal system is fixed in the centre of gravity of the satellite body and the z-axis points in the direction of the particular face.

In this thesis, it will be compared two cases depending on the attitude:

- The satellite advancing vertically (one small face points to the Earth):

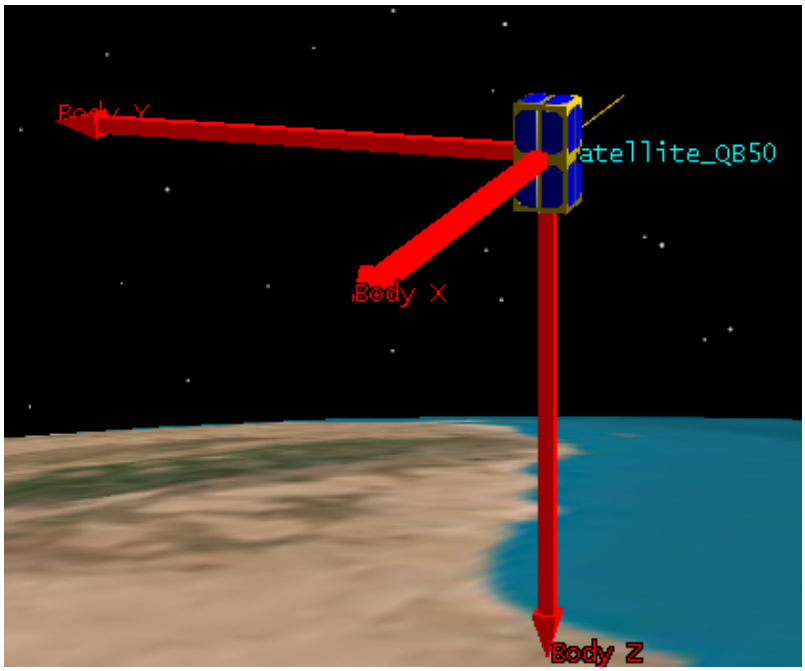

Figure 4.3: The body coordinates system if QB50 advances vertically

- The satellite advancing horizontally (one big face points to the Earth):

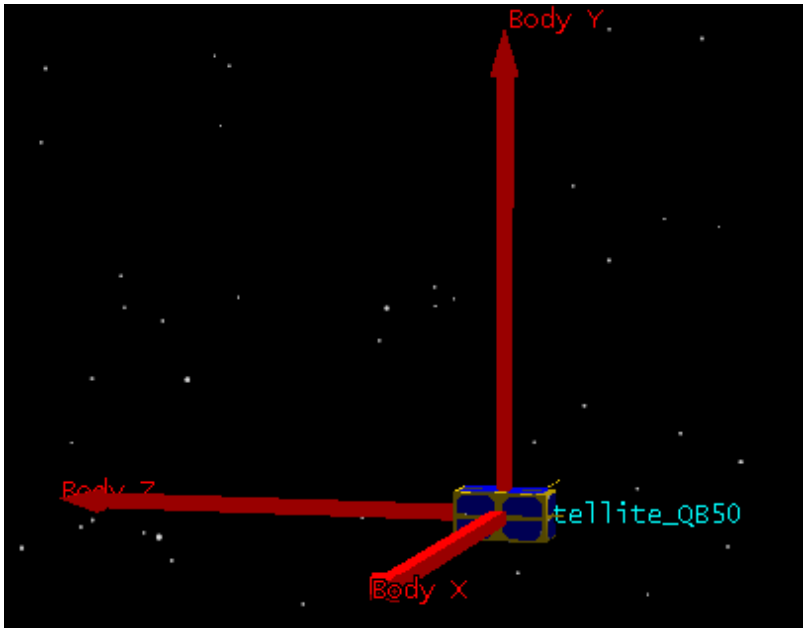

Figure 4.4: The body coordinates system if QB50 advances vertically

4.8.2. Inertia properties

After defining the reference frame of QB50, the inertia properties have to be determined. They cannot be defined exactly, due to the position of the elements inside the structure is still unknown; therefore a simple model will be used.

The double CubeSat has a mass of 2 kg, but the distribution of the mass it is not considered uniform in this thesis. The centre of mass will be displaced 1 cm each axis from the geometric centre[5], in order to take into account all the non-symmetrical components that could be in the nanosatellite. Therefore, the gravity centre is situated at (0.01, 0.01, 0.01) m. Figure 4.5 that lies in the plane x = 0.01 m, shows a schema of the situation of the QB50's gravity centre considered:

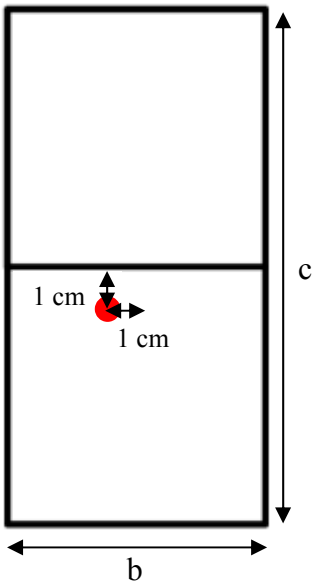

Figure 4.5: Schema of the centre of mass in the plane x = 0.01 m

In order to define correctly the inertia matrix, the parallel axis theorem or Huygens-Steiner theorem [22] will be used. The moment of inertia is given by:

$$I_O = I_{GC} + m \cdot r^2 \tag{4.3}$$

where I_O is the moment of inertia about an axis passing through the point O (0.01, 0.01, 0.01) m, I_{GC} is the moment of inertia of the object about an axis passing through its geometric centre, m is the mass of QB50, and r is the distance between the two axes.

The inertia matrix of the gravity centre is:

[5] The maximum distance which can be displaced the centre of mass of a CubeSat with respect to the geometric centre is 2 cm, it is specified in section 2.1

$$I_o = \begin{pmatrix} \frac{m(b^2+c^2)}{12} + mr^2 & -\frac{mab}{4} & -\frac{mac}{4} \\ -\frac{mab}{4} & \frac{m(a^2+c^2)}{12} + mr^2 & -\frac{mbc}{4} \\ -\frac{mac}{4} & -\frac{mbc}{4} & \frac{m(a^2+b^2)}{12} + mr^2 \end{pmatrix} \quad (4.4)$$

where r is the perpendicular distance between the parallel axes ($r = \sqrt{0.01^2 + 0.01^2}$ m), m is the mass of the satellite (m = 2 kg), a is the x-side of the satellite (a = 0.1 m), b is the y-side of the satellite (b = 0.1 m), and c is the z-side of the satellite (c = 0.2 m).

Then applying the corresponding values, the inertia matrix is:

$$I_o = \begin{pmatrix} 8.533 \cdot 10^{-3} & -5 \cdot 10^{-3} & -1 \cdot 10^{-2} \\ -5 \cdot 10^{-3} & 8.533 \cdot 10^{-3} & -1 \cdot 10^{-2} \\ -1 \cdot 10^{-2} & -1 \cdot 10^{-2} & 4.133 \cdot 10^{-3} \end{pmatrix} \quad (4.5)$$

4.8.3. Disturbing torques

During the lifetime, QB50 is subjected to variable disturbances resulting from various properties of LEO environment. The disturbing torques play a main role to determine the attitude [23]. However, as this thesis is a first approximation of QB50 mission, they will not be taken into account. Otherwise, they have to be considered in future studies. The major environmental disturbances acting on the satellite emerge from:

- Gravity gradient
- Aerodynamic drag
- Solar radiation pressure
- Magnetic disturbance

Gravity gradient torque

Any non-symmetrical object of finite dimensions in orbit is subjected to a gravitational torque, because of the variation in the Earth's gravitational force around the object. This gravity gradient torque results from the inverse square gravitational force field. Actually, as the gravitational field decreases with the square of the distance from the Earth's centre, the whole satellite is not attracted with the same gravitational force by the Earth. The formula, which defines the gravity gradient torque, is:

$$\vec{T}_{gg} = \frac{3\mu}{r^3}(\vec{r}\ x\ I\vec{r}) \quad (4.6)$$

where μ is the gravitational parameter of the Earth, r the distance between the geometrical centre of the satellite and the Earth centre, and I the matrix inertia.

Aerodynamic drag torque

As QB50 orbits in a LEO, the aerodynamic drag becomes the main disturbance torque, because it depends directly on the atmosphere density. The aerodynamic drag torque varies due to density variations, satellite velocity and cross-sectional area.

$$\vec{T}_A = \vec{r}\ x\ \vec{F}_D \tag{4.7}$$

where $|\vec{r}|$ is the distance between the geometric center and the centre of mass, and $\vec{F}_D$ is the atmospheric drag force (look at section 3.2.2).

Solar radiation pressure torque

Radiation incident on a spacecraft's surface produces a force, which results in a torque about the spacecraft's centre of mass. Because the solar radiation varies as the inverse square of the distance from the Sun, the solar radiation pressure is essentially altitude independent for satellite in Earth orbit. The major factors determining the radiation torque on a spacecraft are: the intensity and spectral distribution of the incident radiation, the geometry of the surface and its optical properties, and the orientation of the Sun vector relative to the spacecraft. This torque can be defined as:

$$\vec{T}_{SRP} = \vec{r}\ x\ \vec{F}_{SRP} \tag{4.8}$$

where $|\vec{r}|$ is the distance between the centre of pressure and the centre of mass, and $\vec{F}_{SRP}$ is the solar radiation pressure force (see section 3.2.4).

Magnetic disturbance torque

Magnetic disturbance torque results from the interaction between the satellite's residual magnetic field and the geomagnetic field. The primary sources of magnetic disturbance torques are: spacecraft magnetic moments, eddy currents and hysteresis. Of these, the spacecraft's magnetic moment is usually the dominant source.

$$\vec{T}_M = \vec{B}\ x\ \vec{D} \tag{4.9}$$

where $\vec{B}$ is the earth magnetic field and $\vec{D}$ the residual dipole.

4.9. Solar and geomagnetic activity

Solar parameters play an important role for the design of a mission and for the lifetime predications. However, such predictions are complex and difficult to perform, due to the Sun's activity is defined by 11-year cycle during which its activity can vary strongly [24]. Furthermore, the Sun is characterized by a second cycle: the Sun's rotation cycle, which has a period of approximately 27 days. Hence, solar activity predictions are quite difficult.

The particle and radiation fluxes coming from the Sun, which perturb the Earth's atmosphere, are:

- **Solar energetic particles (SEP):** They consist of protons, electrons and heavy ions with energy ranging from a few tens of keV to GeV. Solar Energetic Particles (SEPs) can originate from two processes: by solar wind, which is a stream of charged particles ejected from the external layer of the Sun, or by shock waves associated with Coronal Mass Ejection (CMEs). However, only about 1% of the CMEs produce strong SEP events. Moreover, these particles interacting with the magnetosphere cause geomagnetic field fluctuations, which affect the atmospheric density.

- **Solar ultraviolet (UV) radiation:** They heat the Earth's atmosphere from the exosphere through the thermosphere, modifying the air properties. The ultraviolet solar radiation consists of two components: the first one related to active regions (sunspots) on the solar disk, and the other to the solar disk itself. The active region component comes from areas of higher temperature and consists mainly of highly ionized atoms, whereas the radiation from the solar disk itself comes from much less ionized atoms.

There are two parameters to describe the solar activity: the solar decimetre-wavelength radio flux ($F_{10.7}$), which is used as an index of solar UV radiation and is well-correlated with the number of active regions (sunspots), and the flux averaged or smoothed, over approximately three solar rotations ($\bar{F}_{10.7}$), which is linearly related to the disk component of the solar UV radiation.

The geomagnetic activity is defined, basically, by the geomagnetic index (K_p) [6], which measures the solar particle radiations by its magnetic effects. This index is measured each 3-hours interval of the universal time day (UT).

Considering the effect of solar activity, it is evident that higher is the level of solar activity, lower is the lifetime of a satellite in orbit. In Table 4.1 there are, roughly, the different levels of solar activity:

Levels of solar activity	$F_{10.7}$	$\bar{F}_{10.7}$	K_p
Low activity	70	70	0
Mean activity	150	150	4
High activity	330	240	8

Table 4.1: Levels of solar activity

[6] Note that there is another geomagnetic index: a_p, but it is derived from K_p

In STK there are two possibilities for the solar activity:

- Use database of STK
- Enter manually the values of $F_{10.7}$, $\bar{F}_{10.7}$ and K_p

In this project, it has been used the database of STK; however it is important to have a global vision of these parameters before mentioned, during the QB50 mission. For this reason, it is possible to see the behaviour of the solar flux $F_{10.7}$ and the sunspot number during the 24th solar cycle (the current solar cycle), in Figures 4.6 and 4.7:

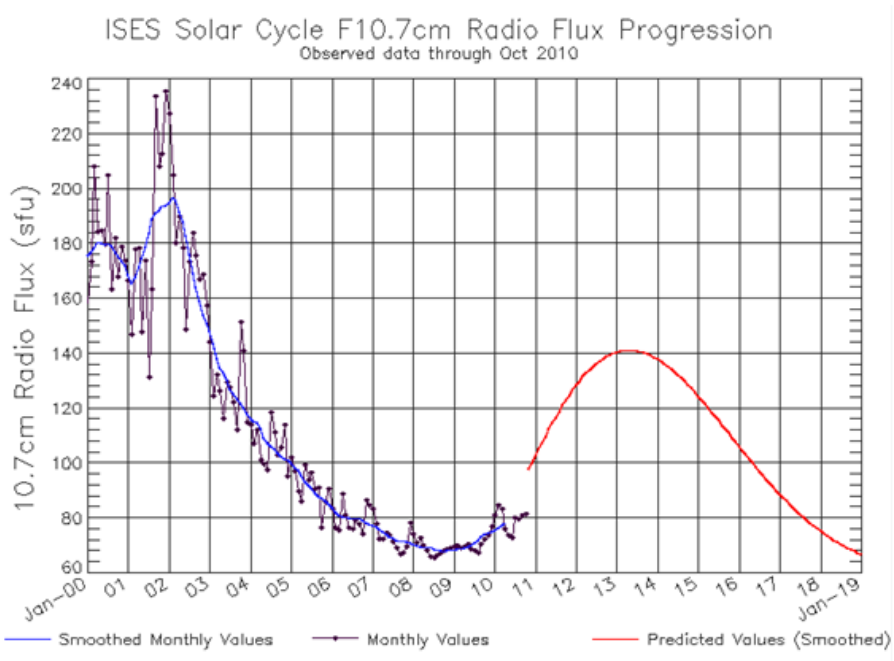

Figure 4.6: Solar flux $F_{10.7}$ during the 24th solar cycle

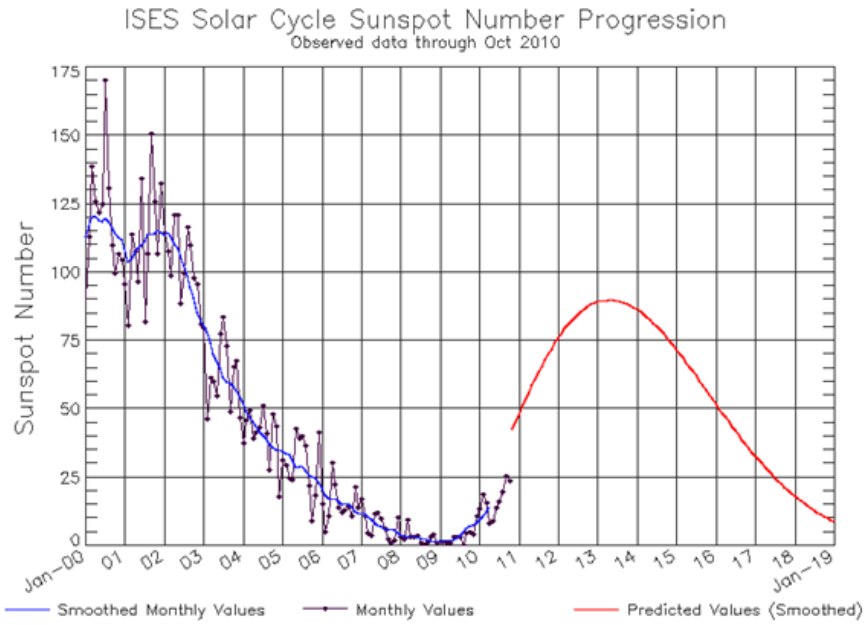

Figure 4.7: Sunspot number during the 24th solar cycle

4.10. Solar radiation pressure area

The solar radiation pressure area is the area perpendicular to the Sun's vector, A_{Sun}. As it is not a dominant perturbation in LEO and the difference between A (the cross-sectional area) and A_{Sun} is small, in this project it is assumed that $A = A_{Sun}$.

4.11. Solar radiation pressure coefficient, C_r

The solar radiation pressure coefficient is needed for the simulation of STK. As it is mentioned previously, the effect of solar radiation pressure is negligible in LEO and it does not affect on lifetime predictions. The C_r value used to simulate the QB50 mission will be 1, which is the mean value.

4.12. Summary of parameters for a double and triple CubeSat

Table 4.2 summarizes the characteristics of a double CubeSat. These values will be used in the STK simulation:

Double CubeSat characteristics	Value
Mass	2 kg
Drag coefficient	2.2
Cross sectional area	0.01667 m^2
Ballistic coefficient	54.5454 kg/m^2
Solar radiation pressure area	0.01667 m^2
Radiation pressure coefficient	1

Table 4.2: Summary of parameters for a double CubeSat

As it is mentioned, some of the double CubeSat results will be compared with the triple CubeSat ones. Concretely in this project, it will be compared the lifetime and the power gathered depending on the attitude. In Table 4.3, there are the main characteristics for a triple CubeSat, which will be used in the STK simulation:

Triple CubeSat characteristics	Value
Mass	3 kg
Drag coefficient	2.2
Cross sectional area	0.02333 m^2
Ballistic coefficient	58.4416 kg/m^2
Solar radiation pressure area	0.02333 m^2
Radiation pressure coefficient	1

Table 4.3: Summary of parameters for a triple CubeSat

5. The Lifetime of QB50

The lifetime of a satellite is one of the most important aspects of a space mission; due to it is the period of time when the satellite carries out its function. Hence the success of the mission depends on it.

In a low-Earth orbit, satellites experience orbital decay and have physical lifetime determined almost entirely by their interaction with the atmosphere. The prediction of satellite lifetime depends on the satellite characteristics, the knowledge of the initial satellite orbital parameters, the drag force, the atmospheric density and the solar and geomagnetic activity.

As it is mentioned previously, the main cause of the orbital decay is the drag caused by the residual atmosphere at low altitudes, where the atmosphere exerts a significant effect. The result of this friction effect is the altitude decreases quickly. To keep a constant altitude, a regular altitude boost is needed to counteract orbital decay. Unfortunately QB50 will be completely passive and no orbit control will be possible.

The forecast of the QB50 lifetime has the objective to choose the correct initial altitude to accomplish the minimum lifetime required, which is about three months for a double CubeSat. To choose the initial altitude, it will be introduced in STK the main parameters influencing the decay of the satellite, before defined. As pointed out on section 4.7 the lifetime will be calculated with two different atmospheric density models: Jacchia 1971 and NRLMSISE 2000. Once the initial altitude is selected for a double CubeSat, it will be calculated the lifetime of a triple CubeSat.

Finally, it has to be said that the launch is planned for June 2014, but the day is still unknown. For this reason, before choosing the initial altitude, some calculi will be done in order to see if the launch day is an important parameter that greatly affects the QB50 lifetime.

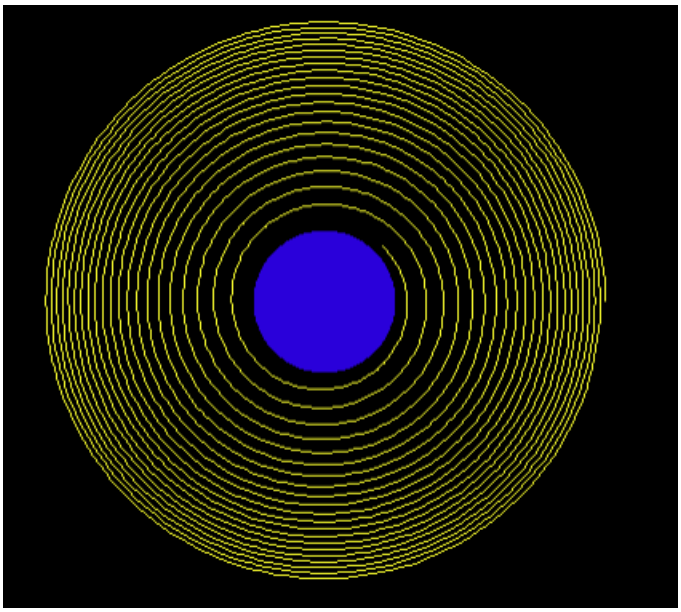

Figure 5.1: Diagrammatic view of how a satellite decays in a low Earth orbit[7]

5.1. Initial altitude choice

First of all, before computing the initial altitude, it has to be known if the launch day plays an important role. Hence fixing all the parameters, it will be studied the lifetime as a function of the date. The days studied will be: 1st, 5th, 10th, 15th, 20th, 25th and 30th of June. With these values it will be able to see if there is a tendency, and if the lifetime varies greatly. Concretely, the model used to do the computation is Jacchia 1971 and the altitude is 330 km. These two considerations are arbitraries. Afterwards an extensive study will be done focusing in these two parameters. The rest of the parameters introduced in STK are defined before (see section 4.12). Table 5.1 contains the results:

Date	Lifetime (days)
1st of June	93
5th of June	93
10th of June	93
15th of June	93
20th of June	93
25th of June	92
30th of June	91

Table 5.1: Lifetime depending on the launch date

[7] The radial scale has been drawn very much enlarged to show how the spiral opens out toward the end of the satellite's life, when it undergoes the re-entry phase

Table 5.1 shows that there is a soft decreasing tendency of the lifetime depending on the launch date. However, this tendency appears at the end of the month, due to in the first three weeks the lifetime seems to be constant. The difference between the launch taking place at the beginning of the month or at the end is just two days, which represents 2.22% respect 90 days. Hence, the day chosen for the launch in this project will be the 15th of June, because is the half of the month and the lifetime is the most probable; due to approximately the first three weeks have the same lifetime. Furthermore the error, which could be committed, is not representative, less than 3%.

Once the date has been chosen, it is time to decide the initial altitude. By one hand, the minimum altitude permitted in the QB50 mission is 320 km; hence it will be the first altitude examined. By the other hand, the maximum altitude permitted is 330 km. Lifetime is computed by each kilometre of this range of altitudes and for both models, Jacchia 1971 (the most restrictive model, look at section 4.7) and NRLMSISE 2000 (one of the last update models). The results are shown in Table 5.2:

Initial altitude (km)	**Lifetime**	
	Jacchia 1971 (days)	**NRLMSISE 2000 (days)**
320	75	80
321	77	82
322	79	84
323	80	85
324	82	87
325	84	89
326	86	91
327	88	92
328	89	94
329	91	96
330	93	98

Table 5.2: Lifetime as a function of the initial altitude and the atmospheric density model

Looking at Table 5.2 it is easy to see the difference, in lifetime terms, between the two models. In order to ensure the minimum lifetime of three months, the initial altitude must comply that the nanosatellite will be in orbit three months with both models. The first initial altitude that fulfil the minimum lifetime is 329 km. Nevertheless, if the launch takes place at the end of June, then the lifetime measured with Jacchia 1971 would not be enough, as it could be seen in Table 5.2. Therefore, in order to take into account all the possibilities, the initial altitude will be 330 km.

Now, that the initial altitude is clear, there are some basic results of the orbit that will be helpful for the analysis performed in the following sections. These results could be seen in Table 5.3:

Semi major axis	6708.14 km
Eccentricity	0
Orbital period	5467.82 sec
Mean motion	15.8016 revs/day
Velocity	7.70847 km/sec

Table 5.3: Orbital results

5.2. Lifetime estimation of a double CubeSat

Once it has been chosen the date of launch (15th of June), the initial altitude (330 km), and the atmospheric density model (NRLMSISE 2000), it can be simulated the lifetime with STK. Figure 5.2 shows the behaviour of the double CubeSat during its lifetime. Also this graph will show the exactly date when the nanosatellite will decay.

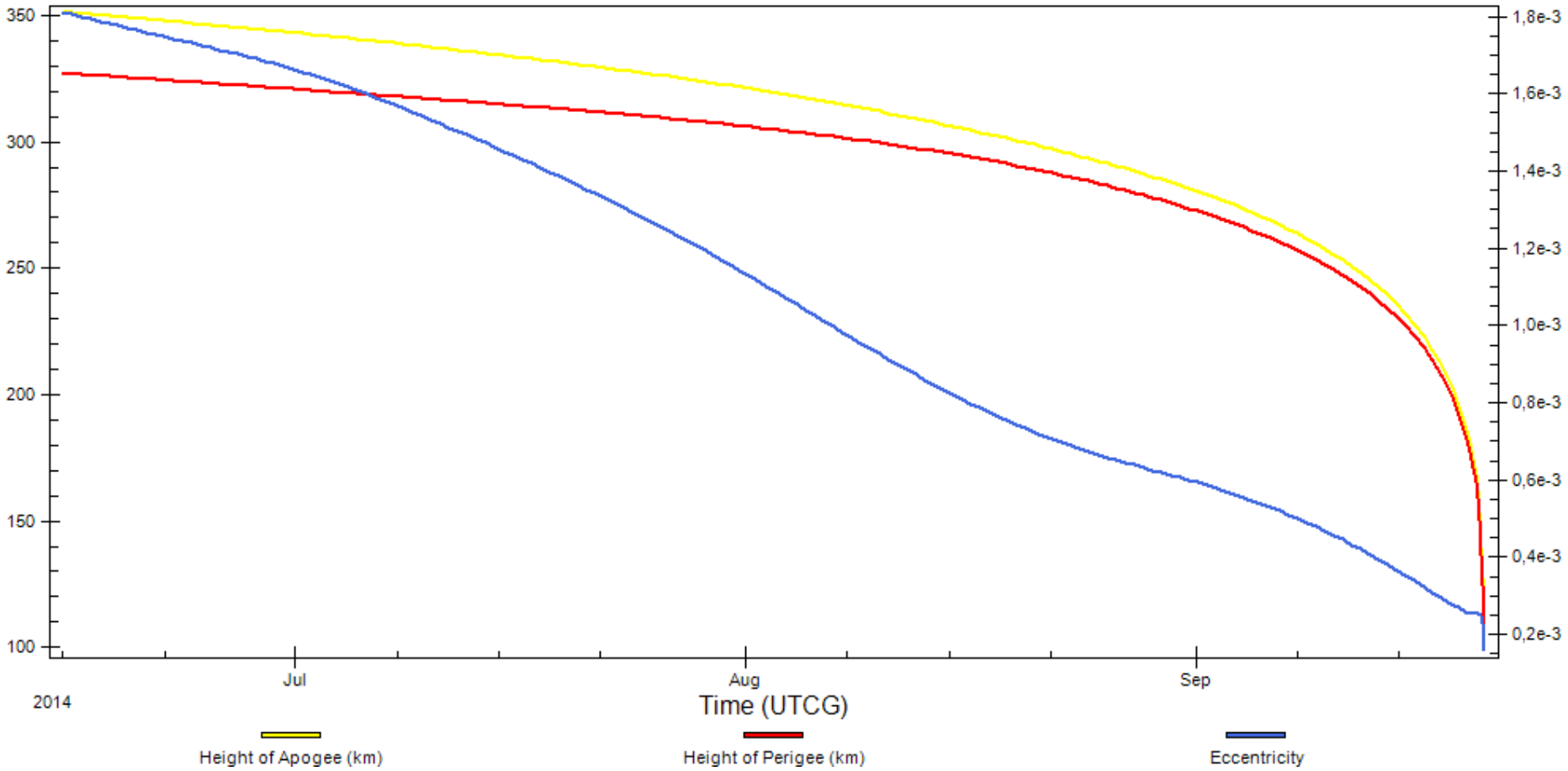

Figure 5.2: Lifetime estimation of a double CubeSat

The results presented in Figure 5.2 estimate a lifetime of 98 days, more than 3 months, the minimum lifetime expected for this mission. So, starting the space mission on 15th of June 2014, STK forecasts that it will finish on 20th of September 2014 at 19:16:54.280, after 1566 orbits.

Looking at the form of the graph, it is strange that despite having a circular orbit, height of apogee and perigee are separated approximately 21 km at the beginning. This variation happens due to the equatorial bulge. As it is mentioned previously, concretely in section 3.2.1, the altitude of a circular orbit with respect to the ground is not constant; it is larger close to the poles and lower close to the equator ($R_{equator}$ = 6378 km, R_{polar} = 6357 km). The difference between both radii is approximately 21 km, the same distance between apogee and perigee at the beginning of the mission that Figure 5.2 shows. As the lifetime advances, this distance becomes lower until the nanosatellite decays definitively.

5.3. Lifetime estimation of a triple CubeSat

As it is commented before, some of the double CubeSat results will be compared with the triple CubeSat ones, and the lifetime is one of them. The initial orbit, the launch day, the atmospheric density model and the rest of parameters are the same for a double and a triple CubeSat, instead of the inertia matrix, the mass, the cross-sectional area and solar pressure area, as it can be seen in section 4.12. Note that the centre of mass of the triple CubeSat has not been displaced. Figure 5.3 shows the graph which has the results:

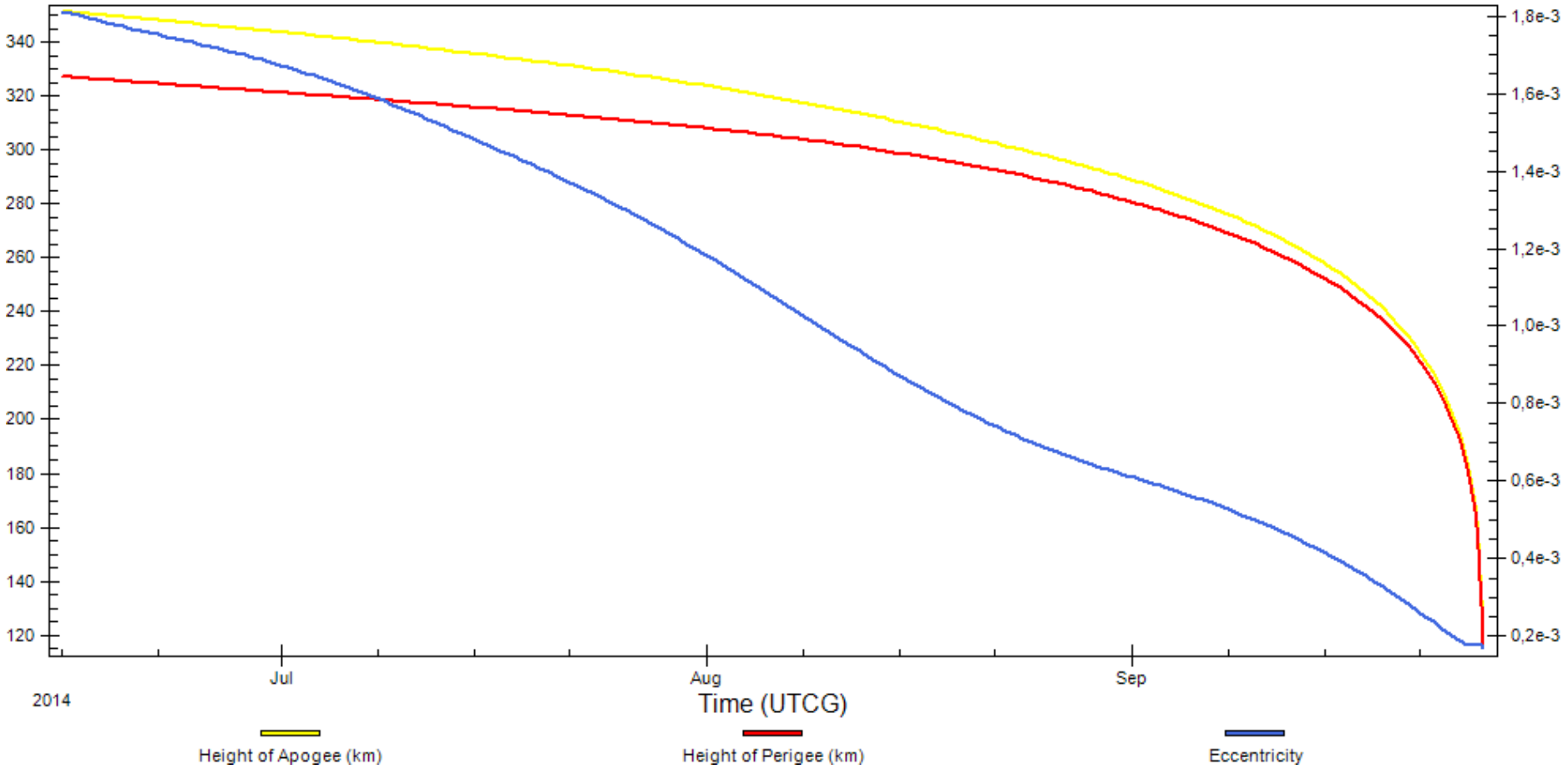

Figure 5.3: Lifetime estimation of a triple CubeSat

The results presented in Figure 5.3 estimate a lifetime of 104 days, more than 3 months, the minimum lifetime expected for the mission. Hence, starting the space mission on 15th of June 2014, STK forecasts that it will finish on 26th of September 2014 at 14:07:12.609, after 1658 orbits. Also the lifetime, computed with Jacchia 1971, is about 99 days; thus the minimum lifetime it is achieved.

What strikes of these results is the difference between the double and the triple CubeSat lifetime. A plausible explanation could be that the centre of mass of the triple CubeSat has not been displaced, which generates less torques than in the double CubeSat.

Looking at Figure 5.3, it can also be seen that the apogee and perigee are also displaced approximately 21 km at the beginning of the mission. As it is explained for the double CubeSat, it happens because of the equatorial bulge.

6. Access

6.1. Determination of the footprint

Due to the antennas are considered omnidirectional, one can assume that the whole area the satellite can see is the same area that antennas have access. In order to have a global vision about the field of view, there are some parameters that have to be defined [25]. Figure 6.1 shows a schema of the field of view:

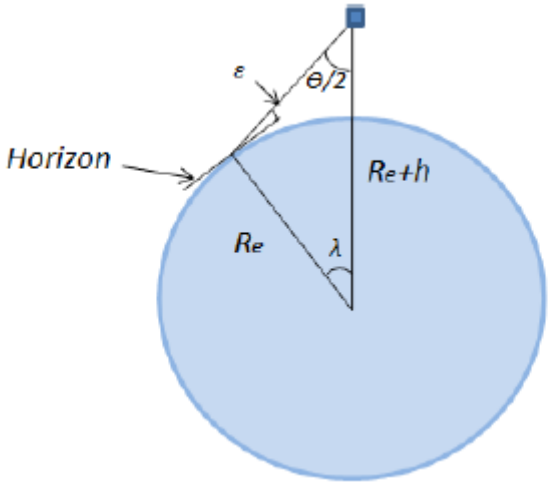

Figure 6.1: Field of view

$$\theta = 2 \cdot arcsin\left(\frac{R_e \cdot sin(90° + \varepsilon)}{R_e + h}\right) \tag{6.1}$$

$$\lambda = 180° - \frac{\theta}{2} - (90° + \varepsilon) \tag{6.2}$$

where $\theta/2$ is the cone angle of the sensor located in the nanosatellite, R_e is the radii of Liège (R_e = 6365.4 km), ε is the minimal elevation of QB50 respect the horizon (ε =10°), h is the apogee/perigee altitude (h = 330 km), and λ is the angle between the double CubeSat and Liège, which vertex is located in the Earth's centre.

Then, the footprint length L_{FP} and area A_{FP} can be calculated as:

$$\mathrm{L_{FP}} = 2 \cdot \lambda \cdot \left(\frac{2 \cdot \pi \cdot R_e}{360}\right) \tag{6.3}$$

$$A_{FP} = 2 \cdot \pi \cdot {R_e}^2 \cdot \left(1 - sin(90° - \lambda)\right) \tag{6.4}$$

The results are shown in Table 6.1:

	Perigee/Apogee (330 km)
θ	138.868°
λ	10.566°
L_{FP}	$2.348 \cdot 10^3$ km
A_{FP}	$4.317 \cdot 10^6$ km^2

Table 6.1: Satellite's field of view

The footprint of QB50, with a length of 2348 km and an area of $4.317 \cdot 10^6$ km^2, is displayed in Figure 5.2. In this figure it can be seen that the satellite passing over Liège, almost covers the entire Western Europe, instead of Portugal, the south-west of Spain and the south of Italy.

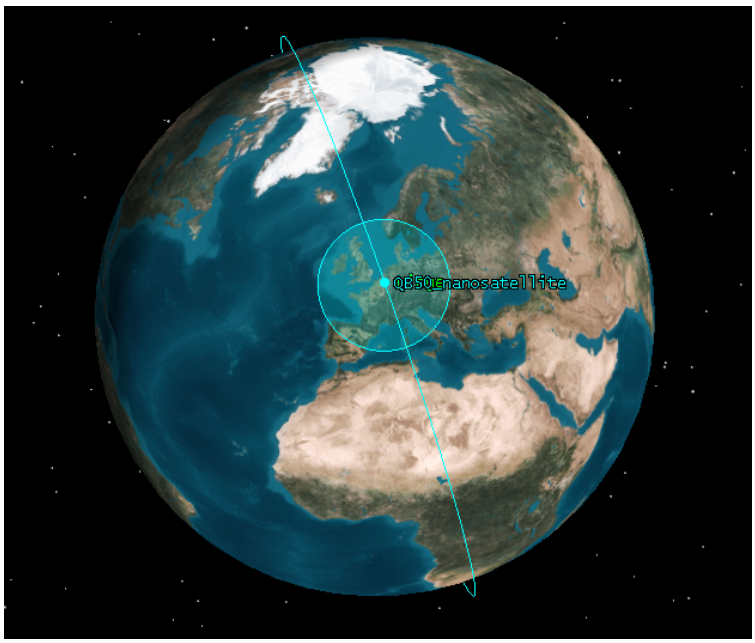

Figure 6.2: QB50's footprint

6.2. Ground station access

It is essential for the mission design to know the time available when the QB50 can establish communication with the ground station in Liège. As it is mentioned previously, it is considered a minimal elevation of QB50 respects the horizon, in order to take into account the obstacles around the ground station. This constraint is about 10° above the horizon. Figure 6.3 shows the accesses between the satellite and the Liège GS during 25th of July 2014:

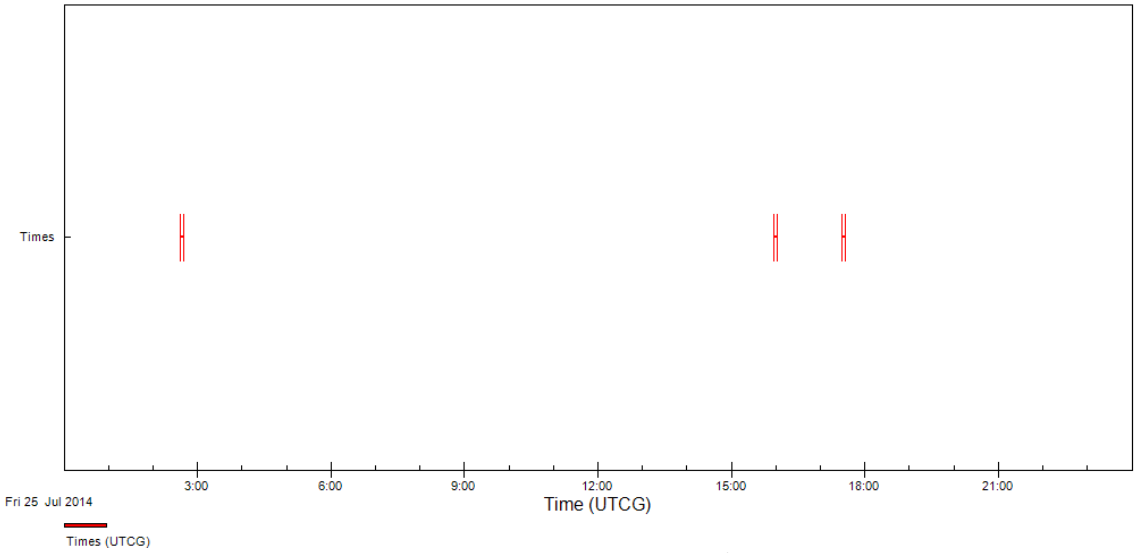

Figure 6.3: GS access time during 25th of July

Looking at this graph, it can be seen that the interval accesses are represented by segments with different thicknesses, depending on the duration of each access. It has been represented this short period of time instead of the graph including all the lifetime, because of as the lifetime is about 98 days, there are lots of accesses; therefore the graph including all of them is not too clear.

In Appendix A, the details of the access periods for each day of QB50 lifetime are displayed. From this simulation, the global statistics will be presented in Table 6.2:

Ground Station Access	**Duration (s)**
Minimum	6.369
Maximum	335.901
Mean	243.405
Total	70344.129

Table 6.2: Access global statistics

Each access will have a mean duration of 4.057 minutes. It can then be deduced that, on average, the satellite will be visible 11.964 min/day. From the Appendix A, it can also be seen that there will be at least 3 accesses per day which ensures a daily communication link between the GS in Liège and the satellite.

7. Sunlight periods

During the mission, there will be some periods when the satellite will not be illumined. It occurs when the Earth blocks the sunlight, or if there is a moon eclipse between Earth and Sun. The first cause appears much more frequently than the moon eclipse because of the high frequency at which the satellite rotates around the Earth. Indeed, QB50 will perform 15.8016 revolutions per day; therefore, times of sunlight and darkness follow each other in very short periods. The two consequences, of the Earth blocking the sunlight or the moon eclipses to the QB50, are the umbra and penumbra periods, which can be seen in Figure 7.1:

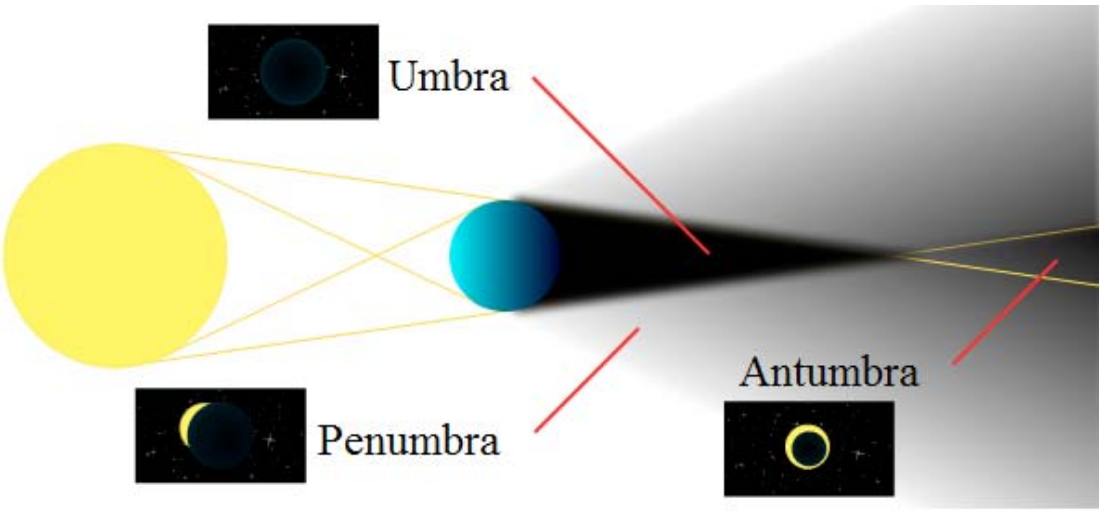

Figure 7.1: Schema of sunlight, penumbra and umbra periods

As the QB50's orbit is defined, it is possible to calculate the duration the satellite will be in sunlight, in penumbra and in umbra. Figure 7.2 shows these periods:

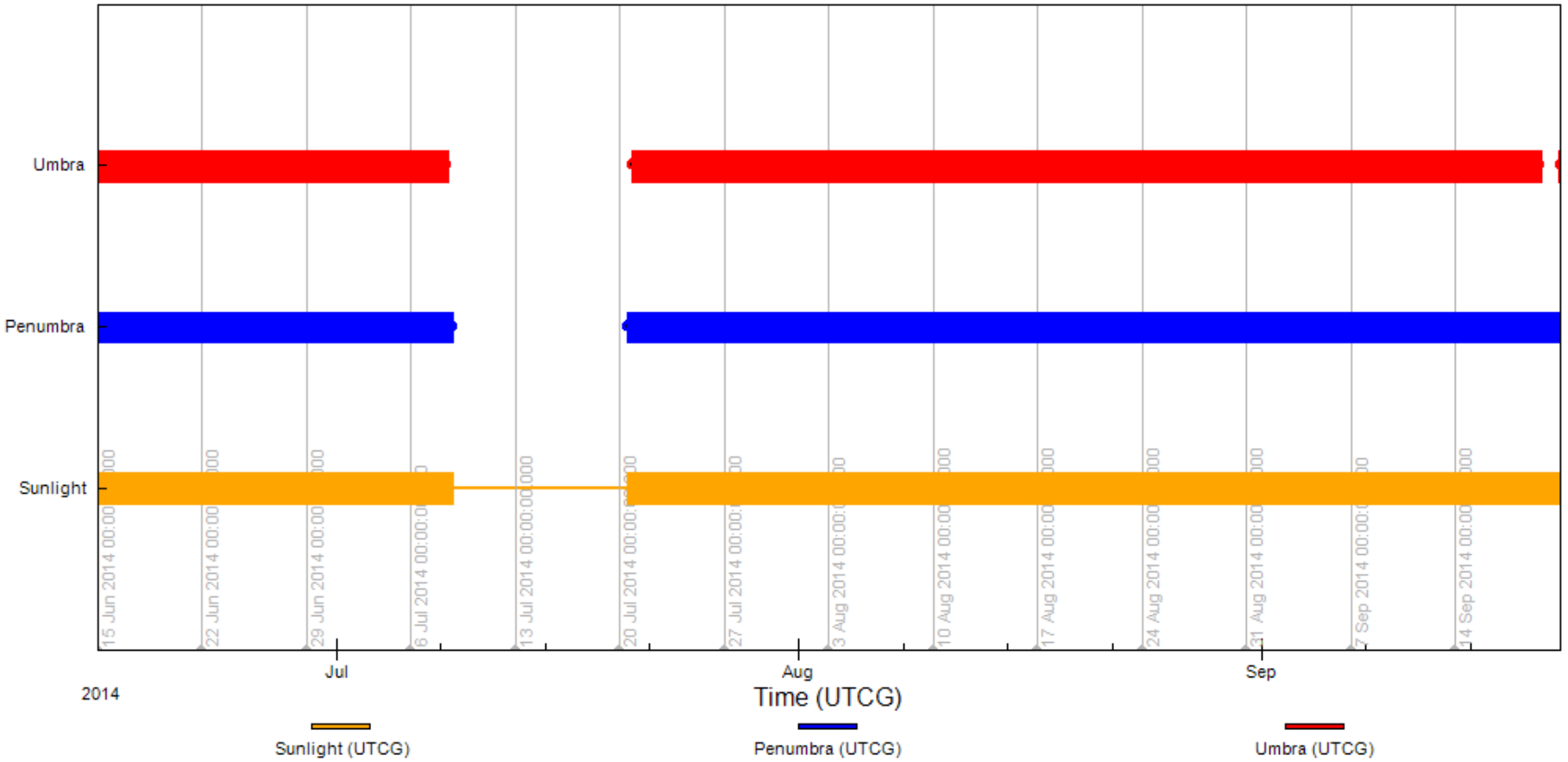

Figure 7.2: Lighting times graph

As this graph is not too clear, due to it is not possible to see the different time intervals of umbra, penumbra and sunlight, Figure 7.3 shows these periods during 25th and 26th of July 2014. However, the most important thing to note in Figure 7.2 is that every day during the QB50 lifetime, the satellite will have periods of sunlight, penumbra and umbra periods, instead of the between the days 8th and 20th of July, and 19th and 20th of September[8]. Concretely, the first period starts the 8th of July 2014 at 21:15:14.262 and it finishes the 20th of July 2014 at 13:45:12.996, and the second one is comprised between 19th of September 2014 at 18:06:08.753 and 20th of September 2014 at 21:56:39.469. During the first period, the satellite receives constant light all the time because of there are not eclipses; hence, there are not penumbra and umbra periods. Concerning the second period, there will not be umbra periods, even though there will be penumbra periods, as it can be seen in Figure 7.2.

It happens because of the high orbital inclination (explained in section 3.1), which causes the non-presence of equatorial orbits. During these periods, as the orbital plane is approximately perpendicular to the sunlight direction, the Earth cannot block the sunlight to the satellite, whatever the Sun position. This phenomenon it is also treated in section 8.6.

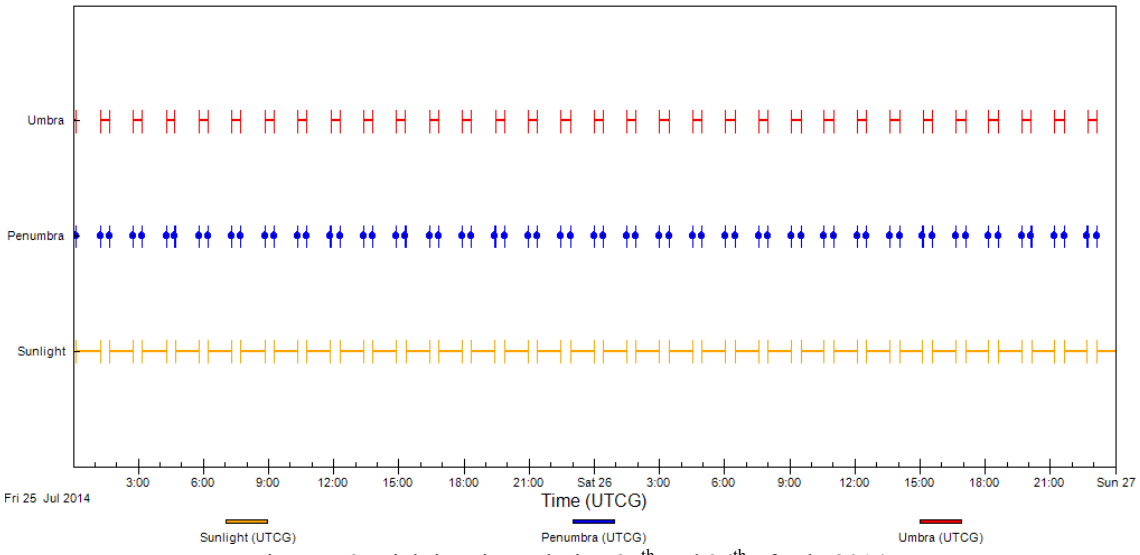

Figure 7.3: Lighting times during 25th and 26th of July 2014

[8] Note that these periods could change when all the orbital parameters will be finally defined, basically the argument of perigee, RAAN and true anomaly

Below, in Tables 7.1, 7.2 and 7.3, it could be seen the minimum, maximum, mean and total duration of sunlight, penumbra and umbra periods:

Sunlight Times	Duration (min)
Minimum	651.960
Maximum	1009798.734
Mean	4340.569
Total	5963942.325

Table 7.1: Global statistics of sunlight times

Penumbra Times	Duration (s)
Minimum	7.893
Maximum	454.021
Mean	19.020
Total	51733.914

Table 7.2: Global statistics of penumbra times

Umbra Times	Duration (s)
Minimum	12.547
Maximum	2171.230
Mean	1819.482
Total	2450842.864

Table 7.3: Global statistics of umbra times

Therefore, QB50 will be 70.442% of its time in sunlight, 0.611% in penumbra and 28.947% in umbra periods. As expected, the penumbra periods are very short due to the low height of the QB50's orbit.

During one orbit, the maximum duration of an umbra period is 36.119 min, which represents 39.709% of the orbit. It means that during the periods when the satellite is inside the Earth's shadow, the satellite must operate with batteries because of solar panels are not illumined. Otherwise, the sunlight periods are the time intended to recharge the batteries. The minimum duration of a sunlight period is 10.866 min; it means that the batteries have to be able to be charged in this time, in order to ensure the right functioning of the double CubeSat, if a peak demand is required.

8. Power system

A power system (SP) failure is one of the principal causes for losing a space mission; therefore the electrical power provision for space vehicles is an important requirement for satellite payloads. To provide uninterrupted electrical power, the satellite needs to be in working order, thus it is indispensable the power supply unit.

The principal functions of the power system are:

- Power source
- Power conditioning
- Power distribution
- Power storage
- Power protection

In Figure 8.1 there is a schema of how it works the power system. Basically, the satellite generates power with solar panels from the solar irradiation. Then this power has to be conditioned as the requirements of satellite. Part of this power is distributed in different subsystems, and the other part is stored in batteries for being used during eclipses or peak demands.

The power system has to control the good function of the energy. It means that if there is a subsystem wasting too much energy, this system must cut off the connection and notify this malfunction to the on board computer. Furthermore, the power system has to know always the Maximum Power Point Tracking (MPPT) to determine the correct solar panels function.

Finally, the power system has to be able to shut down all the subsystems, instead of communication subsystem, which has to send the pertinence beacon signals when an emergency occurs. When this emergency is solved, the PS has to be able to start up on its own.

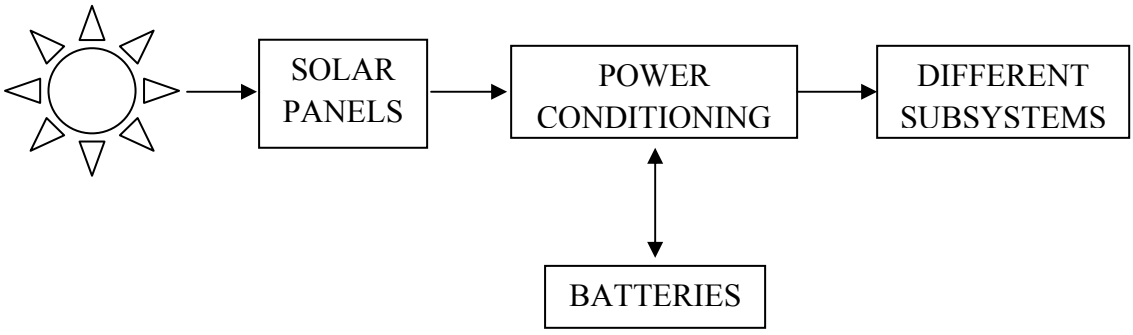

Figure 8.1: Basic schema of the power system

8.1. Power generation

The electrical energy is the form of energy that uses all the subsystems of QB50, thus it is necessary to convert the power received by the Sun to electrical energy [26]. In general, a spacecraft power system consists of two main sources:

- **Primary energy source:** It converts the primary energy into electrical power. In this case, the solar energy will be the primary energy source. Moreover, QB50 will use solar panels to capture this energy, due to the limited dimensions of the CubeSat.

- **Secondary energy source:** The principal aim of this source is to replace the primary energy source when this is not available. To carry out this function, the energy has to be correctly stored and the electrical power has to be delivered to the satellite and its payload when necessary. This is the case when the solar panels cannot capture the solar energy, because of the satellite is eclipsed. How long this secondary energy source is used, is determined in section 7. Concretely, it will have to be able to work continuously during 36.119 minutes.

There are two different options instead of using solar cells, but they cannot be used for different reasons. The first one is the conversion from nuclear to electrical power, using the heat produced by radioactive decay of Plutonium-238, but the disadvantage is the risk of spreading nuclear matter. The second one is using batteries which are charged before launch, but the problem is the low power that they offer, combined with the time of the mission, and the limited dimensions and weight of the double CubeSat.

8.2. Solar cells

Solar cells are devices which use the photoelectric effect to convert electromagnetic radiation that falls on them into electricity. They are constructed from a semiconductor material, like silicon, linked to a metal conductor and covered by a layer of anti-reflective glass [27].

Individual cells, otherwise known as photovoltaic (PV) cells, are assembled together as panels or modules which are then further grouped together as arrays.

Operation

When photons of electromagnetic radiation strike a semiconductor material, they can reflect off the surface, pass through without striking anything, or can be absorbed by electrons in the material's crystal lattice. These electrons are in the valence band. Absorbing energy from a photon, however, can excite them into the so called "conduction band", where they are free to move throughout the material. The excited electron leaves behind a free space in the lattice which can be filled by an electron from

a neighbouring atom. This leaves another space which is filled by an electron from the next atom, and so on.

Photovoltaic cells are limited by the "band gap", or energy difference between the valence and conduction bands. Photons, with exactly this energy, create one electron-hole pair in which case all their energy goes to electrical output. However, photons of lower energies are absorbed as heat and do not contribute at all to usable energy. Similarly photons, which higher energies, are partly wasted as extra energy. As the Sun emits radiation across the whole range of photon energies, large parts of the spectrum will not contribute to electrical power, limiting cell efficiency.

Other limitations on efficiency include optical losses such as reflection, electrical resistance within the cell and connectors, and impurities and defects in the crystal structure.

Types of cell

Most common solar cells are of the silicon p-n junction type. Other types of cells, such as thin film cells, light absorbing dyes and organic/polymer cells do exist, but these are rarely used for spacecraft panels.

P-n junction cells consist of two types of silicon with slightly different electrical properties placed in contact. Excited electrons are diffused across this junction to recombine with holes, but can only flow one way due to the electric field created by the imbalance of charge (because of the different way the two types of silicon react to incident radiation). The effect of the diode leads to a current flow in one direction, which can then proceed down any connected wire to the load. These cells can then be single junction or multi-junction.

Single junction cells are the first generation panels. They have just two types of silicon. Multi-junction cells consist of many different semiconductor materials (for example gallium arsenide GaAs, germanium Ge and gallium indium phosphide GaInP) sandwiched together in layers. It creates a cell with several different band gaps, allowing photons of much different energy to excite electrons and therefore allowing larger parts of the electromagnetic spectrum to be covered. Modern multi-junction cells can reach efficiencies of up to 30%, while typical solar cell efficiencies are currently of 27%. In this thesis, the BOL (Beginning Of Life) efficiency considered will be of 30%, like in OUFTI-1 mission.

Solar cell thermal properties

According to Azurspace properties [28], the emissivity (ε) and the absorpvity (α) of their Triple Junction GaAs Solar Cell are:

$\varepsilon = 0.86$

$\alpha = 0.91$

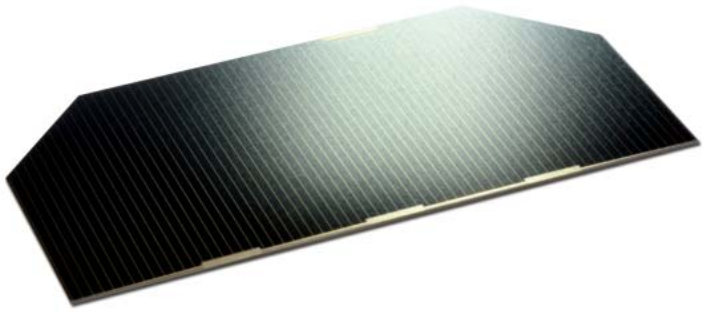

Figure 8.2: QB50's high efficiency solar cells

8.3. Energy storage

As it is mentioned previously, the power which will not be used at same time as it is produced will have to be stored. There are two ways of doing this, with batteries or flywheels.

The flywheel stores the energy as kinetic energy. However, when the flywheel accelerates or de-accelerate, the attitude of satellite could change. Hence, to compensate this problem it has to be used two flywheels. The problem is that it increases the weight and for this reason it is not possible to use this method in QB50 mission.

Therefore, the way chosen for storing the energy is the batteries. It will allow the satellite to use this energy stored when it occurs a solar eclipse or in peak demands. For choosing the battery model, there are some aspects that have to be taken into account: dimensions, weight, capacity and charging characteristics. It is also important to note that the batteries cannot be overcharged or discharged through the solar panels.

8.4. Power conditioning

It is important to obtain the power, but also to regulate it for using it in the best conditions for the satellite. Hence, the power conditioner is a device intended to improve the quality of the power that is delivered to all the subsystems. It plays an important role, due to it is necessary to protect, control and provide the power to each subsystem of the double CubeSat (first, the most important subsystems receive the power, and so on) with the correct voltage and the necessary power for each task.

8.5. Power budget

It has to be known the energy needed to choose the right number of batteries and solar cells for the spacecraft. The incoming power depends on the double CubeSat attitude, and the payload demands influence the outgoing power and the stored energy.

8.6. Power gathered

For a good design of the power supply system, the specifications for the entire system should be known, in order to estimate the amounts of incoming, outgoing and stored energy. There are several factors to be taken into account. For example, the outgoing energy depending on the payload demands, the type of the batteries and the solar panels.

8.6.1. Power gathered for a double CubeSat

In order to obtain a good estimation of the power collected, it is important to take into account the behaviour of the satellite depending on the attitude. For this reason, it will be done two graphs of the power gathered. The first one represents the QB50 advancing vertically (Figure 8.3), the other one represents the satellite advancing horizontally (Figure 8.4).

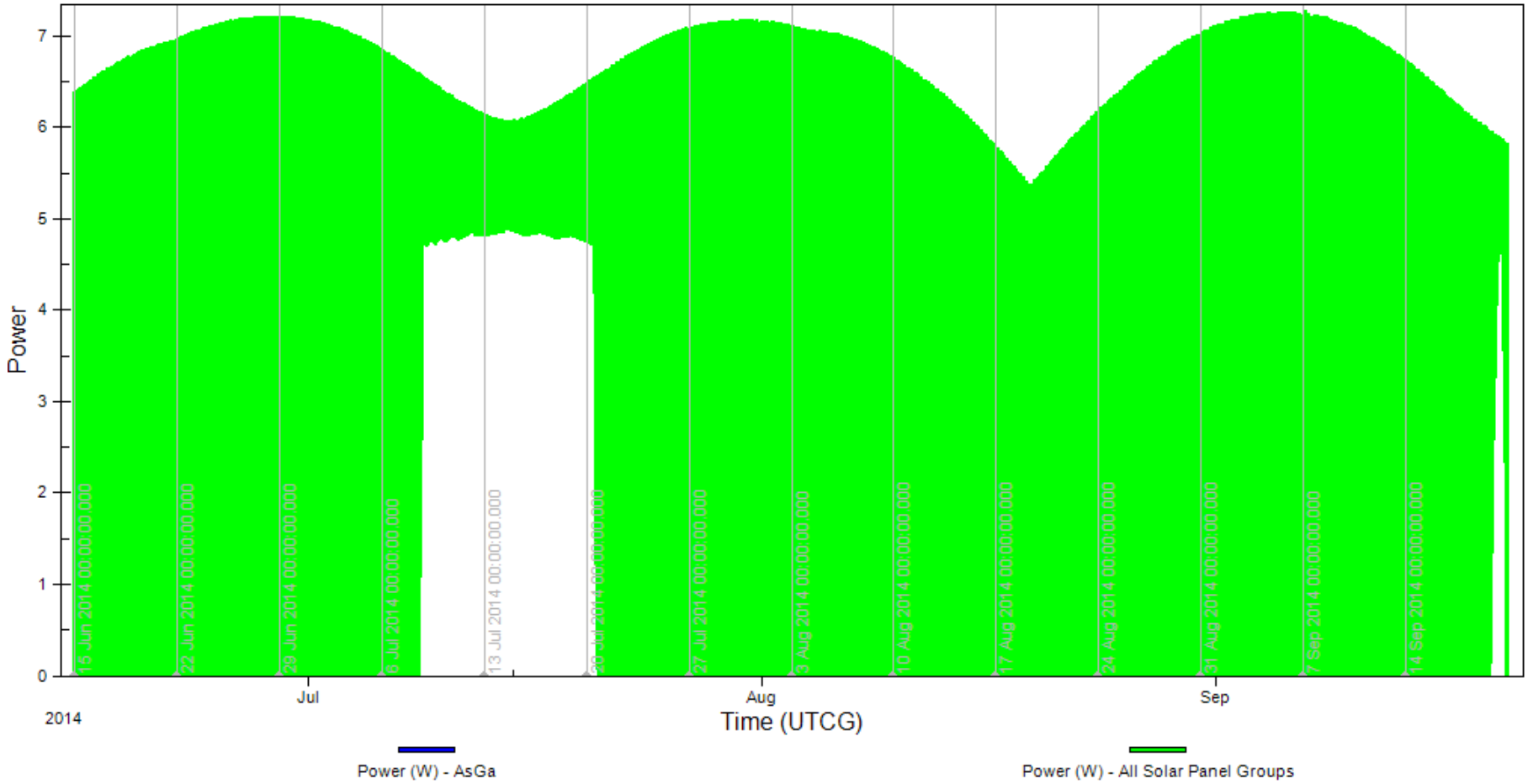

Figure 8.3: Power collected graph of double CubeSat advancing vertically

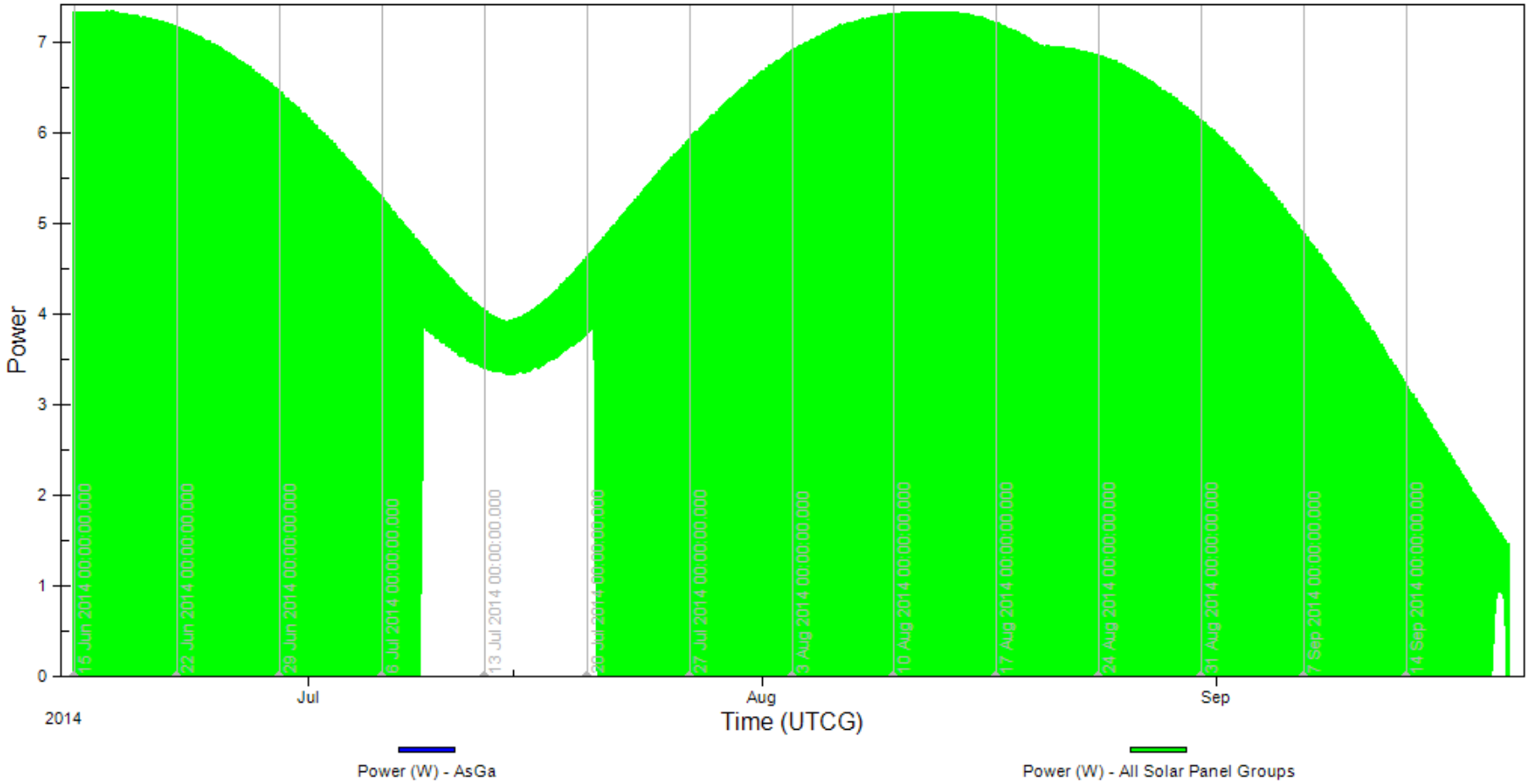

Figure 8.4: Power collected graph of double CubeSat advancing horizontally

First of all, comment that the satellite receives sunlight each day of its lifetime. Comparing the two graphs of double CubeSat, one concludes that the attitude plays an important role on the power gathered, as it could be seen analyzing the graphs, due to the different forms that they present.

By one hand, looking at the graphs related with the double CubeSat, concretely the graph where the satellite advances vertically (Figure 8.3), the highest value reached for the nanosatellite is 7.244 W, it is achieved on 6th of September 2014. There are three high peaks of power during the lifetime of QB50 and also three low peaks. However, what is really striking is what happens between 8th of July 2014 at 21:15:14.262 and 20th of July 2014 at 13:45:12.996[9]. During this period, the satellite is not hidden by the Earth or the Moon; it is always illumined by the Sun. Therefore during these days, if there are not demand peaks, the satellite will not use the batteries and it will be able to load them. It also happens between 19th of September 2014 at 18:06:08.753 and 20th of September 2014 at 21:56:39.469, but it is a shorter period.

By the other hand, Figure 8.4, which contents the graph when the satellite advances horizontally, presents two high peaks and two low peaks, it means that there are less peaks than the other attitude case, but they are more marked. Concretely, the highest peak is 7.340 W, which is greater compared with the highest peak of Figure 8.3. However, the total power gathered is lower when the satellite advances horizontally, as it could be seen comparing the areas of both graphs.

Not only there are differences between both cases of attitude, but also they present some similarities like obviously, the periods without the Earth or the Moon blocking the sunlight. The duration is the same, instead of the average of the power gathered, which is lower when the QB50 advances horizontally, as it is commented. Hence, during the first period of continuing sunlight (between 8th and 20th of July 2014), the minimum values achieved for the QB50 are quite different depending on the attitude, due to whereas the nanosatellite advancing vertically has approximately a constant minimum value of 4.8 W, the double CubeSat advancing horizontally has a low peak, as it could be seen in Figures 8.3 and 8.4.

Taking into account all these aspects, the best attitude option for the double CubeSat would be advancing vertically, because the total power gathered during its lifetime is higher than when the satellite advances horizontally, and the peaks are less marked.

Moreover, these graphs do not allow seeing with detail the power gathered and the periods of time when the satellite cannot capture solar energy. For this reason, Figures 8.5 and 8.6 shows the power collected on 25th of July 2014[10] during 5 hours (9:00-14:00), depending on the attitude.

[9] This phenomenon has been mentioned previously in section 7

[10] Note that the day chosen is not included in the periods without eclipses

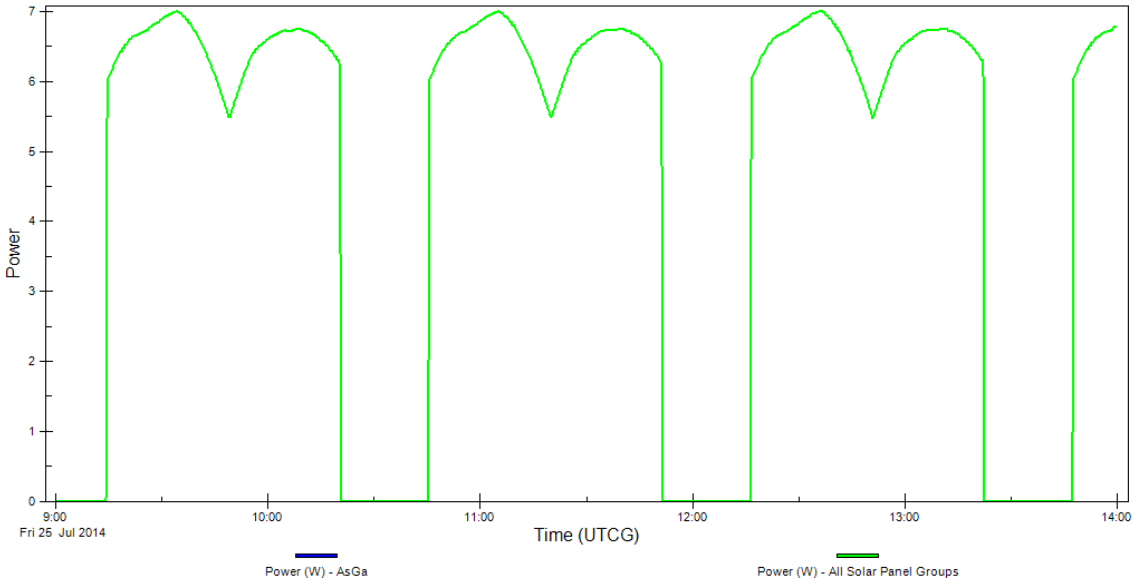

Figure 8.5: Power collected by a double Cubesat advancing vertically during 5 hours

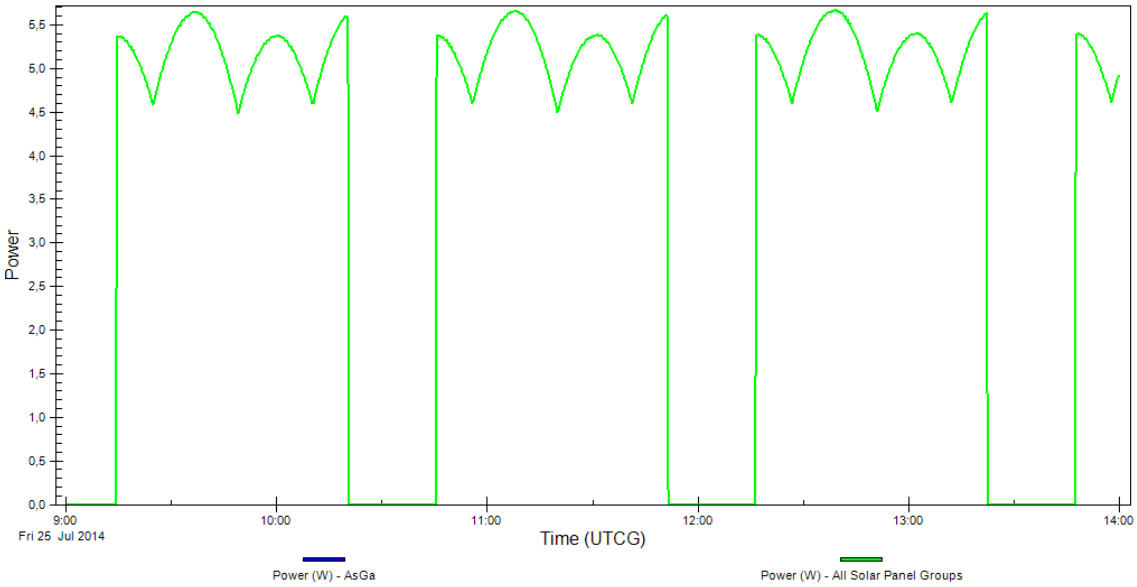

Figure 8.6: Power collected by a double CubeSat advancing horizontally during 5 hours

As it could be deduced looking at both figures, they present a similar form, instead of the top, where the double CubeSat advancing horizontally have more peaks. Finally, comment that they have, obviously, the same duration of sunlight and eclipse periods.

8.6.2. Power gathered for a triple CubeSat

The last point of study for a triple CubeSat is the power collected. It will be predicted the power gathered depending on the attitude, advancing vertically (Figure 8.7) and horizontally (Figure 8.8). Furthermore, as it has been done with the double CubeSat previously, it will be presented with detail the power gathered on 25th of July 2014 during 5 hours (9:00-14:00), in Figures 8.9 and 8.10.

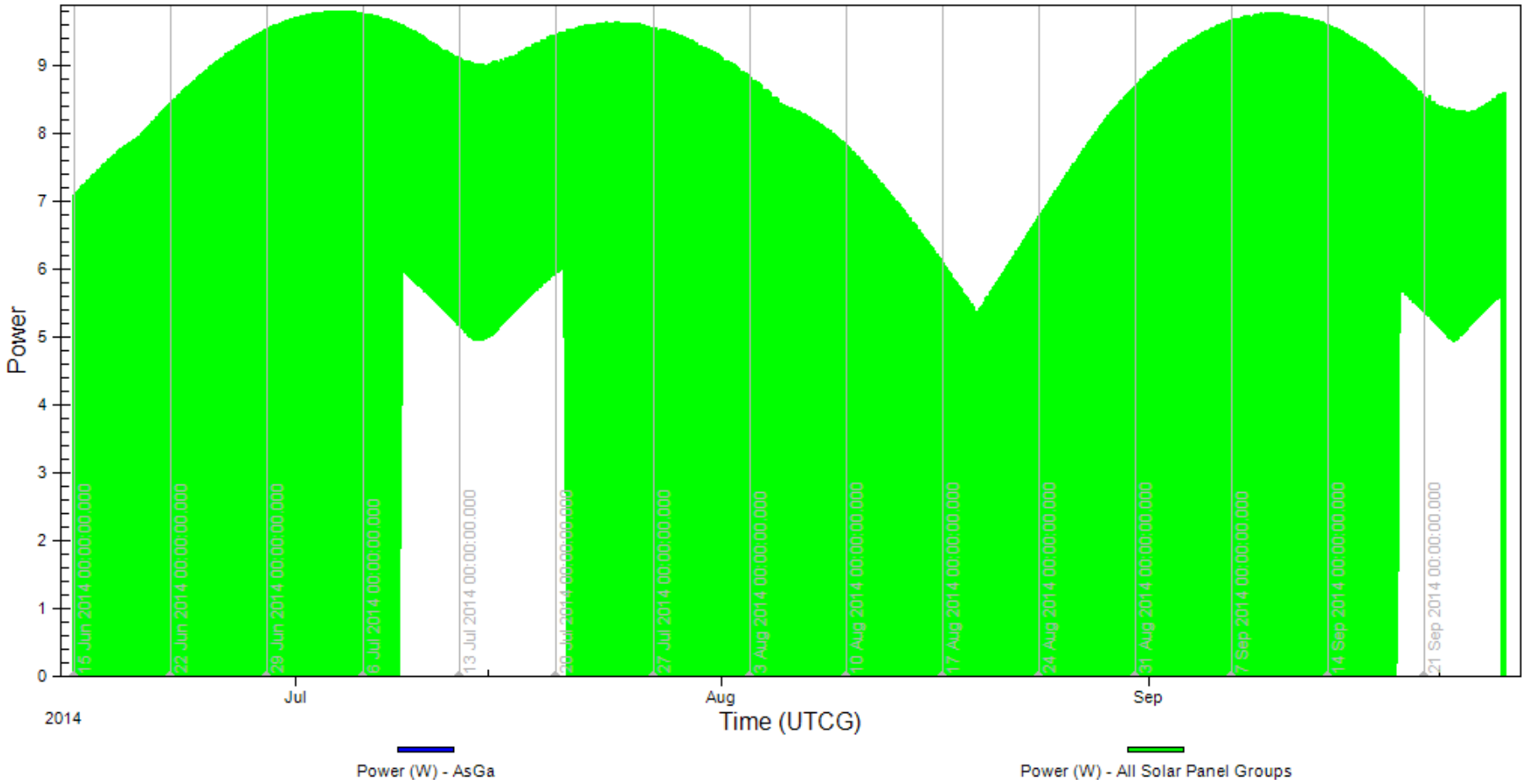

Figure 8.7: Power collected graph of triple CubeSat advancing vertically

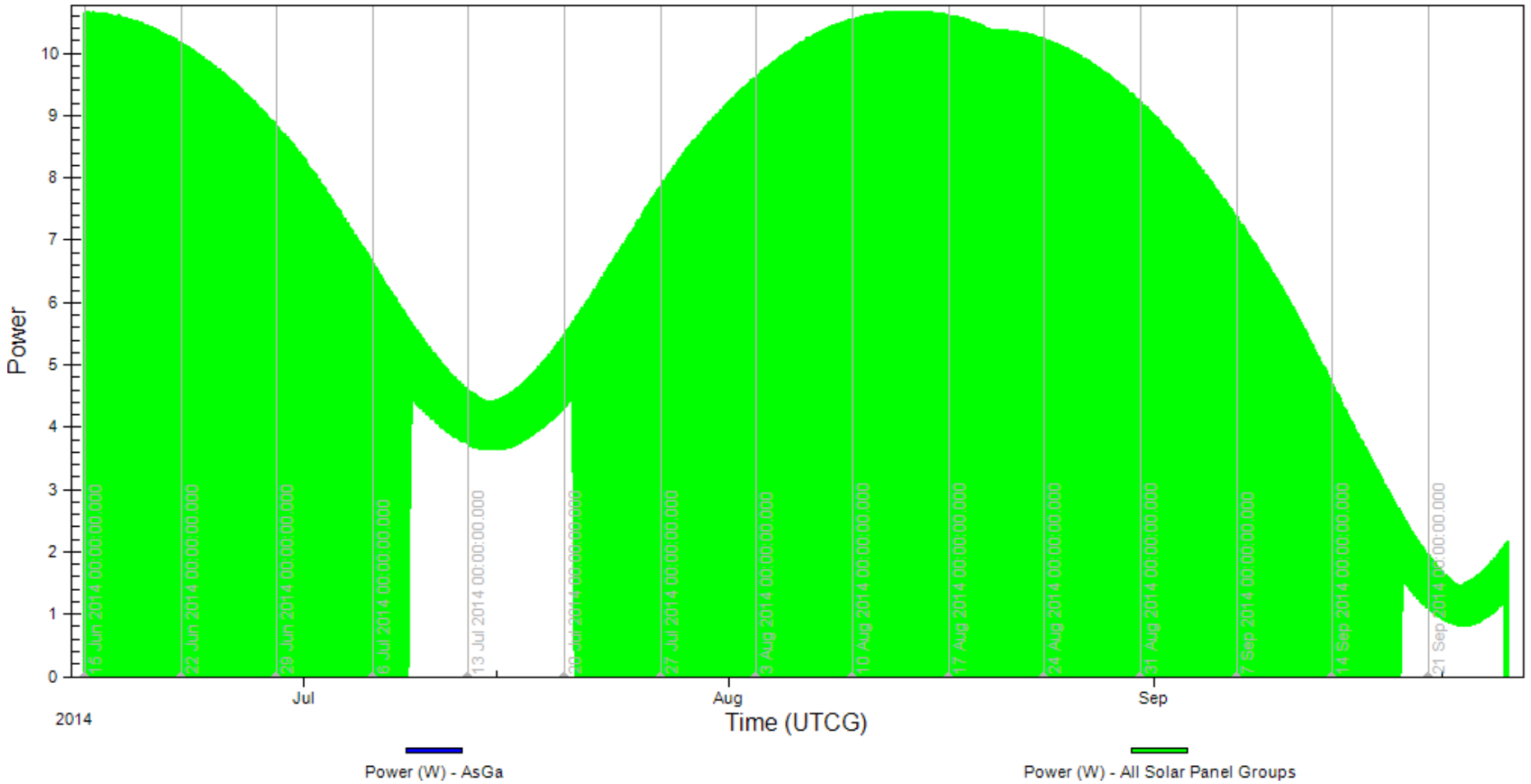

Figure 8.8: Power collected graph of triple CubeSat advancing horizontally

Looking at the four graphs of power gathered, it can be seen that the double and triple CubeSat, grouped by the type of attitude, have a relatively similar form even though the values are quite different. Obviously, the triple CubeSat collect more power than the double CubeSat, due to the lateral faces of the triple CubeSat are bigger; thus the solar panels are bigger too.

Focusing on the graph which includes the information of the triple CubeSat advancing vertically, it presents a highest value of 9.809 W. It has two periods of time when the satellite is not hidden by the Earth or the Moon. The first one (between 8th and 20th of July 2014) is the same as the double CubeSat, but the second one is longer. It happens because the triple CubeSat has a longer lifetime than the double one (see Figures 5.2 and 5.3). This second period of time, when the satellite is always illumined by the Sun, takes place between the 19th of September 2014 at 05:56:00 and the 26th of September 2014 at 13:04:00. It is shorter than the first one, but probably if the satellite's lifetime were longer, it will have similar duration.

Concerning the second graph of triple CubeSat (Figure 8.8), it has a highest value of 10.671 W achieved on 13th of August. It is almost 1 W higher than the triple CubeSat advancing vertically. However, as it happens with the double CubeSat, the total power collected for the triple CubeSat advancing horizontally is lower. Otherwise, during the two periods, when the satellite is always lighted, it takes place the two low peaks of Figure 8.8.

Therefore, the best attitude option for the triple CubeSat would be advancing vertically, because although the satellite advancing horizontally has a higher peak of power, the total power gathered during the triple CubeSat lifetime is higher when the satellite advances vertically, and this graph presents more constant values.

Figures 8.9 and 8.10 show the power gathered between 9:00-14:00 on 25th of July 2014.

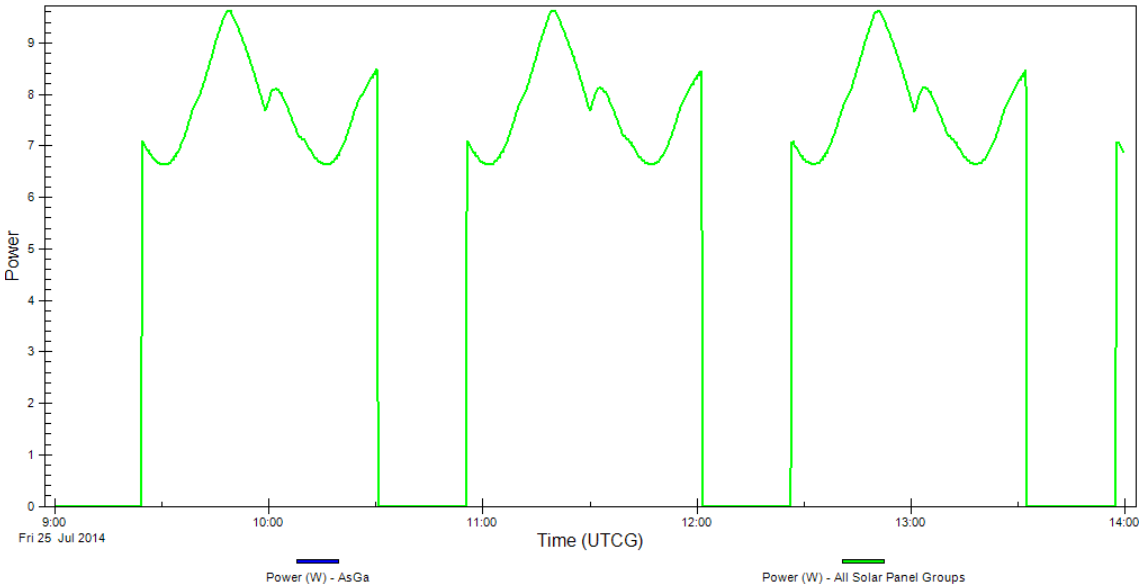

Figure 8.9: Power collected by a triple Cubesat advancing vertically during 5 hours

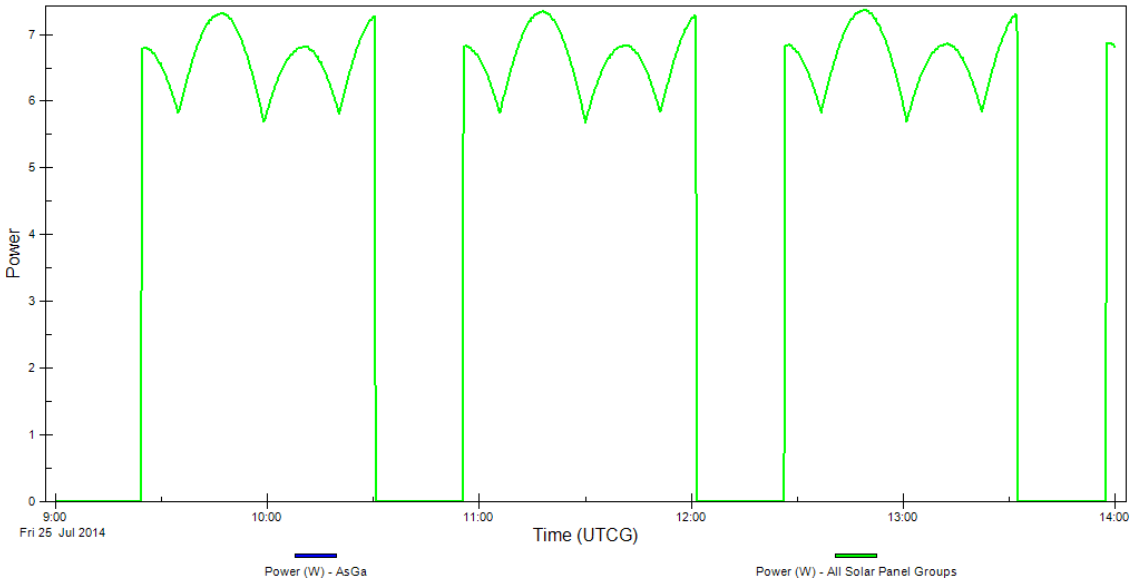

Figure 8.10: Power collected by a triple Cubesat advancing horizontally during 5 hours

As it happens with the double CubeSat, both figures present a similar form instead of the top, where there are slight changes.

Obviously, the sunlight and eclipse periods are the same for the double and triple CubeSat. Therefore, the triple CubeSat's batteries will have to accomplish the results presented in section 7. It means that these batteries will have to work continuously 36.199 minutes if required, and the minimum period of recharge will be about 10.866 minutes.

9. SEET: Space Environment and Effects Tool

An important point of this project is the application of SEET on the QB50 mission. SEET is a new tool of STK designed to evaluate the effects of the space environment on the spacecraft [29]. So, it will be helpful in QB50 due to it provides extensive information on the space environment, based on the averaging of large amounts of historical data.

Furthermore of applying SEET on the QB50 mission, a tutorial of this tool will be done in order to give some help for the next students, who will use SEET tool in a near future. This tutorial is located in Appendix B. The structure of this tutorial will be related, obviously, with the QB50 mission. Hence, it will be described step by step how to obtain the graphs and reports desired.

Focusing on the Space Environment and Effects Tool possibilities, SEET provides comprehensive modelling of the space environment, with the capability to predict various effects of the near-Earth environment on a space vehicle. This tool also provides five module models that can be used in the spacecraft missions:

- **The magnetic field module:** It computes the magnetic field along the satellite path, as well as performing field-line tracing, using standard models.
- **The radiation environment module:** It computes the expected ionizing dose rate and energetic particle fluxes experienced by a satellite along its trajectory, due to the trapped electron and proton populations, as well as the integrated total dose and fluence (flux integrated over time).
- **The vehicle temperature module:** It computes the expected temperature of a satellite exposed to direct solar and reflected Earth radiation, using simple thermal balancing equations.
- **The particle impacts module:** It computes the probabilistic distribution of small mass particles incident on a spacecraft.
- **The South Atlantic anomaly transit (SAA) module**: It computes the entrance and exit times and probable fluxes for a satellite crossing the SAA, a region of space with a greater concentration of ionizing radiation.

9.1. The magnetic field module

As it is commented, this module computes the magnetic field along the satellite path, as well as performing field-line tracing, using standard models. The range of output is available from the Earth's surface out to a few tens of Earth radii (about 120,000 km).

The Earth's magnetic field can be represented approximately as a magnetic dipole, with one pole near the geographic North Pole and the other near the geographic South Pole. The standard coefficients that represent the geomagnetic field have to be adjusted periodically, because of the locations of the poles and the strength of the field vary over time [30]. These standard coefficients with their standard mathematical description are known as the International Geomagnetic Reference Field (IGRF). The standard coefficients of IGRF are maintained in tables having nodal values added about once every five years. During this time, the coefficients are linearly interpolated to approximate their slow change over time.

The full description of the IGRF main field is a multi-pole spherical harmonic expansion containing over 100 coefficients:

$$V(r,\theta,\lambda,t) = R\sum_{n=1}^{N_{max}}\left(\left(\frac{R}{r}\right)^{n+1}\sum_{m=0}^{n}(g_n^m(t)\cos(m\lambda) + h_n^m(t)\sin(m\lambda))P_n^m(\theta)\right) \quad (9.1)$$

where *r, θ, λ* are geocentric coordinates (*r* is the distance from the centre of the Earth, *θ* is the colatitude and *λ* is the longitude), *R* is the IGRF reference radius (6371.2 km), $g_n^m(t)$ and $h_n^m(t)$ are the harmonic coefficients at time *t*, and $P_n^m(\theta)$ are the Schmidt semi normalized associated Legendre functions of degree *n* and order *m*.

In addition to the main field, the solar wind affects on the Earth's main field, creating a magnetic draping effect that alters the basic dipole at high altitudes. The contribution to the magnetic field due to the solar wind interaction is called the external field and is modelled by Olson-Pfitzer model [31].

The region in which the Earth's total magnetic field (main and external) exerts the dominant influence on charged particle motions is called the magnetosphere (500-60.000 km), in which there are the Van Allen radiation belts, solar energetic particles, and galactic cosmic rays. Such high-energy particles are the main factors that cause the degradation of components of the satellite. However, QB50 will orbit in a LEO; hence the influence of these factors will be lower than other satellites orbiting in higher altitudes.

Main field options

- **IGRF:** This option provides magnetic field calculations based on the full harmonic expansion of IGRF coefficients. The model coefficients at the epoch of interest are linearly interpolated from the ICRF coefficient tables, the nodes of which are spaced approximately every five years.
- **Fast-IGRF:** This option provides a specially tuned version of the IGRF harmonic expansion. It returns a field strength estimate accurate to within 1% of the full-IGRF option, but it is significantly faster.

- **Centered-dipole:** This option is an approximation of the Earth's magnetic field, with parameters derived from the IGRF coefficients. The dipole position and orientation is fixed with respect to the ECEF coordinate system origin with its axis tilted southward and rotated eastward compared to the ECEF Z and X axes. The IGRF coefficients determine the degree of tilt. The Centered-dipole model is a good choice when computational speed is a high priority.

Other user-selectable parameters

- **IGRF-update rate:** The harmonic coefficients of the IGRF main-field change slowly with time and are maintained in tables having nodal values added every five years typically. Between these nodes, the coefficients are linearly interpolated. The "update rate" determines how frequently the IGRF model coefficients are re-interpolated from the table. The default update rate is 1 day, which should be sufficient for most applications. However, for long periods it should be increased this value.

- **Field-line refresh rate:** This is the time period of the frequency at which the magnetic field lines will be reconstructed in the solar-magnetic coordinate system, using the defined magnetic field model. The default refresh rate of 5 minutes represents a reasonable compromise for most situations.

9.2. The radiation environment module

The Earth's trapped particle radiation belts were discovered at the beginning of the space. Consequently, considerable efforts were invested in building models of the trapped proton and electron populations, culminating in the NASA AP-8 and AE-8 models. Nevertheless, the CRRES mission has demonstrated that the trapped particle radiation environment is much more complex than the static environment described by the old models [32].

The concept of trapped particle radiation

The motions of charged particles entering the magnetosphere from the solar wind and undergoing acceleration or resulting from the decay of neutrons produced by cosmic ray interactions with the neutral atmosphere, are dominated by the magnetosphere magnetic field [33]. Figure 9.1 shows a schema of these charged particles:

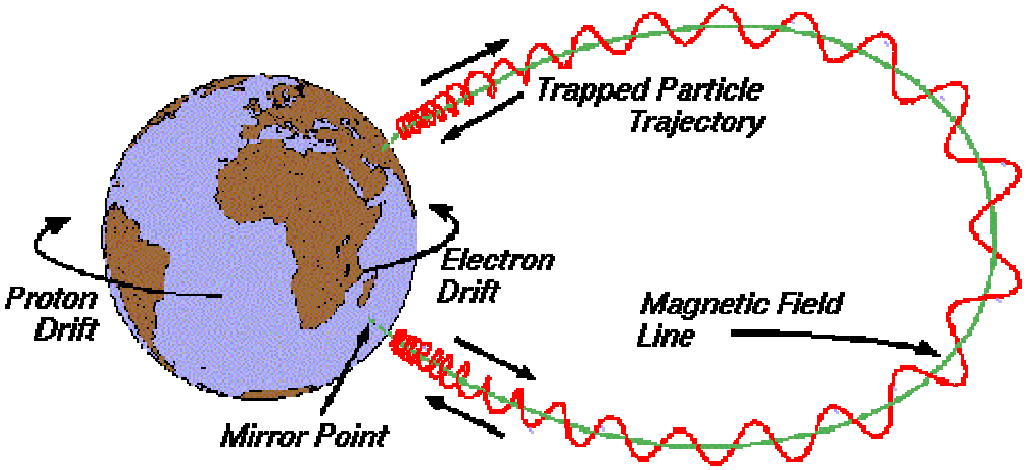

Figure 9.1: Representation of charged particles trapped in the Earth's magnetic field

The population of charged particles trapped by the Earth's magnetic field consists mainly of protons with energies between 100 keV and several hundred MeV and electrons with energies between a few tens of keV and 10 MeV.

The trapped proton population

The energetic (above 10 MeV) trapped proton population is confined to altitudes below 20,000 km, while lower energy protons cover a wider region, with protons below 1 MeV reaching geosynchronous altitudes. Figure 9.2 shows the distribution of trapped protons with energies above 10 MeV, as predicted by the NASA AP-8 MAX model.

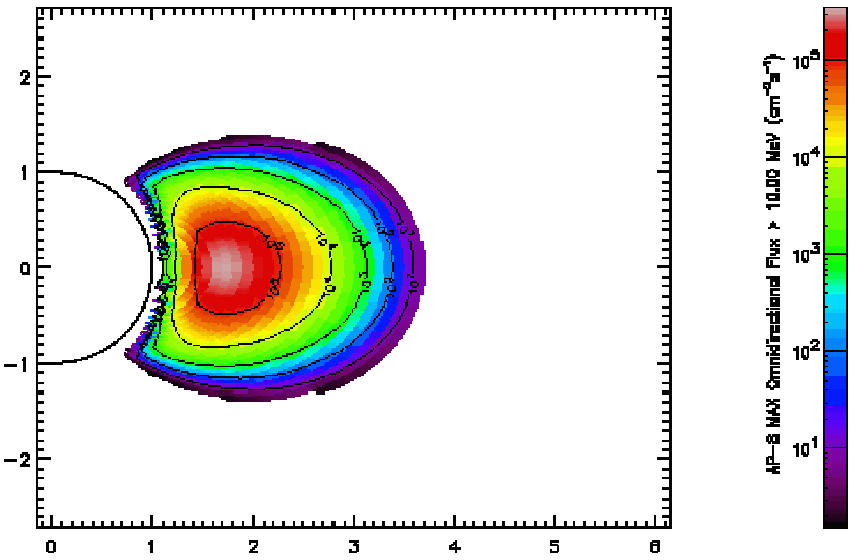

Figure 9.2: Distribution of trapped proton flux >10 MeV

The trapped electron population

The trapped electron population distribution is characterised by two zones of high intensities, below altitudes of one Earth radius and above two Earth radii in the magnetic equatorial plane, respectively, which are separated by a region of low intensities. The location and extent of the inner and outer belts depends on electron

energy, with higher energy electrons confined more to the inner belt, and lower energy electrons populating the outer belt to altitudes beyond geosynchronous orbit. Figure 9.3 shows the trapped electron population above 1 MeV.

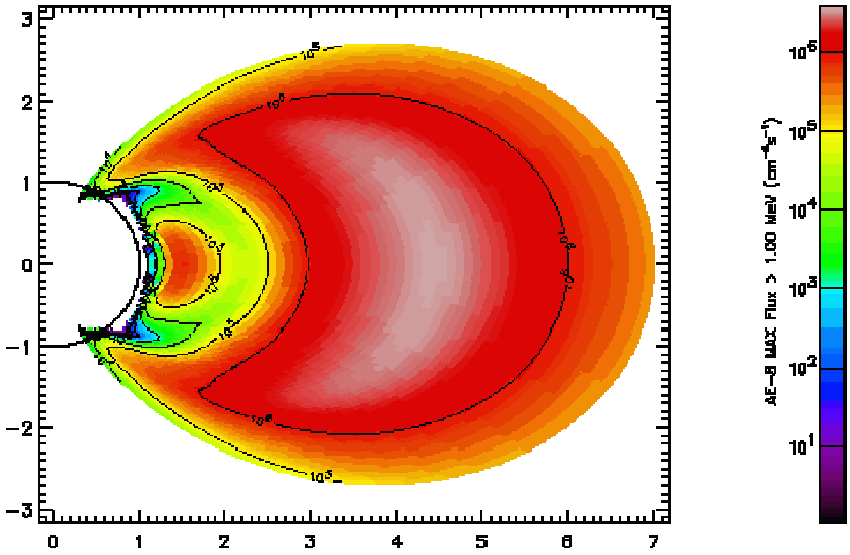

Figure 9.3: Distribution of trapped electron flux >1 MeV

9.2.1. SEET radiation environment module

The radiation environment which is collected by the satellite causes degradation in different devices on QB50, for this reason it is important to know information on satellite dosage and incident energetic particle flux. The total dose is computed by integrating the instantaneous dosage rate over time, where the dosage rate itself depends on the incident energetic particle flux and shielding parameters (material type and thickness) of a shielded instrument.

Hence, during the satellite trajectory this module computes the expected dosage rate and accumulated ionizing dose due to energetic electron and proton particle fluxes, for a range of user-specified shielding thicknesses.

First of all, it has to be decided which radiation environment model using. The different models are explained below:

APEXRAD

It is a radiation model to predict the amount of radiation received, based on data collected by the APEX Space Radiation Dosimeter [34]. The results of this model are given by four shielding thicknesses fixed; it means that only the prescribed sets of shielding thicknesses may be used. These values are: 0.108966, 2.0955, 5.9055 and 11.6205 mm

CRRESRAD

It is a radiation model that predicts the amount of radiation received based on data collected by the Combined Release and Radiation Effects Satellite (CRRES) Space Radiation Dosimeter [35], for radiation dosages behind shielding thicknesses of 2.0955, 5.9055, 11.6205 and 22.5171 mm.

Radiation-only

It is a radiation model that gives the results for the three values of shielding thicknesses that APEXRAD and CRRESRAD share: 2.0955, 5.9055 and 11.6205 mm.

For long scenarios APEXRAD, CRRESSRAD or Radiation-Only option should be selected. The problem is that these three models do not specifically compute proton or electron fluxes or provide constituent dosage rate and dose information, they only compute combined information from all constituent sources.

CRRES

It is a flux model based on CRRESELE [36], an electron flux model for energies between 0.5-6 MeV, and CRRESPRO [37], a proton flux model for energies between 0.1-100 MeV. These models are based on data collected by CRRES instrumentation.

NASA

It is a flux model based on NASA AE-8 radiation belt maps for electron flux for energies between 0.04 and 7.0 MeV, and NASA AP-8 radiation belt maps for proton flux for energies between 0.1 and 400 MeV.

If the model selected is CRRES or NASA, it will be able to use SHIELDOSE-2 [38], which is a radiation transport model that uses the electron and proton fluxes computed by the flux models, to estimate the absorbed total dose as a function of depth in a specified shielding material. Outputs include total and particular dosage rates of electrons, bremsstrahlung and protons. When SHIELDOSE-2 is active the shielding thicknesses has to be defined as well as the following options[11]:

- **Detector Type**: It has to be selected the type of material under Aluminium shielding to be used for dose computations. The materials for being chosen are: Aluminium, Graphite, Silicon, Air, Bone, Calcium, Gallium, Lithium, Silicon Dioxide, tissue and water.

- **Detector Geometry:** It has to be selected the geometry of the material under Aluminium shielding. The possible options are the followings:

[11] The shielding thicknesses parameters of QB50 are defined and explained in Appendix B

- **Finite-slab:** The detector is embedded in one side of a planar slab of Aluminium shielding material, and is irradiated through the slab from the other side.
- **Semi-infinite slab:** The detector has the same geometry as the finite slab, except that the Aluminium shielding material has no boundary behind the irradiated surface.
- **Spherical:** The detector is embedded at the centre of a solid sphere of Aluminium and irradiated from all directions.

- **Nuclear Attenuation Mode:** It has to be selected the degree of nuclear attenuation for dose computations. Possible values are: nuclear attenuation (due to local charged secondary energy deposition), and nuclear attenuation including neutrons.

In Figure 9.4 it can be seen a schema showing how it works the radiation environment module:

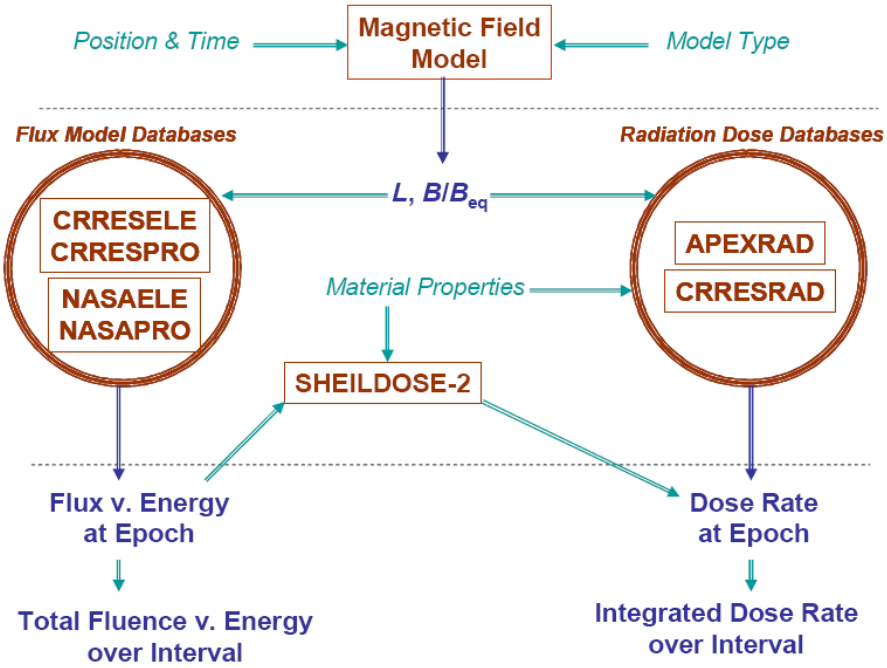

Figure 9.4: Radiation Environment Model Interdependencies

9.2.2. SEET radiation environment module applied to OUFTI-1

SEET is a new tool of STK; hence it is interesting to see if its results are closer to other applications used to predict the radiation. For this reason, it will be applied STK/SEET to OUFTI-1 and it will be compared these results with the Vincent Beukelaers' thesis [8], who used SPENVIS software.

As it is mentioned before, SEET radiation environment module has five different models. They are classified in two groups. The first one includes APEXRAD,

CREESRAD and Radiation-only models. They are able to compute only total dose information. The second group includes NASA and CREES. They provide more complete information. As it is pointed out previously, the CRRES mission has demonstrated that the trapped particle radiation environment is much more complex than the static environment described by the old models. Hence, CREES will be the model used to forecast the total radiation dose with STK/SEET.

Figures 9.5 and 9.6 show the predicted radiation dose for OUFTI-1 during its lifetime, provided by SPENVIS and STK/SEET, respectively.

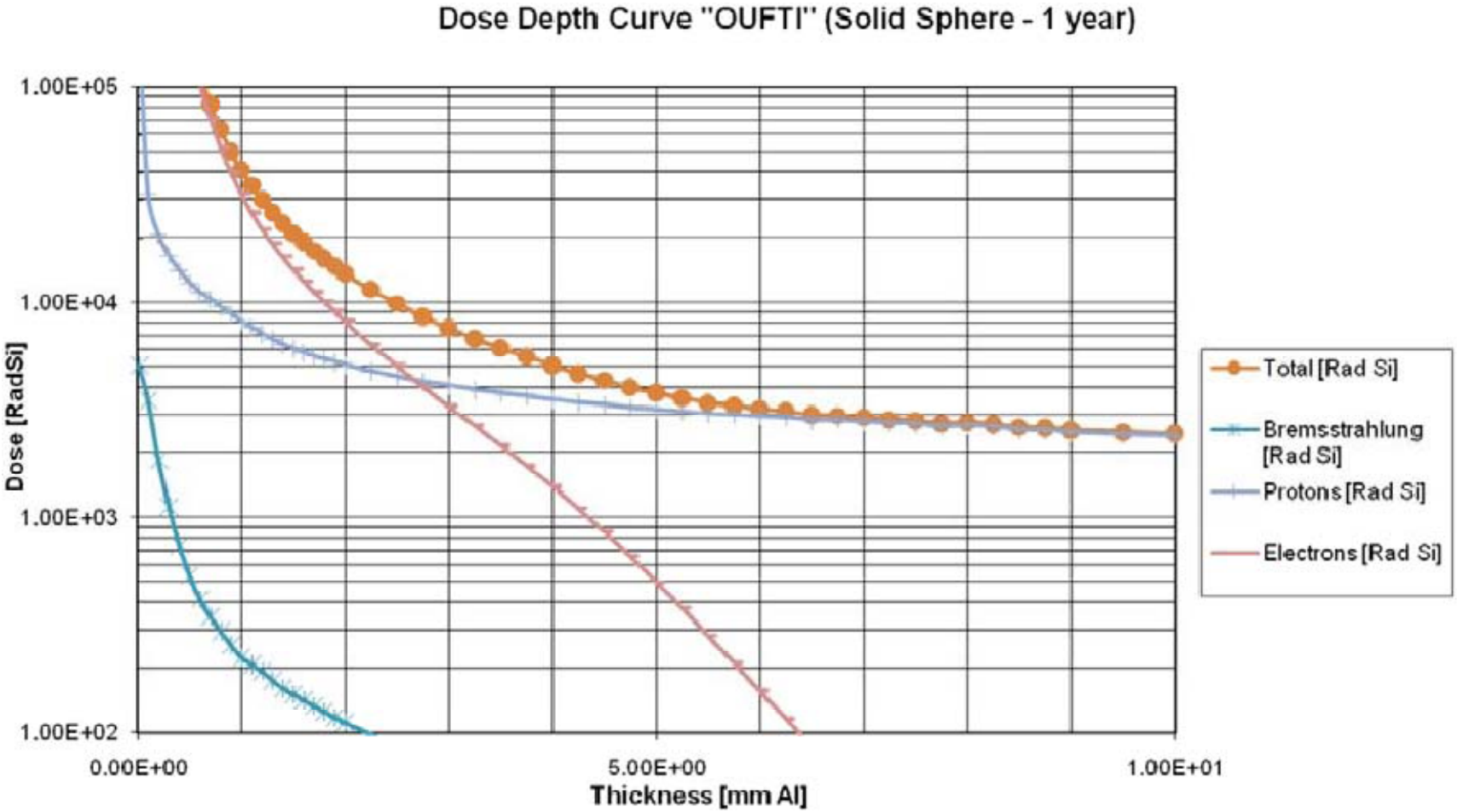

Figure 9.5: Radiation dose received for OUFI-1 provided by SPENVIS

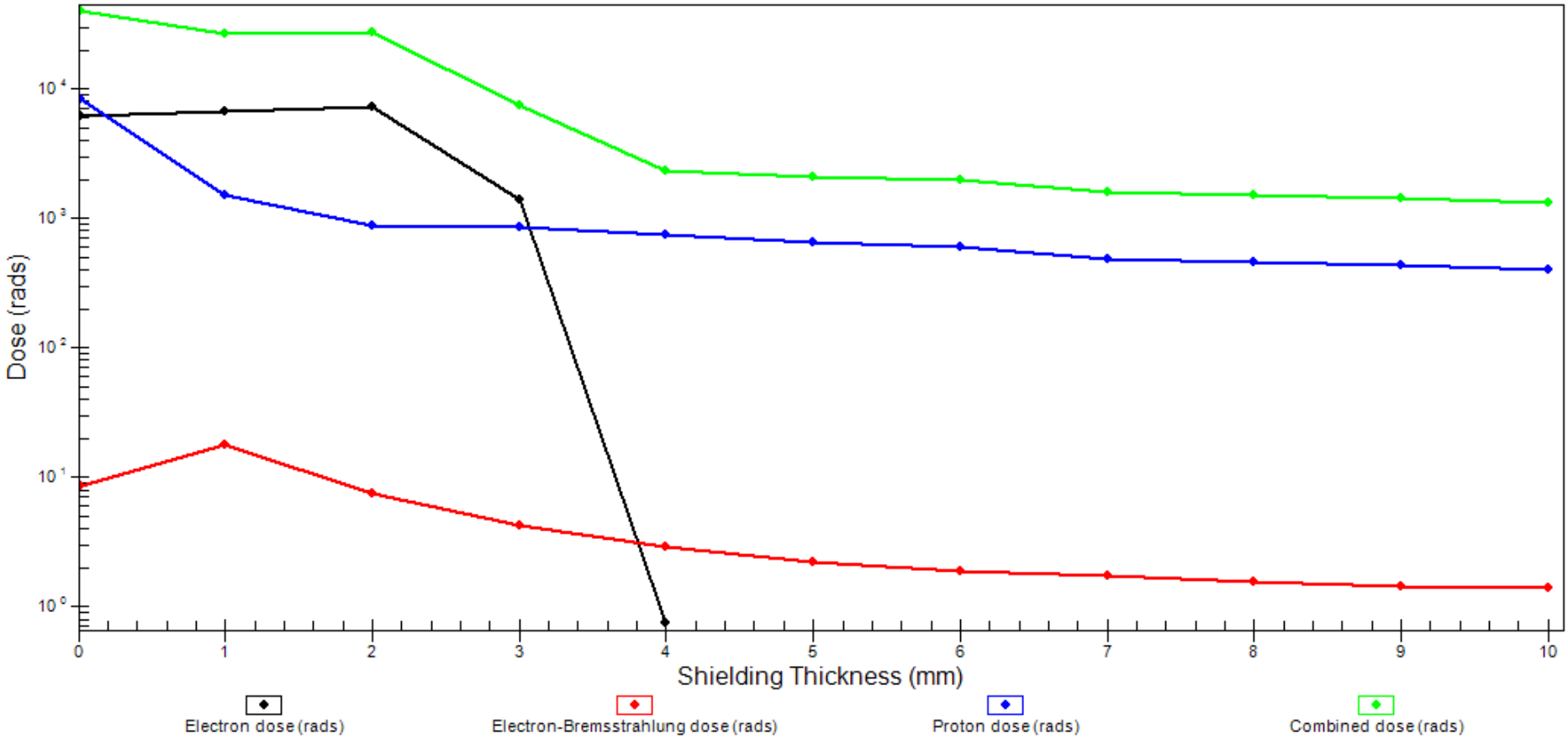

Figure 9.6: Radiation dose received for OUFI-1 provided by STK/SEET

In both graphs are represented the total, electron, bremsstrahlung and proton radiation doses. At first glance, one concludes that the total and proton radiation curves from both figures roughly have similar form even though the values, due to the values provided by SPENVIS software are slight greater than the STK/SEET ones. Concerning the bremsstrahlung and electron radiation doses, their curves show significant variations depending on the software used.

Nevertheless, what really strikes is the big difference between the radiation values of all curves provided by SPENVIS and STK/SEET in the range of 0 to 2 mm of shielding thickness. The SPENVIS curves reach very high radiation values when the shielding thickness is 0 mm compared with SEET results. However, when the shielding thickness increases, the radiation values of the SPENVIS graphs fall significantly. Otherwise, the SEET radiation values remain approximately constant during this range.

Moreover, the most important curve is the total radiation dose, because it is the sum of all the energetic particles which cause radiation damage to electronic components, solar cells and materials. For these reason, in Figure 9.7 it can be seen this curve more detailed. Furthermore, in order to compare the total radiation curves more accurately, both curves will be superimposed (Figure 9.8).

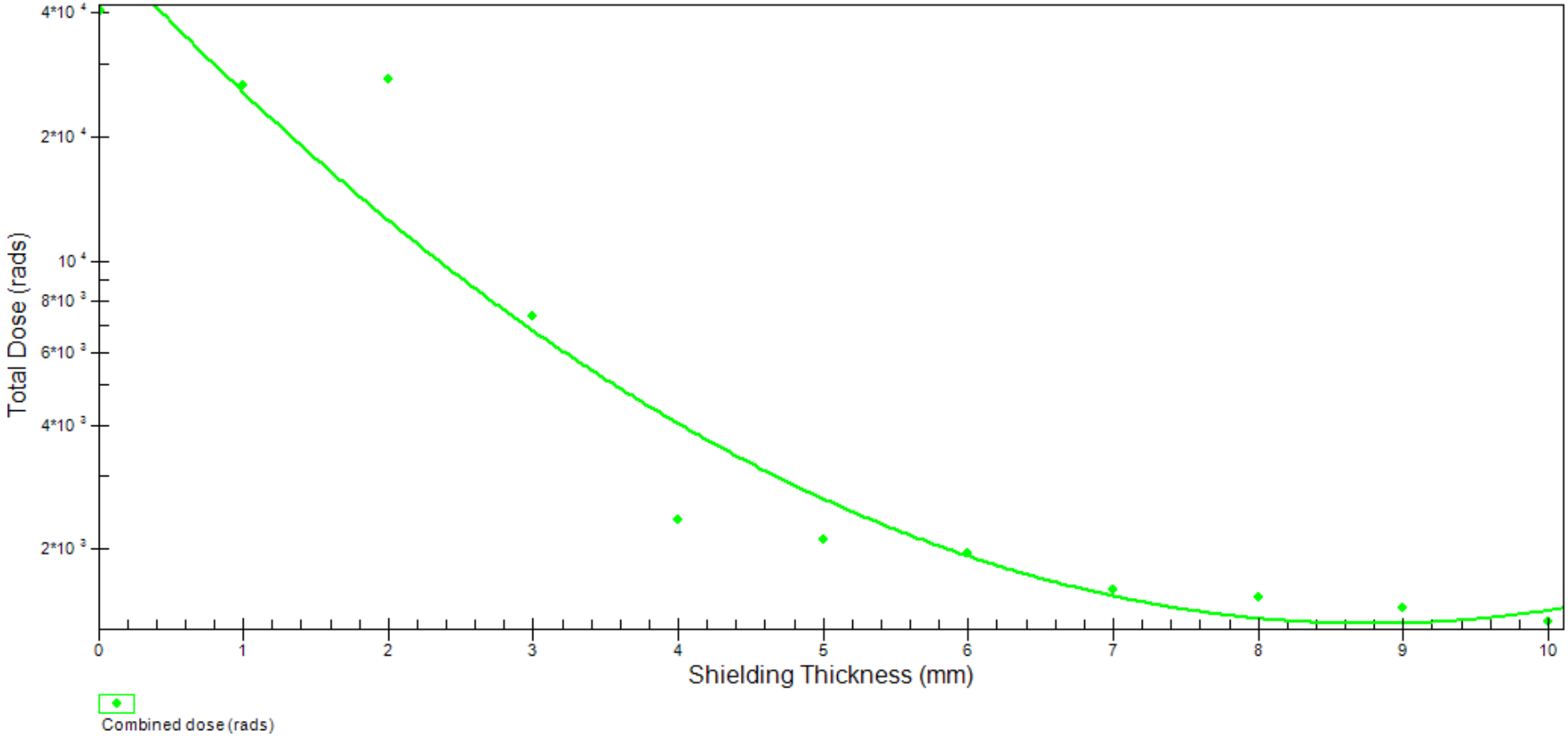

Figure 9.7: Regression curve of total radiation dose received for OUFI-1 provided by STK/SEET

First of all, it has to be commented that the graph presented in Figure 9.7 is a regression curve. As it is known, a regression is an approximation, hence it always presents some errors; however, this regression curve is closer the SPENVIS one than the real curve obtained joining all the points of the graph.

Nevertheless, analyzing more deeply the points of the graph, it should be noted that the graph could be divided in three parts. The first part includes the range of shielding thickness between 0 and 2 mm. During this range, the radiation values remain approximately constants. The second part includes the range of shielding thickness between 2 and 4 mm, where the radiation values fall significantly. This fall of radiation values is related with the behaviour of the electron dose curve (look at Figure 9.6). And finally, the third part includes the rest of shielding thickness values (4-10 mm). During this range, the radiation values become again more or less constants. However, the differences between each three parts are softly hidden for the regression curve.

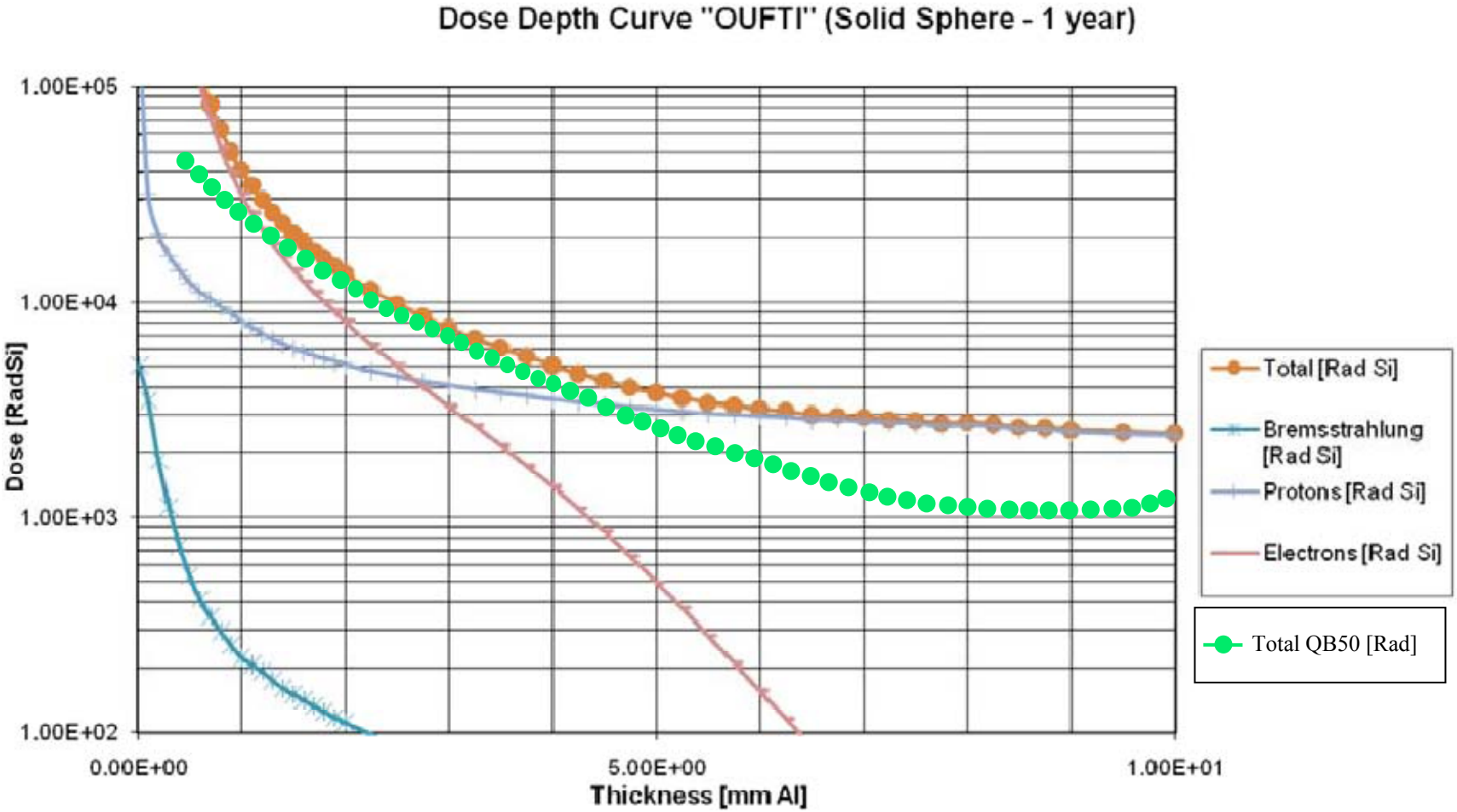

Figure 9.8: Comparison between the curves of total radiation dose

Now, that the curves of total radiation dose are superimposed, it is possible to analyze more accurately both graphs. As it has been pointed out in Figures 9.5 and 9.6, the radiation values provided by SPENVIS are slight greater, above all after the thickness achieves the value of 5 mm. However, the thickness predicted for OUFTI-1 is 1.925 mm. For this value of thickness, the dose radiation provided by SPENVIS is 14 krad, and the dose radiation provided by the regression curve of STK/SEET is 13.233 krad. The error committed is 5.479%

Actually, these results are not too displaced; therefore STK/SEET is a good tool to forecast the radiation dose that will receive the double CubeSat during the mission.

9.2.3. SEET radiation environment module applied to QB50

Once it has been demonstrated that SEET is a good tool to compute the radiation of QB50, the prediction of radiation dose will be done. In Figure 9.9 it is represented the total, electron, bremsstrahlung and proton radiation dose forecasted for QB50, and in Figure 9.10 it is represented the regression curve of total radiation dose.

In order to define the shielding thickness of QB50, it has been taken into account the design of OUFTI-1 due to the external structure will be at least similar. Hence, the thickness of solar panels is 1.5 mm and the total shielding thickness, considering the skeleton of QB50, is 1.925 mm.

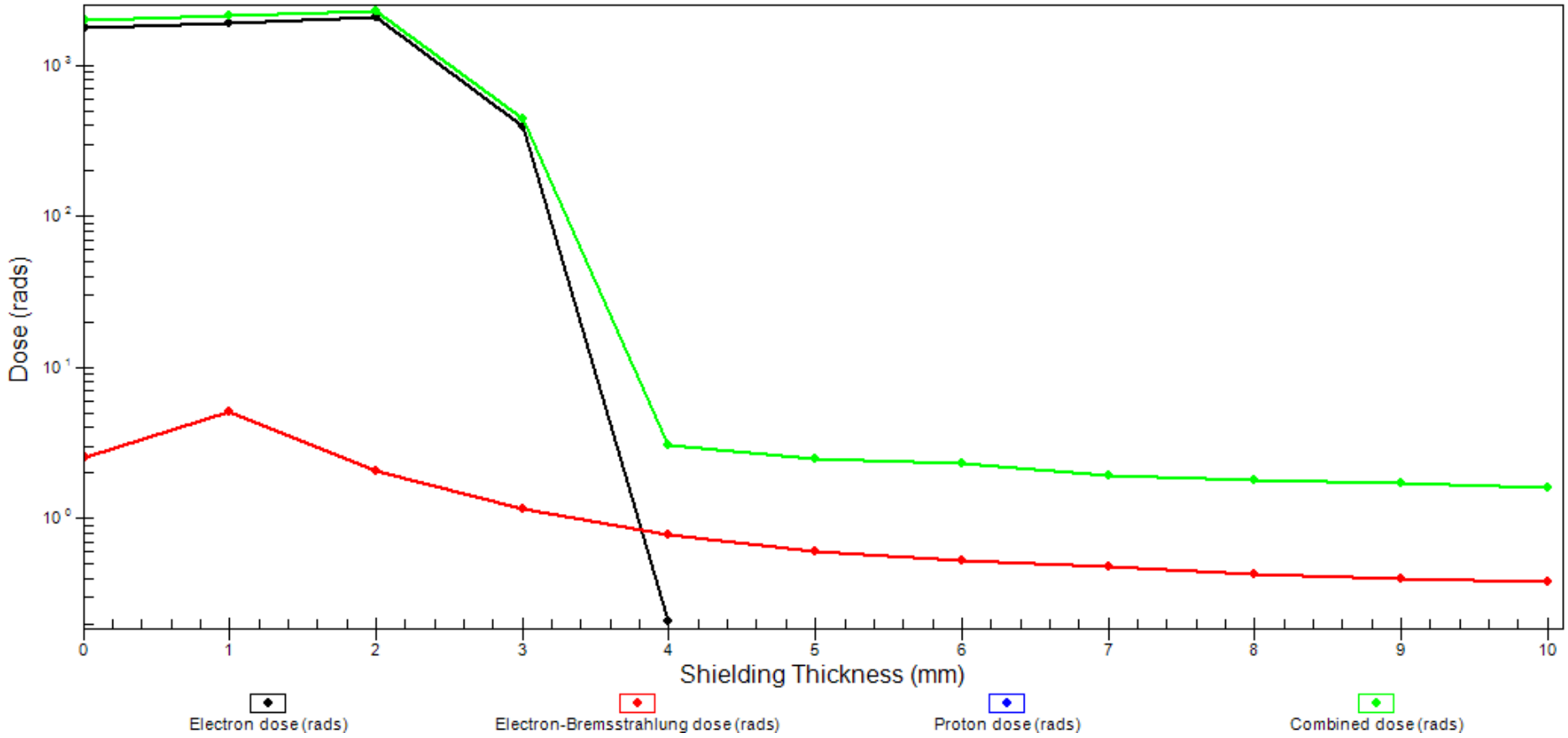

Figure 9.9: Radiation dose received for QB50

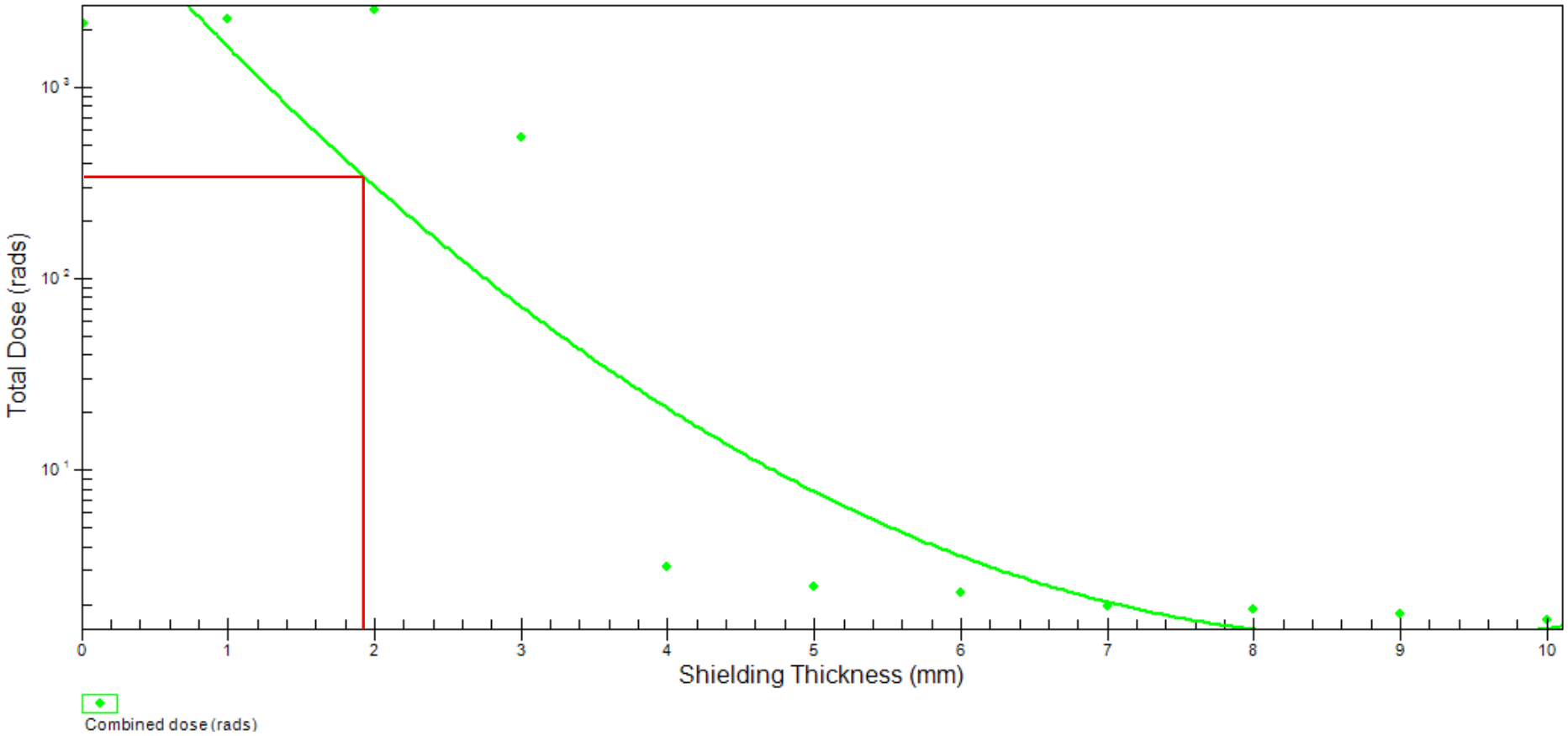

Figure 9.10: Regression curve of total radiation dose received for QB50

Looking at Figure 9.9 what strikes is the non-presence of proton dose. It is related with the Van Allen radiation belts. As QB50 is very close to the Earth, the nanosatellite is far away from Van Allen radiation belts. Hence, the radiation received for the double CubeSat is low. Moreover, the electron and bremsstrahlung doses have similar form than Figure 9.6, even though the radiation values are quite different.

Focusing on Figure 9.10, it can be seen the regression curve of the total radiation dose received for QB50. Its form is similar to the OUFTI-1's curve (Figure 9.7), instead of the radiation values. Obviously, the values of dose radiation received for QB50 are lower than results of OUFTI-1, due to the altitude and lifetime are lower. While OUFTI-1 orbits between 1447 km and 354 km and its lifetime is about 1 year, QB50 orbits in a circular orbit of 330 km and the lifetime forecasted is about 98 days.

Focusing on the shielding thickness of QB50 planned (1.925 mm), the total radiation dose predicted by STK/SEET is 342.5499 rad. It seems to be a lower radiation dose if it is compared with OUFTI-1. However, as it is said before, there are two main factors that have to be taken into account in order to understand the results: the lifetime and the altitude. The first factor does not need explanation due to longer lifetime means more radiation received. The second one is related with the Van Allen radiation belts. As commented previously, QB50 will be far away from Van Allen radiation belts; therefore the dose radiation received for the nanosatellite decreases substantially.

In principle, with these low values of radiation dose predicted, the electronic components of the double CubeSat would not have problems in this aspect. Nevertheless, in future developments it has to be done a precise analysis in order to know more accurately the dose radiation received.

9.3. The vehicle temperature module

This module calculates the expected temperature of a spacecraft exposed to direct solar and reflected Earth radiation, using thermal balancing equations. The temperature computations are based on models for either spherical objects [39], or planar objects with a specified orientation [40].

The Sun or Earth radiation can be either absorbed or reflected by opaque spacecraft material. The total thermal radiation transferred of a spacecraft will be a function of reflectivity, emissivity, surface area, temperature and geometric orientation. This model accounts all the sources of emitted and absorbed energy, along with some internal heat dissipation, following the thermal equilibrium equation:

$$E_{\text{absorbed}} + E_{\text{dissipated}} = E_{\text{emitted}} \tag{9.2}$$

where the energy absorbed ($E_{absorbed}$) represents the fraction of the incoming radiation that is absorbed by the material, independent of the incident angle of the radiation. The energy dissipated ($E_{dissipated}$) is the radiation converted in heat energy because of some

electrical or mechanical operations. And the energy emitted ($E_{emitted}$) represents the fraction of energy emitted relative to an ideal blackbody at the same temperature.

Applying the Stefan-Boltzmann law, the average external temperature T_0 of a spacecraft may be modelled as:

$$\sigma_B T_0^4 = \left[\left(\frac{(Q_{Sun} + Q_{ER})\eta_0 + Q_i}{\varepsilon_0}\right) + Q_{IR}\right]\frac{1}{A_0} \tag{9.3}$$

where σ_B is the Stefan-Boltzmann constant, Q_{Sun} is the direct thermal power from the Sun, Q_{ER} is the power due to sunlight reflected from the Earth, Q_{IR} is the radiant infrared power emitted from the Earth due to its temperature, Q_i is the power from the heat produced inside the spacecraft, η_0 is the material absorptivity of the spacecraft, A_0 is the total radiating surface area, and ε_0 is the surface emissivity of the spacecraft. All the power sources contribute while the spacecraft is illumined; only the emissive-infrared component from the Earth (Q_{IR}) and internally-generated heat (Q_i) play a role, while the spacecraft is in the shadow of the Earth.

The absorbed portion of the incoming energy and emitted infrared energy are function of the Earth's atmosphere, the clouds and the gas concentrations. The albedo of the Earth is a measure of how it reflects sunlight into space by the Earth's atmosphere, clouds, oceans and land surfaces. Typically 30% of solar energy at optical wavelengths may be reflected and thereby contributes to Q_{ER}.

The rest of solar energy raises the Earth's temperature because it is absorbed by the atmosphere and Earth's surfaces contributing to Q_{IR}. The Earth's albedo, the power per unit area from the Sun and the spacecraft's distance from the Earth and Sun are therefore used in combination to estimate how affects the radiated power to the spacecraft.

There are two models to determine the reflected incidence of incoming radiation: a plate and a sphere model. For QB50, the selection will be a sphere.

In order to calculate the temperature that the double CubeSat will receive during its lifetime, a graph is created. Figure 9.11 shows the temperature in K as a function of time.

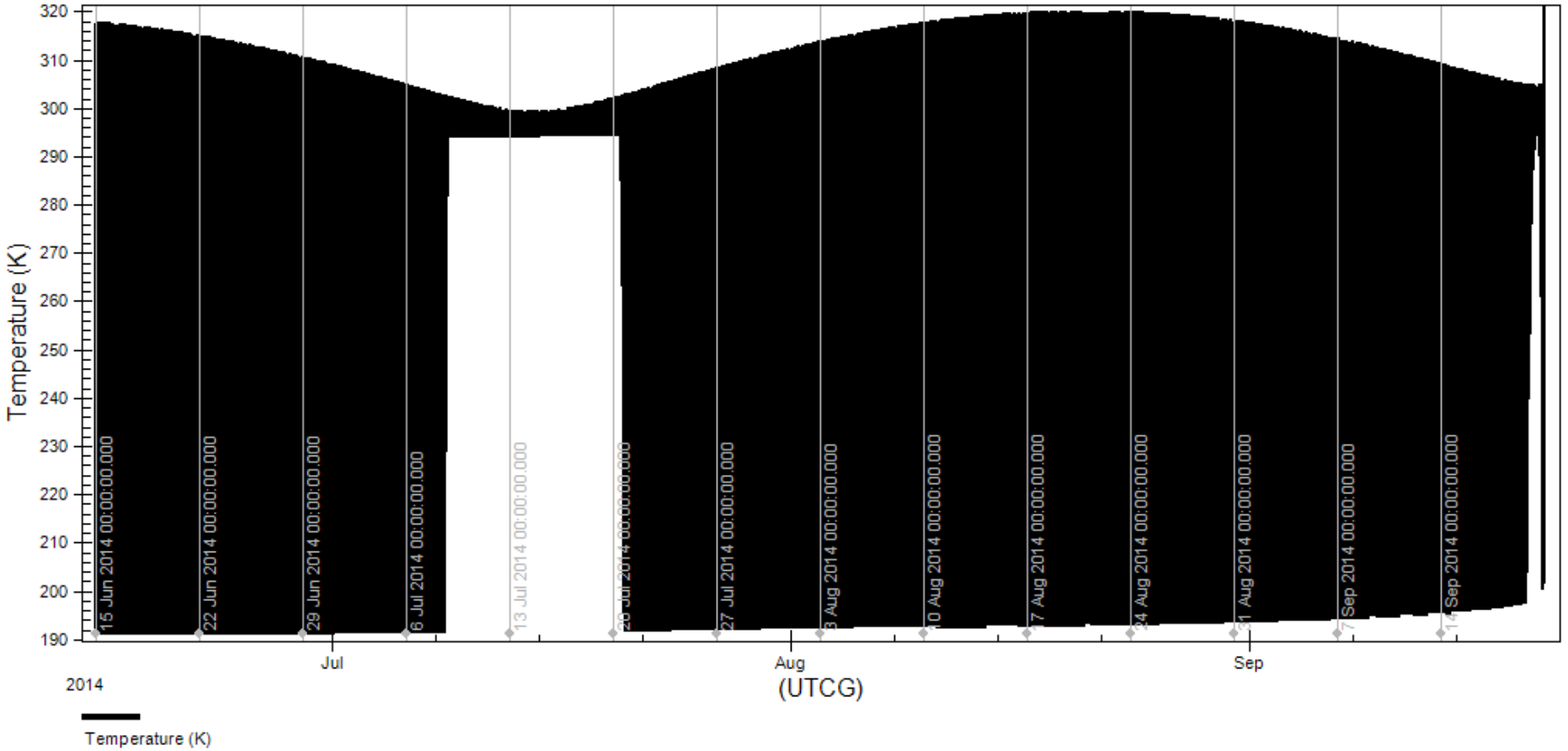

Figure 9.11: Temperature achieved for QB50 during its lifetime

Looking at the graph, it could be said that the maximum temperature achieved for QB50 is 320.047 K, without considering the re-entry phase, at the end of which the nanosatellite is disintegrated. Comparing this graph with Figure 8.3, which represents the power collected graph of a double CubeSat advancing vertically, one concludes that they have, obviously, a similar form. For the intermediate temperatures, it has to be taken into account the solar heating when the satellite enters into the Earth's shadow, because the satellite loses temperature progressively. Between the days of 8th to 20th of July, and 19th to 20th of September, the satellite is always illumined because of the Earth does not intersect the trajectory between the QB50 and the Sun. During these periods the temperature fluctuates between 294.238 and 302.431 K.

9.4. The particle impacts module

About 10,000 space debris objects are currently catalogued, but the number of debris larger than 1 cm is estimated to be around 60,000. The danger of these objects comes from their high relative velocity with respect to the satellite and the intensity of the impact can be extremely high.

This module computes the probabilistic number of small particles impacting the spacecraft of a given cross-sectional area and orbit, during a specified time period. These impacts can cause significant damage to spacecraft. They could have two different origins: meteoroids [41] or artificial debris [42]. The probable impact rate on a satellite is determined from the modelled particle environment and the cross-sectional area of the satellite. The surface material of satellite has to be specified because it plays an important role. Figure 9.12 shows how affect the particle impacts.

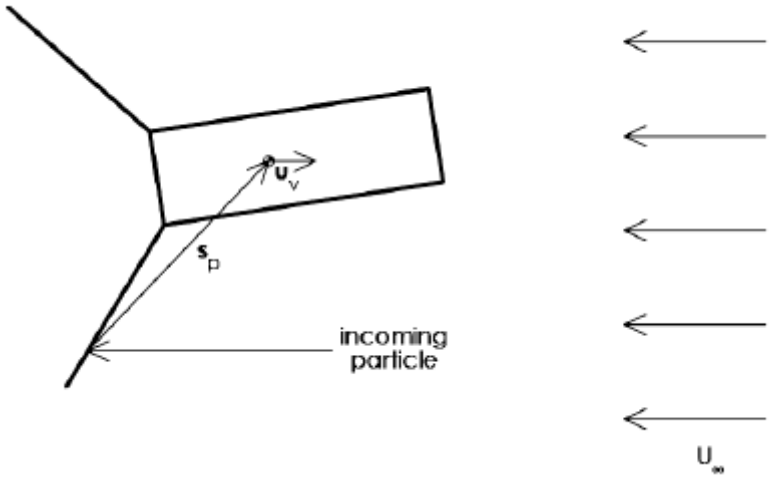

Figure 9.12: Schema of how affect the particle impacts

Meteors

The meteor showers occur when the Earth passes through the dust trails of comets. Commonly, the meteoroids' mass is between the range of 1 μg –10 mg and reaching velocities between 12 km/s and 70 km/s. Meteor showers have two important characteristics: the radiant, which is the point in the sky where meteors come from, and the number of shower meteors per hour, specified with Zenithal Hourly Rate (ZHR). There are peaks of ZHR higher than 10,000 when the spacecraft crosses a dense comet dust trail, but usually the normal value of ZHR is approximately 200. SEET's Meteor Environment model is largely based on a database of 50 parameterized annual meteor showers.

Debris

Orbital debris consist of numerous objects with different origins like inactive satellites, parts of spacecraft produced by an accident, explosion, collision or erosion. This model calculates an average impact velocity profile and the orbital debris particle flux at a given time as a function of particle size, satellite average altitude (values included in the range of 300-2250 km), orbital inclination, and the $\bar{F}_{10.7}$ solar activity index for the previous 13 months. The debris environment module calculates the particle flux that would be capable of causing damage to satellite surface. Figure 9.13 shows the locations of debris around the Earth.

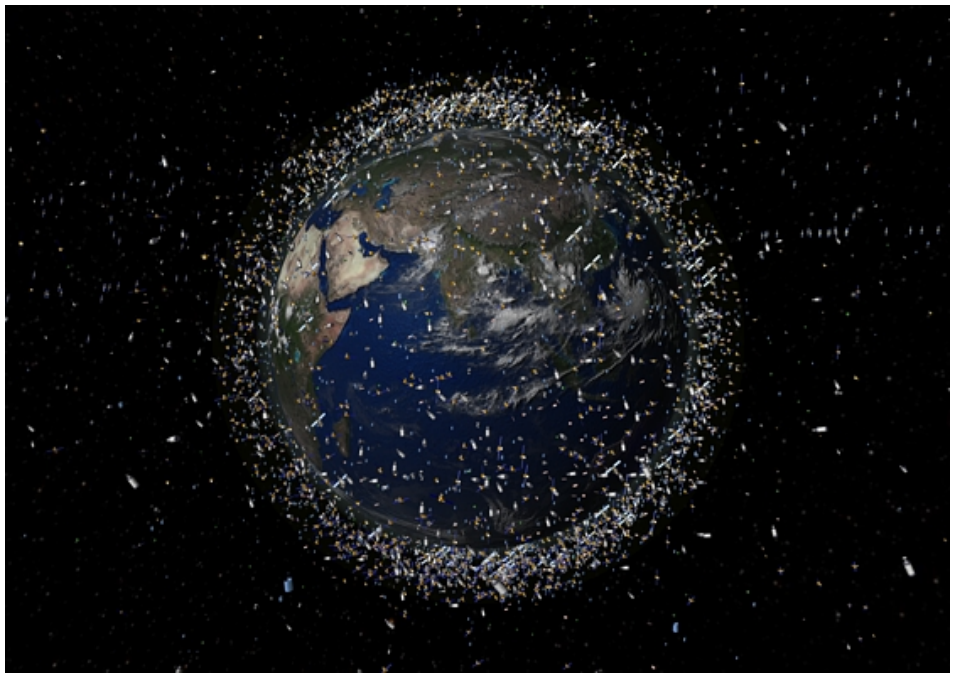

Figure 9.13: Debris around the Earth

In order to compute the particle impacts received for the double CubeSat, Figure 9.14 shows the impact rate during its lifetime.

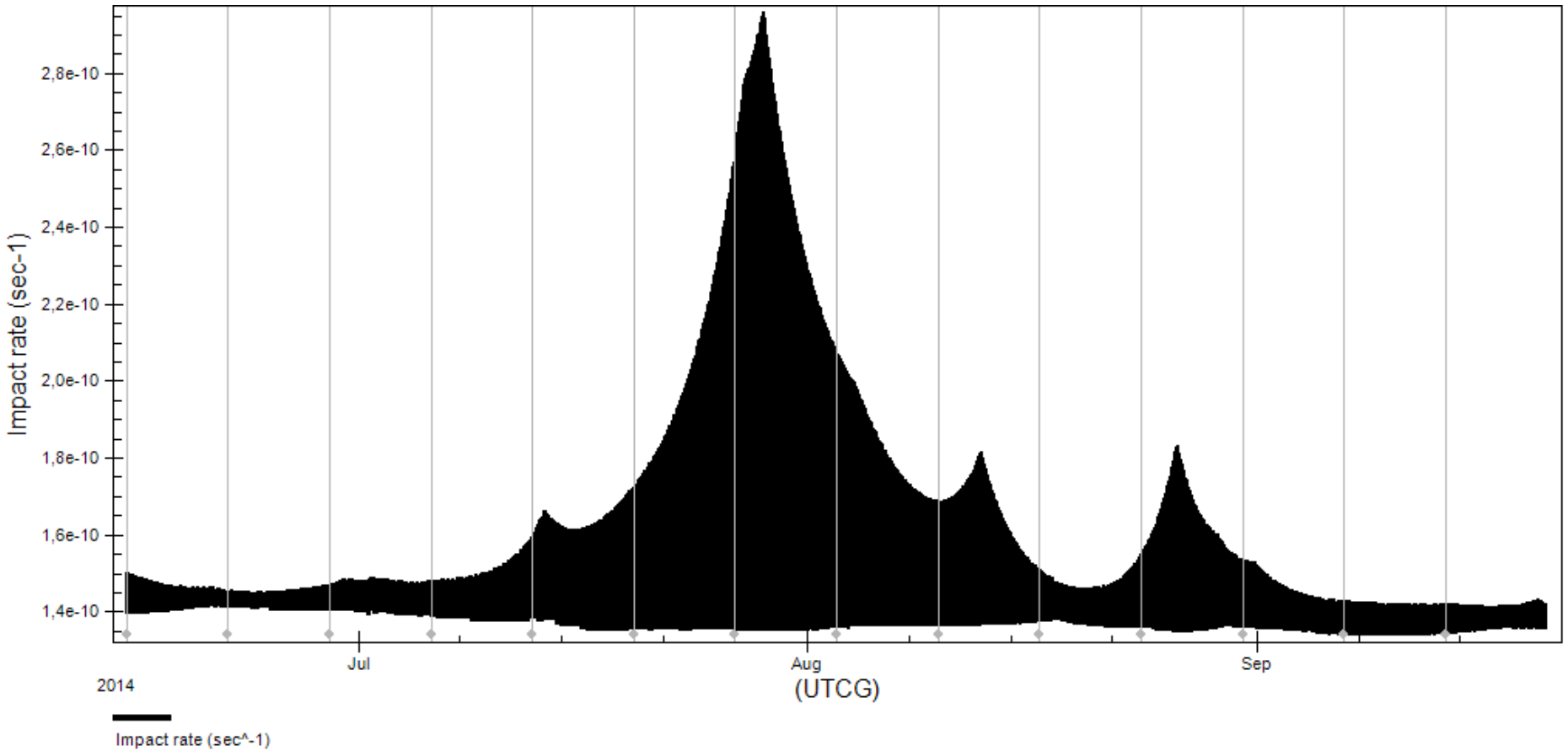

Figure 9.14: Particle impacts rate of QB50

Looking at Figure 9.14, one concludes that there are some peaks during the mission period, but the most important one is the peak achieved on 28th of July with a value of $2.9583 \cdot 10^{-10}$ s^{-1}. It happens because of the variation of the South delta Aquariids meteor shower activity [43]. South delta Aquariids meteor streams are groups of meteoroids originating from dust grains ejected from an unknown comet. These small dust grains (meteoroids) are distributed along the parent comet's orbit concentrated close to the comet nucleus with fewer grains farther away from the nucleus. The South delta Aquariids annual shower is a brief, but intense, meteor shower.

Nevertheless, although on 28th of July is reached the highest peak, the impact rate values are still low; hence it does not seem to be an issue of concern.

9.5. South Atlantic anomaly transit (SAA)

The South Atlantic anomaly is a region of space where there is an increased concentration of ionizing radiation. The electronic parts of the satellite can be spoiled because of this radiation. For this reason, it has to be known when the satellite is in this zone for decreasing the electronic damage.

The Earth's magnetic field, where are trapped protons and electrons by the Van Allen radiation belts, is approximately a tilted dipole pattern at low altitudes. This inclination makes the centre of the Earth and the centre of the magnetic dipole pattern to be displaced; therefore, there is a portion of the inner radiation belt closer to the Earth than others. This region is known as the South Atlantic anomaly, and it is located in the coast of Brazil.

This module computes the entrance and exit times and probable fluxes for a satellite crossing the SAA region. For all flux-related output is needed to be specified the energy channel parameter. The SAA module covers altitudes from 400 km through 1700 km. Thus QB50 is not within this range of altitudes, this module will not be used in this project.

10. Conclusions

This project constitutes a detailed mission analysis of the QB50 double CubeSat in terms of lifetime, ground station accesses, sunlight periods, power collected, radiation environment, vehicle temperature and particle impacts predictions. Furthermore, it has been estimated the lifetime and the power gathered of a triple CubeSat. Another important goal has been the application of the SEET tool of STK to the QB50 nanosatellite, because it is the first time that this tool is used in the University of Liège for the mission analysis of a satellite.

First of all, analyzing the orbit and its evolution in time, it has been obtained with STK a lifetime of 98 days for a double CubeSat, more than the minimum lifetime of three months required. Moreover, the lifetime predicted for a triple CubeSat has been 104 days. Note that the centre of mass of the triple CubeSat has not been displaced of its geometric centre. This aspect can explain the difference of lifetime between both nanosatellites.

Once the lifetime has been forecasted, the second step has been to determine the ground station accesses. The footprint of QB50 have a length of 2348 km and an area of $4.317 \cdot 10^6$ km^2. Each access between the GS in Liège and the satellite will have a mean duration of 4.057 minutes, and the satellite will be visible 11.964 min/day on average. Furthermore, there will be at least 3 accesses per day which will ensure a daily communication link.

The sunlight, penumbra and umbra periods also have been computed. Concretely, QB50 will be 70.442% of its time in sunlight, 0.611% in penumbra and 28.947% in umbra. The maximum duration of an umbra period is 36.119 minutes, which represents 39.709% of the orbit. Hence, during this interval of time, the nanosatellite will operate with batteries. Otherwise, the minimum duration of a sunlight period is 10.866 minutes.

When the sunlight periods have been defined, the power gathered for a double and triple CubeSat is estimated depending on the attitude. For the double and triple CubeSat, taking into account all these aspects, the best attitude option would be advancing vertically, because the total power gathered during its lifetime is higher than when the satellite advances horizontally.

Finally, it is applied the SEET tool in QB50. However, before being applied to the double CubeSat, it has been demonstrated that this tool is valid to predict the radiation, applying it in OUFTI-1 CubeSat and comparing its results with the radiation values provided by SPENVIS. The total radiation dose predicted has been 342.5499 rad. Thus it is a low value of radiation dose; the electronic components of the double CubeSat would not have problems in this aspect. Nevertheless, in future developments it has to be done a precise analysis, in order to know more accurately the dose radiation received.

SEET tool also allows the prediction of the vehicle temperature and the particle impacts that will receive the nanosatellite during its lifetime. Concretely, the maximum temperature achieved for QB50 is 320.047 K. Concerning the particle impacts, the maximum peak of the impact rate is reached on 28th of July, with a value of $2.9583 \cdot 10^{-10}$ s^{-1}, because of the variation of the South delta Aquariids meteor shower activity. However, it does not seem to be an issue of concern.

In order to summarize these results, Table 10.1 includes all of them and allows taking an overview of this project.

		Type		Results
Lifetime		Double CubeSat		98 days
		Triple CubeSat		104 days
Access		Footprint	Length	2348 km
			Area	$4.317 \cdot 10^{6}$ km^2
		Ground Station access	Minimum duration	6.369 s
			Maximum duration	5.598 min
			Mean duration	4.057 min
			Total duration	19.540 h
			Average duration	11.964 min/day (3 accesses/day)
Sunlight periods		Sunlight periods		70.442%
		Penumbra periods		0.611%
		Umbra periods		28.947%
Power gathered		Double CubeSat	Advancing vertically (highest value)	7.244 W
			Advancing horizontally (highest value)	7.340 W
		Triple CubeSat	Advancing vertically (highest value)	9.809 W
			Advancing horizontally (highest value)	10.671 W
SEET	**Radiation environment**	Total radiation dose		342.5499 rad
	Vehicle temperature	Maximum		320.047 K
	Particle impacts	Maximum impact rate		$2.9583 \cdot 10^{-10}$ s^{-1}

Table 10.1: Summary of results

Appendix

A. GS Accesses

Access	Start Time (UTCG)	Stop Time (UTCG)	Duration (sec)
1	15 Jun 2014 09:16:50.433	15 Jun 2014 09:22:03.435	313.002
2	15 Jun 2014 10:50:31.582	15 Jun 2014 10:52:43.660	132.078
3	15 Jun 2014 22:40:53.332	15 Jun 2014 22:45:00.920	247.588
4	16 Jun 2014 00:13:08.190	16 Jun 2014 00:17:33.417	265.227
5	16 Jun 2014 09:39:51.487	16 Jun 2014 09:45:27.387	335.901
6	16 Jun 2014 23:03:09.075	16 Jun 2014 23:08:36.889	327.814
7	17 Jun 2014 08:31:07.068	17 Jun 2014 08:35:00.845	233.777
8	17 Jun 2014 10:03:12.641	17 Jun 2014 10:07:53.970	281.329
9	17 Jun 2014 23:26:06.638	17 Jun 2014 23:31:29.825	323.187
10	18 Jun 2014 08:53:23.197	18 Jun 2014 08:58:47.016	323.819
11	18 Jun 2014 22:16:59.464	18 Jun 2014 22:21:31.903	272.439
12	18 Jun 2014 23:49:44.126	18 Jun 2014 23:53:41.419	237.293
13	19 Jun 2014 09:16:01.546	19 Jun 2014 09:21:33.055	331.508
14	19 Jun 2014 22:38:59.277	19 Jun 2014 22:44:30.836	331.558
15	20 Jun 2014 08:06:38.898	20 Jun 2014 08:10:57.922	259.024
16	20 Jun 2014 09:39:01.621	20 Jun 2014 09:43:20.881	259.260
17	20 Jun 2014 21:31:26.830	20 Jun 2014 21:32:49.576	82.746
18	20 Jun 2014 23:01:36.707	20 Jun 2014 23:06:50.456	313.749
19	21 Jun 2014 08:28:34.438	21 Jun 2014 08:34:04.384	329.946
20	21 Jun 2014 21:51:47.738	21 Jun 2014 21:56:35.766	288.027
21	21 Jun 2014 23:24:56.517	21 Jun 2014 23:28:25.935	209.418
22	22 Jun 2014 07:20:45.644	22 Jun 2014 07:20:52.013	6.369
23	22 Jun 2014 08:50:48.930	22 Jun 2014 08:56:14.750	325.820
24	22 Jun 2014 22:13:28.029	22 Jun 2014 22:19:00.564	332.535
25	23 Jun 2014 07:40:51.323	23 Jun 2014 07:45:26.481	275.158
26	23 Jun 2014 09:13:27.261	23 Jun 2014 09:17:25.359	238.098
27	23 Jun 2014 21:04:58.075	23 Jun 2014 21:07:19.325	141.250
28	23 Jun 2014 22:35:43.368	23 Jun 2014 22:40:48.050	304.682
29	24 Jun 2014 08:02:23.656	24 Jun 2014 08:07:56.709	333.053
30	24 Jun 2014 21:25:16.431	24 Jun 2014 21:30:13.970	297.539
31	24 Jun 2014 22:58:44.044	24 Jun 2014 23:01:47.984	183.940
32	25 Jun 2014 06:53:22.757	25 Jun 2014 06:55:07.275	104.518
33	25 Jun 2014 08:24:13.092	25 Jun 2014 08:29:33.294	320.202
34	25 Jun 2014 21:46:34.364	25 Jun 2014 21:52:06.490	332.126
35	26 Jun 2014 07:13:42.915	26 Jun 2014 07:18:27.911	284.996
36	26 Jun 2014 08:46:28.382	26 Jun 2014 08:50:08.511	220.129
37	26 Jun 2014 20:37:22.328	26 Jun 2014 20:40:10.849	168.521
38	26 Jun 2014 22:08:25.533	26 Jun 2014 22:13:22.836	297.304
39	27 Jun 2014 07:34:50.068	27 Jun 2014 07:40:24.380	334.313
40	27 Jun 2014 20:57:24.075	27 Jun 2014 21:02:26.879	302.804
41	27 Jun 2014 22:31:04.614	27 Jun 2014 22:33:48.496	163.882
42	28 Jun 2014 06:25:10.307	28 Jun 2014 06:27:22.834	132.527
43	28 Jun 2014 07:56:13.106	28 Jun 2014 08:01:28.881	315.774
44	28 Jun 2014 21:18:17.123	28 Jun 2014 21:23:48.405	331.282
45	29 Jun 2014 06:45:12.426	29 Jun 2014 06:50:02.486	290.060
46	29 Jun 2014 08:18:03.261	29 Jun 2014 08:21:31.053	207.792
47	29 Jun 2014 20:08:30.567	29 Jun 2014 20:11:31.648	181.081
48	29 Jun 2014 21:39:41.916	29 Jun 2014 21:44:34.543	292.627
49	30 Jun 2014 07:05:52.682	30 Jun 2014 07:11:27.153	334.470
50	30 Jun 2014 20:28:09.292	30 Jun 2014 20:33:14.142	304.850
51	30 Jun 2014 22:01:55.623	30 Jun 2014 22:04:28.304	152.680

52	1 Jul 2014 05:55:41.629	1 Jul 2014 05:58:03.889	142.261
53	1 Jul 2014 07:26:47.845	1 Jul 2014 07:32:01.159	313.314
54	1 Jul 2014 20:48:35.065	1 Jul 2014 20:54:05.656	330.591
55	2 Jul 2014 06:15:18.631	2 Jul 2014 06:20:09.725	291.094
56	2 Jul 2014 07:48:10.010	2 Jul 2014 07:51:33.166	203.156
57	2 Jul 2014 19:38:19.825	2 Jul 2014 19:41:22.653	182.828
58	2 Jul 2014 21:09:31.167	2 Jul 2014 21:14:22.430	291.263
59	3 Jul 2014 06:35:30.335	3 Jul 2014 06:41:04.244	333.909
60	3 Jul 2014 19:57:30.770	3 Jul 2014 20:02:34.848	304.077
61	3 Jul 2014 21:31:14.626	3 Jul 2014 21:33:47.582	152.957
62	4 Jul 2014 05:24:53.501	4 Jul 2014 05:27:11.474	137.973
63	4 Jul 2014 06:55:56.016	4 Jul 2014 07:01:09.224	313.208
64	4 Jul 2014 20:17:26.889	4 Jul 2014 20:22:57.132	330.243
65	5 Jul 2014 05:44:00.244	5 Jul 2014 05:48:48.477	288.233
66	5 Jul 2014 07:16:46.965	5 Jul 2014 07:20:14.088	207.123
67	5 Jul 2014 19:06:48.647	5 Jul 2014 19:09:42.723	174.076
68	5 Jul 2014 20:37:51.893	5 Jul 2014 20:42:45.256	293.363
69	6 Jul 2014 06:03:41.661	6 Jul 2014 06:09:14.310	332.649
70	6 Jul 2014 19:25:27.164	6 Jul 2014 19:30:27.502	300.338
71	6 Jul 2014 20:59:00.160	6 Jul 2014 21:01:44.897	164.737
72	7 Jul 2014 04:52:45.407	7 Jul 2014 04:54:43.070	117.663
73	7 Jul 2014 06:23:36.162	7 Jul 2014 06:28:51.526	315.364
74	7 Jul 2014 19:44:51.137	7 Jul 2014 19:50:21.165	330.028
75	8 Jul 2014 05:11:15.805	8 Jul 2014 05:15:56.849	281.044
76	8 Jul 2014 06:43:52.838	8 Jul 2014 06:47:31.783	218.945
77	8 Jul 2014 18:33:56.820	8 Jul 2014 18:36:28.758	151.938
78	8 Jul 2014 20:04:42.580	8 Jul 2014 20:09:41.164	298.584
79	9 Jul 2014 05:30:25.038	9 Jul 2014 05:35:55.317	330.279
80	9 Jul 2014 18:51:57.074	9 Jul 2014 18:56:49.942	292.868
81	9 Jul 2014 20:25:11.750	9 Jul 2014 20:28:17.122	185.371
82	10 Jul 2014 04:19:23.116	10 Jul 2014 04:20:28.917	65.801
83	10 Jul 2014 05:49:46.594	10 Jul 2014 05:55:05.818	319.224
84	10 Jul 2014 19:10:46.225	10 Jul 2014 19:16:15.557	329.332
85	11 Jul 2014 04:37:03.764	11 Jul 2014 04:41:32.116	268.352
86	11 Jul 2014 06:09:26.531	11 Jul 2014 06:13:23.115	236.583
87	11 Jul 2014 17:59:47.799	11 Jul 2014 18:01:33.309	105.509
88	11 Jul 2014 19:30:01.646	11 Jul 2014 19:35:07.700	306.054
89	12 Jul 2014 04:55:38.614	12 Jul 2014 05:01:04.574	325.960
90	12 Jul 2014 18:16:59.150	12 Jul 2014 18:21:39.306	280.156
91	12 Jul 2014 19:49:49.072	12 Jul 2014 19:53:20.312	211.240
92	13 Jul 2014 05:14:25.418	13 Jul 2014 05:19:49.179	323.761
93	13 Jul 2014 18:35:10.465	13 Jul 2014 18:40:37.509	327.044
94	14 Jul 2014 04:01:22.695	14 Jul 2014 04:05:30.563	247.868
95	14 Jul 2014 05:33:26.761	14 Jul 2014 05:37:44.263	257.502
96	14 Jul 2014 18:53:47.390	14 Jul 2014 18:59:01.842	314.452
97	15 Jul 2014 04:19:20.369	15 Jul 2014 04:24:38.684	318.316
98	15 Jul 2014 17:40:32.315	15 Jul 2014 17:44:51.782	259.467
99	15 Jul 2014 19:12:51.233	15 Jul 2014 19:16:50.417	239.184
100	16 Jul 2014 04:37:30.498	16 Jul 2014 04:42:58.024	327.526
101	16 Jul 2014 17:58:02.109	16 Jul 2014 18:03:23.596	321.487
102	17 Jul 2014 03:24:11.748	17 Jul 2014 03:27:46.835	215.087
103	17 Jul 2014 04:55:51.770	17 Jul 2014 05:00:30.872	279.102
104	17 Jul 2014 18:15:57.879	17 Jul 2014 18:21:19.949	322.071
105	18 Jul 2014 03:41:28.030	18 Jul 2014 03:46:33.241	305.212
106	18 Jul 2014 05:14:55.162	18 Jul 2014 05:16:46.062	110.899
107	18 Jul 2014 17:02:36.283	18 Jul 2014 17:06:21.706	225.423
108	18 Jul 2014 18:34:16.478	18 Jul 2014 18:38:43.171	266.693
109	19 Jul 2014 03:58:59.216	19 Jul 2014 04:04:27.809	328.592
110	19 Jul 2014 17:19:19.190	19 Jul 2014 17:24:29.307	310.117
111	19 Jul 2014 18:53:28.578	19 Jul 2014 18:55:02.707	94.129

112	20 Jul 2014 02:45:32.591	20 Jul 2014 02:48:11.400	158.809
113	20 Jul 2014 04:16:38.927	20 Jul 2014 04:21:37.798	298.871
114	20 Jul 2014 17:36:30.657	20 Jul 2014 17:41:57.398	326.740
115	21 Jul 2014 03:01:58.999	21 Jul 2014 03:06:42.331	283.332
116	21 Jul 2014 04:34:40.003	21 Jul 2014 04:37:50.522	190.519
117	21 Jul 2014 16:23:14.114	21 Jul 2014 16:25:58.499	164.384
118	21 Jul 2014 17:54:02.127	21 Jul 2014 17:58:53.627	291.501
119	22 Jul 2014 03:18:48.278	22 Jul 2014 03:24:12.753	324.475
120	22 Jul 2014 16:38:59.714	22 Jul 2014 16:43:48.606	288.893
121	22 Jul 2014 18:12:03.704	22 Jul 2014 18:15:07.516	183.812
122	23 Jul 2014 03:35:44.666	23 Jul 2014 03:40:58.985	314.320
123	23 Jul 2014 16:55:22.849	23 Jul 2014 17:00:48.457	325.607
124	24 Jul 2014 02:20:51.084	24 Jul 2014 02:24:57.758	246.674
125	24 Jul 2014 03:52:52.490	24 Jul 2014 03:56:57.236	244.746
126	24 Jul 2014 17:12:04.798	24 Jul 2014 17:17:15.997	311.198
127	25 Jul 2014 02:36:53.932	25 Jul 2014 02:42:05.651	311.719
128	25 Jul 2014 15:57:02.628	25 Jul 2014 16:01:13.027	250.399
129	25 Jul 2014 17:29:06.969	25 Jul 2014 17:33:08.930	241.961
130	26 Jul 2014 02:53:04.675	26 Jul 2014 02:58:27.306	322.630
131	26 Jul 2014 16:12:31.460	26 Jul 2014 16:17:46.075	314.615
132	27 Jul 2014 01:38:05.374	27 Jul 2014 01:41:06.164	180.790
133	27 Jul 2014 03:09:21.334	27 Jul 2014 03:14:05.404	284.070
134	27 Jul 2014 16:28:20.611	27 Jul 2014 16:33:43.455	322.844
135	28 Jul 2014 01:53:12.427	28 Jul 2014 01:57:57.286	284.859
136	28 Jul 2014 03:26:00.522	28 Jul 2014 03:28:43.089	162.567
137	28 Jul 2014 15:13:32.120	28 Jul 2014 15:16:27.290	175.170
138	28 Jul 2014 16:44:25.004	28 Jul 2014 16:49:09.097	284.093
139	29 Jul 2014 02:08:34.056	29 Jul 2014 02:13:54.192	320.136
140	29 Jul 2014 15:27:54.071	29 Jul 2014 15:32:41.107	287.036
141	29 Jul 2014 17:00:55.277	29 Jul 2014 17:03:51.813	176.536
142	30 Jul 2014 02:23:59.073	30 Jul 2014 02:29:08.454	309.381
143	30 Jul 2014 15:42:45.521	30 Jul 2014 15:48:07.796	322.274
144	31 Jul 2014 01:07:41.644	31 Jul 2014 01:11:34.678	233.034
145	31 Jul 2014 02:39:31.223	31 Jul 2014 02:43:36.666	245.442
146	31 Jul 2014 15:57:50.657	31 Jul 2014 16:03:02.202	311.545
147	1 Aug 2014 01:22:07.705	1 Aug 2014 01:27:08.968	301.264
148	1 Aug 2014 14:41:31.370	1 Aug 2014 14:45:19.651	228.281
149	1 Aug 2014 16:13:09.484	1 Aug 2014 16:17:23.139	253.655
150	2 Aug 2014 01:36:38.722	2 Aug 2014 01:41:57.197	318.475
151	2 Aug 2014 14:55:16.135	2 Aug 2014 15:00:18.679	302.544
152	2 Aug 2014 16:29:10.238	2 Aug 2014 16:30:42.063	91.825
153	3 Aug 2014 00:20:33.214	3 Aug 2014 00:22:28.952	115.738
154	3 Aug 2014 01:51:10.887	3 Aug 2014 01:56:03.630	292.743
155	3 Aug 2014 15:09:18.071	3 Aug 2014 15:14:39.560	321.489
156	4 Aug 2014 00:33:41.963	4 Aug 2014 00:37:57.192	255.229
157	4 Aug 2014 02:05:52.187	4 Aug 2014 02:09:20.157	207.970
158	4 Aug 2014 13:53:57.920	4 Aug 2014 13:54:52.226	54.306
159	4 Aug 2014 15:23:29.465	4 Aug 2014 15:28:28.718	299.254
160	5 Aug 2014 00:47:13.629	5 Aug 2014 00:52:19.707	306.079
161	5 Aug 2014 14:05:52.242	5 Aug 2014 14:10:01.102	248.860
162	5 Aug 2014 15:37:53.153	5 Aug 2014 15:41:42.170	229.017
163	6 Aug 2014 01:00:45.578	6 Aug 2014 01:05:59.002	313.424
164	6 Aug 2014 14:18:42.868	6 Aug 2014 14:23:49.668	306.800
165	6 Aug 2014 23:43:24.456	6 Aug 2014 23:45:50.898	146.443
166	7 Aug 2014 01:14:16.570	7 Aug 2014 01:18:56.672	280.102
167	7 Aug 2014 14:31:44.359	7 Aug 2014 14:37:02.551	318.192
168	7 Aug 2014 23:55:39.156	7 Aug 2014 23:59:59.360	260.203
169	8 Aug 2014 01:27:56.889	8 Aug 2014 01:31:01.999	185.110
170	8 Aug 2014 13:15:00.108	8 Aug 2014 13:16:31.824	91.716
171	8 Aug 2014 14:44:51.535	8 Aug 2014 14:49:43.448	291.913

172	9 Aug 2014 00:08:06.158	9 Aug 2014 00:13:10.458	304.300
173	9 Aug 2014 13:26:05.224	9 Aug 2014 13:30:15.253	250.029
174	9 Aug 2014 14:58:07.966	9 Aug 2014 15:01:47.590	219.624
175	10 Aug 2014 00:20:30.102	10 Aug 2014 00:25:39.364	309.262
176	10 Aug 2014 13:37:48.533	10 Aug 2014 13:42:52.341	303.808
177	10 Aug 2014 23:02:06.367	10 Aug 2014 23:04:21.483	135.116
178	11 Aug 2014 00:32:50.150	11 Aug 2014 00:37:27.118	276.967
179	11 Aug 2014 13:49:38.430	11 Aug 2014 13:54:53.727	315.296
180	11 Aug 2014 23:13:07.640	11 Aug 2014 23:17:18.287	250.647
181	12 Aug 2014 00:45:15.001	12 Aug 2014 00:48:24.450	189.449
182	12 Aug 2014 14:01:30.006	12 Aug 2014 14:06:22.679	292.673
183	12 Aug 2014 23:24:19.613	12 Aug 2014 23:29:16.611	296.998
184	13 Aug 2014 12:41:44.471	13 Aug 2014 12:45:36.360	231.889
185	13 Aug 2014 14:13:25.297	13 Aug 2014 14:17:15.692	230.394
186	13 Aug 2014 23:35:25.737	13 Aug 2014 23:40:32.543	306.806
187	14 Aug 2014 12:52:06.829	14 Aug 2014 12:56:59.512	292.683
188	14 Aug 2014 14:25:56.998	14 Aug 2014 14:26:59.313	62.315
189	14 Aug 2014 22:16:26.771	14 Aug 2014 22:17:17.868	51.098
190	14 Aug 2014 23:46:24.079	14 Aug 2014 23:51:08.045	283.966
191	15 Aug 2014 13:02:33.048	15 Aug 2014 13:07:44.786	311.738
192	15 Aug 2014 22:25:41.450	15 Aug 2014 22:29:22.569	221.119
193	15 Aug 2014 23:57:19.129	16 Aug 2014 00:00:58.101	218.972
194	16 Aug 2014 13:12:56.815	16 Aug 2014 13:17:56.769	299.954
195	16 Aug 2014 22:35:26.120	16 Aug 2014 22:40:06.220	280.099
196	17 Aug 2014 11:52:27.756	17 Aug 2014 11:55:27.547	179.791
197	17 Aug 2014 13:23:17.560	17 Aug 2014 13:27:34.176	256.616
198	17 Aug 2014 22:45:03.427	17 Aug 2014 22:50:05.275	301.847
199	18 Aug 2014 12:01:11.087	18 Aug 2014 12:05:36.472	265.385
200	18 Aug 2014 13:33:43.699	18 Aug 2014 13:36:27.312	163.613
201	18 Aug 2014 22:54:28.859	18 Aug 2014 22:59:23.921	295.062
202	19 Aug 2014 12:09:59.714	19 Aug 2014 12:15:00.300	300.587
203	19 Aug 2014 21:32:59.524	19 Aug 2014 21:35:24.470	144.946
204	19 Aug 2014 23:03:43.003	19 Aug 2014 23:08:01.142	258.138
205	20 Aug 2014 12:18:42.559	20 Aug 2014 12:23:48.481	305.922
206	20 Aug 2014 21:40:56.516	20 Aug 2014 21:44:56.465	239.950
207	20 Aug 2014 23:12:53.674	20 Aug 2014 23:15:47.899	174.225
208	21 Aug 2014 12:27:16.287	21 Aug 2014 12:32:02.140	285.852
209	21 Aug 2014 21:48:51.385	21 Aug 2014 21:53:34.124	282.739
210	22 Aug 2014 11:04:39.156	22 Aug 2014 11:07:54.017	194.861
211	22 Aug 2014 12:35:41.273	22 Aug 2014 12:39:38.797	237.525
212	22 Aug 2014 21:56:31.620	22 Aug 2014 22:01:28.827	297.207
213	23 Aug 2014 11:11:30.035	23 Aug 2014 11:15:53.923	263.889
214	23 Aug 2014 12:44:07.434	23 Aug 2014 12:46:26.921	139.487
215	23 Aug 2014 22:03:54.322	23 Aug 2014 22:08:42.755	288.432
216	24 Aug 2014 11:18:15.932	24 Aug 2014 11:23:10.210	294.278
217	24 Aug 2014 20:40:32.785	24 Aug 2014 20:42:36.159	123.374
218	24 Aug 2014 22:10:59.657	24 Aug 2014 22:15:14.793	255.136
219	25 Aug 2014 11:24:48.591	25 Aug 2014 11:29:49.011	300.420
220	25 Aug 2014 20:46:16.669	25 Aug 2014 20:49:57.509	220.840
221	25 Aug 2014 22:17:52.264	25 Aug 2014 22:20:58.621	186.357
222	26 Aug 2014 11:31:04.606	26 Aug 2014 11:35:51.001	286.394
223	26 Aug 2014 20:51:54.427	26 Aug 2014 20:56:21.012	266.585
224	27 Aug 2014 10:06:51.594	27 Aug 2014 10:09:06.798	135.205
225	27 Aug 2014 11:37:02.790	27 Aug 2014 11:41:14.583	251.793
226	27 Aug 2014 20:57:11.767	27 Aug 2014 21:01:59.064	287.297
227	28 Aug 2014 10:11:08.176	28 Aug 2014 10:14:54.172	225.996
228	28 Aug 2014 11:42:45.449	28 Aug 2014 11:45:54.941	189.493
229	28 Aug 2014 21:02:04.646	28 Aug 2014 21:06:54.136	289.489
230	29 Aug 2014 10:15:18.478	29 Aug 2014 10:19:47.371	268.894
231	29 Aug 2014 11:48:45.088	29 Aug 2014 11:49:17.200	32.112

232	29 Aug 2014 21:06:31.369	29 Aug 2014 21:11:06.320	274.951
233	30 Aug 2014 10:19:08.854	30 Aug 2014 10:23:57.380	288.526
234	30 Aug 2014 19:40:12.279	30 Aug 2014 19:42:13.828	121.550
235	30 Aug 2014 21:10:31.563	30 Aug 2014 21:14:33.886	242.323
236	31 Aug 2014 10:22:34.210	31 Aug 2014 10:27:26.026	291.815
237	31 Aug 2014 19:42:50.384	31 Aug 2014 19:46:14.466	204.083
238	31 Aug 2014 21:14:07.330	31 Aug 2014 21:17:11.960	184.630
239	1 Sep 2014 10:25:31.208	1 Sep 2014 10:30:12.832	281.624
240	1 Sep 2014 19:45:09.566	1 Sep 2014 19:49:15.974	246.408
241	1 Sep 2014 21:17:41.846	1 Sep 2014 21:18:34.140	52.294
242	2 Sep 2014 10:27:57.364	2 Sep 2014 10:32:16.179	258.816
243	2 Sep 2014 19:46:57.677	2 Sep 2014 19:51:27.157	269.479
244	3 Sep 2014 08:59:25.862	3 Sep 2014 09:02:03.604	157.742
245	3 Sep 2014 10:29:51.100	3 Sep 2014 10:33:33.464	222.364
246	3 Sep 2014 19:48:09.927	3 Sep 2014 19:52:49.442	279.515
247	4 Sep 2014 08:59:45.355	4 Sep 2014 09:03:21.108	215.754
248	4 Sep 2014 10:31:12.839	4 Sep 2014 10:33:59.958	167.120
249	4 Sep 2014 19:48:43.062	4 Sep 2014 19:53:22.504	279.443
250	5 Sep 2014 08:59:34.657	5 Sep 2014 09:03:42.623	247.966
251	5 Sep 2014 10:32:16.745	5 Sep 2014 10:33:16.867	60.122
252	5 Sep 2014 19:48:34.258	5 Sep 2014 19:53:05.168	270.910
253	6 Sep 2014 08:58:45.375	6 Sep 2014 09:03:11.404	266.030
254	6 Sep 2014 19:47:40.666	6 Sep 2014 19:51:55.550	254.883
255	7 Sep 2014 08:57:12.183	7 Sep 2014 09:01:46.855	274.672
256	7 Sep 2014 18:16:21.335	7 Sep 2014 18:17:31.343	70.007
257	7 Sep 2014 19:45:59.217	7 Sep 2014 19:49:51.109	231.892
258	8 Sep 2014 08:54:50.299	8 Sep 2014 08:59:26.878	276.579
259	8 Sep 2014 18:13:06.247	8 Sep 2014 18:15:29.823	143.576
260	8 Sep 2014 19:43:26.555	8 Sep 2014 19:46:48.607	202.052
261	9 Sep 2014 08:51:34.837	9 Sep 2014 08:56:08.477	273.640
262	9 Sep 2014 18:09:10.845	9 Sep 2014 18:12:10.683	179.838
263	9 Sep 2014 19:39:59.146	9 Sep 2014 19:42:43.881	164.735
264	10 Sep 2014 08:47:20.503	10 Sep 2014 08:51:47.888	267.385
265	10 Sep 2014 18:04:19.259	10 Sep 2014 18:07:40.826	201.567
266	10 Sep 2014 19:35:33.887	10 Sep 2014 19:37:31.091	117.205
267	11 Sep 2014 08:42:01.375	11 Sep 2014 08:46:20.570	259.195
268	11 Sep 2014 17:58:23.384	11 Sep 2014 18:01:57.843	214.459
269	11 Sep 2014 19:30:15.062	11 Sep 2014 19:30:55.405	40.343
270	12 Sep 2014 08:35:30.673	12 Sep 2014 08:39:41.055	250.382
271	12 Sep 2014 17:51:15.645	12 Sep 2014 17:54:56.718	221.073
272	13 Sep 2014 08:27:40.421	13 Sep 2014 08:31:42.665	242.245
273	13 Sep 2014 17:42:47.731	13 Sep 2014 17:46:30.376	222.645
274	14 Sep 2014 08:18:21.090	14 Sep 2014 08:22:17.001	235.911
275	14 Sep 2014 17:32:49.820	14 Sep 2014 17:36:29.347	219.527
276	15 Sep 2014 08:07:20.958	15 Sep 2014 08:11:13.160	232.202
277	15 Sep 2014 17:21:09.804	15 Sep 2014 17:24:40.812	211.008
278	16 Sep 2014 07:54:25.123	16 Sep 2014 07:58:16.413	231.290
279	16 Sep 2014 17:07:32.131	16 Sep 2014 17:10:46.752	194.621
280	17 Sep 2014 07:39:13.680	17 Sep 2014 07:43:05.890	232.210
281	17 Sep 2014 16:51:36.267	17 Sep 2014 16:54:19.938	163.672
282	17 Sep 2014 18:22:32.709	17 Sep 2014 18:22:55.082	22.373
283	18 Sep 2014 07:21:17.845	18 Sep 2014 07:25:10.007	232.163
284	18 Sep 2014 16:32:58.438	18 Sep 2014 16:34:30.162	91.724
285	18 Sep 2014 18:02:23.136	18 Sep 2014 18:04:23.328	120.193
286	19 Sep 2014 06:59:50.653	19 Sep 2014 07:03:35.096	224.443
287	19 Sep 2014 17:38:26.033	19 Sep 2014 17:41:15.367	169.334
288	20 Sep 2014 06:33:16.177	20 Sep 2014 06:36:24.488	188.311
289	20 Sep 2014 17:07:33.149	20 Sep 2014 17:10:35.216	182.066

B. Tutorial

First of all, a scenario has to be defined, which will have to cover the desired time period for the satellite orbit of interest (15 June 2014 - 20 September 2014). After this, it has to be created the QB50 satellite, following the parameters of section 4; the orbit, following the explanation of section 3.3; and finally it has to be added the ground station of interest (Liège).

Once it has been done, it can start the tutorial about the different module models of SEET:

1. Magnetic field module

Configure the Magnetic Field Model

1. Display satellite properties. In the properties panel tree, under Basic, select "SEET Environment". The upper dialog box contains the Magnetic Field parameters. As the QB50 will be in a LEO and considering the time period, 98 days, it will be used the following selections: "Fast-IGRF" as Main Field, "Olson-Pfitzer "as External Field, and "1 day" as IGRF Update Rate.

- It has been chosen Fast-IRGF instead of IGRF due to the longer lifetime of QB50, and because of as it is explained in section 9.1, the results of Fast-IGRF are within 1% of the full-IGRF option, and it is significantly faster than IGRF. The Centered-dipole option is not chosen either due to Fast-IGRF is a better magnetic field approximation.

- Olson-Pfitzer is chosen instead of none external field in order to take into account the solar wind.

- The IGRF Update Rate is about 1 day due to it provides more accurate results.

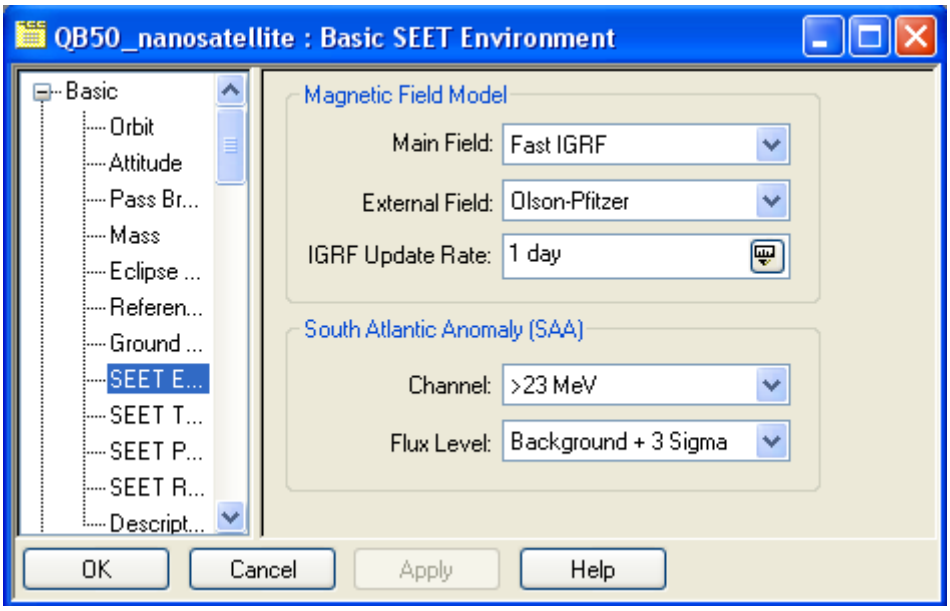

Figure 10.1: SEET Environment panel

Configure the Display 3D Vector

2. Within the satellite properties under 3D Graphics, select “Vector”. In the vector list, select the “Nadir (Centric) Vector”, and deselect the “Show Label” option.

3. In the same vector list, select the “Velocity Vector” and deselect the “Show Label” option.

4. Click the “Add” button to bring up the “Add Vector Geometry Components” dialog. Under the satellite object, select the “SEET Geomagnetic Field” vector and add it to the selected Name list.

5. Back in the 3D Graphics Vector panel, select the “SEET Geomagnetic Field”. Change the colour and deselect “Show Label” option. Select “Show Magnitude”.

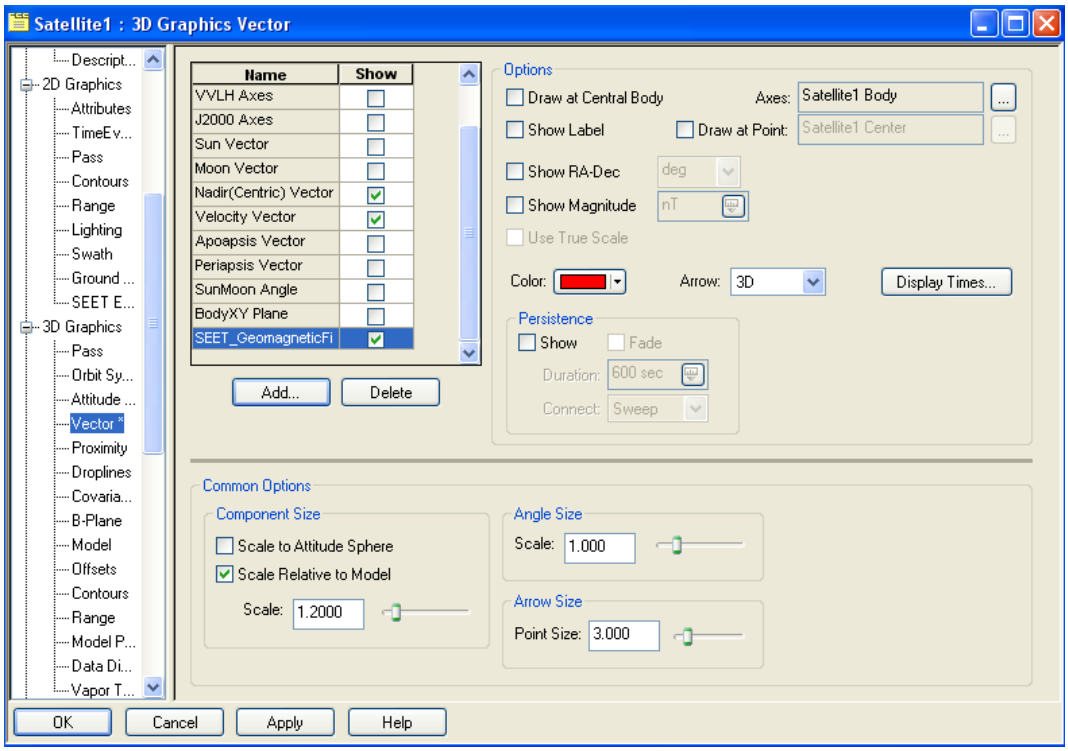

Figure 10.2: 3D Graphics Vector panel

6. To view the vectors selected in the previous step, display the 3D viewing window. On this toolbar, click on the “From/To Position” button and select the “Satellite” for both the menu boxes.

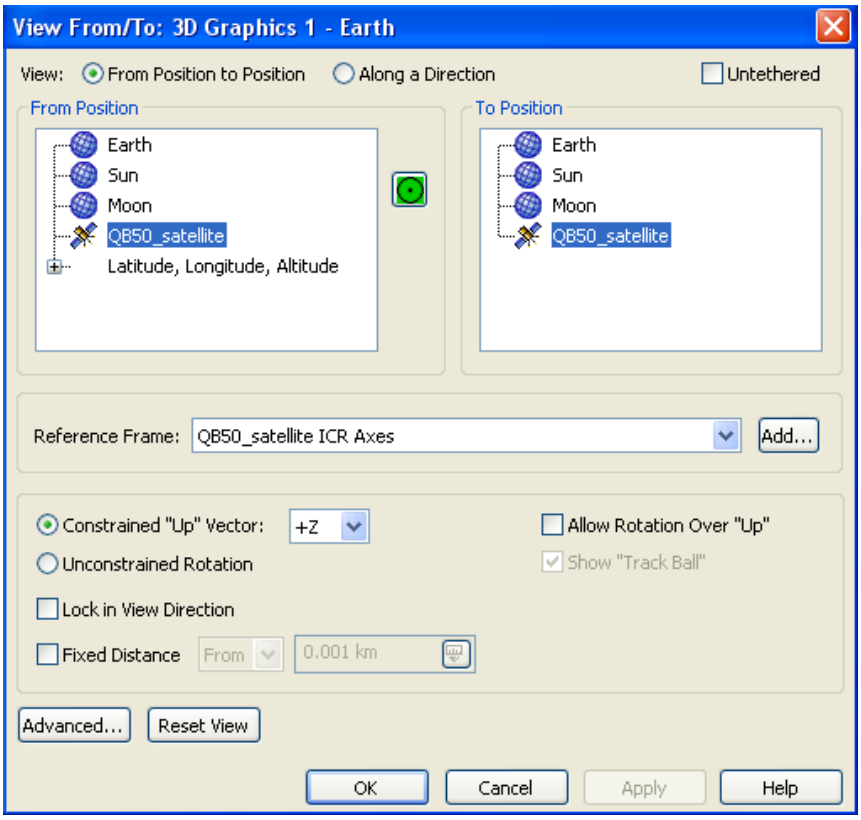

Figure 10.3: 3D viewing window

7. To observe the behaviour of the geomagnetic field vector over time, it has to be used the Animation toolbar.

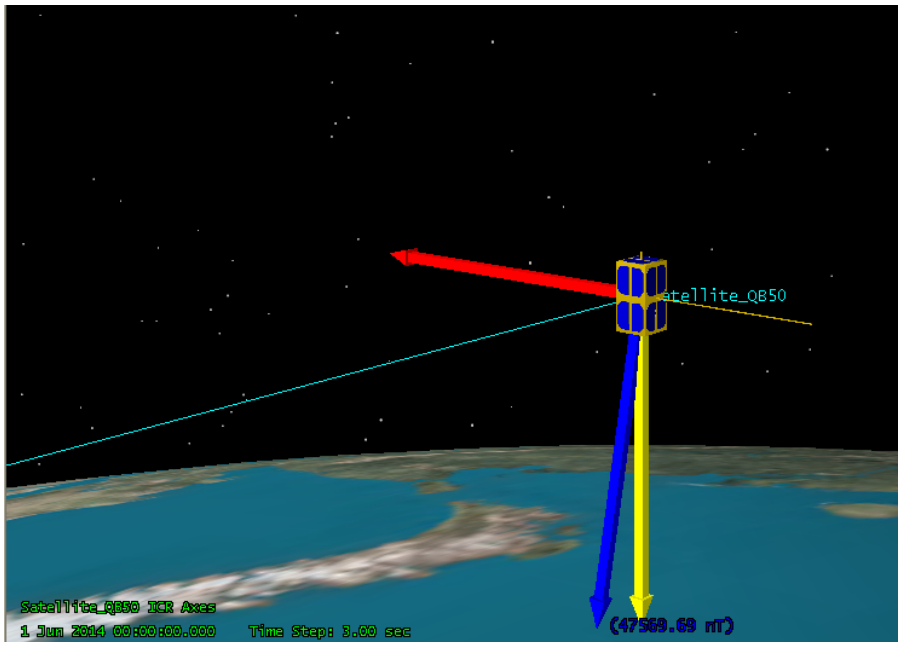

Figure 10.4: Behaviour of the geomagnetic field vector

8. Select “Report & Graph Manager” on the principal menu.

9. In the Report and Graph Manager dialog box, select “My Styles”. Select “New” and then “Report”. Enter a name for the report.

10. In the Report Style dialog box, scroll through the Data Providers list to the “SEET Magnetic Field” data provider. Select “Time”, “B Field-ECF x”, “B Field-ECF y” and “B Field-ECF z” and add them to the Report Contents list. Generate the report.

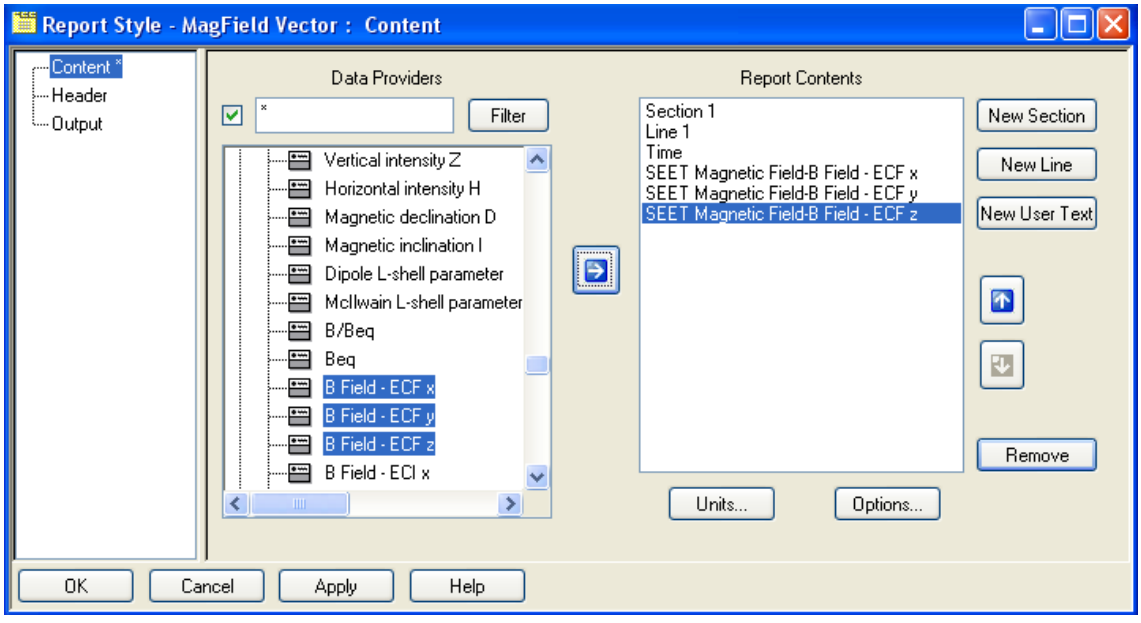

Figure 10.5: SEET Magnetic Field Report Contents

2. The radiation environment module

1. Select the “Scenario Properties”. Under “Basic”, select “Units” then scroll down to “Radiation Shield Thickness” and select “mm”. Returning to “Basic”, select “SEET Radiation”. In the NASA Electron and Proton Activity pane, change the dialog to “Solar Max”.

2. Define the Magnetic Field model following the point 1 of this tutorial.

Configure the Radiation Environment for a long time base dose depth analysis

3. Next step is to configure the Radiation Environment for a long time base line dose depth analysis and generate a graph. For doing this, on the satellite’s Properties page, under “Basic”, select “SEET Radiation”. In the Model panel, confirm that Computational Mode is “CREES”, the Detector Type is “Silicon” and Detector Geometry is “Spherical”. Mark the boxes “Use Nuclear Attenuation” and “Include Neutrons in Nuclear Attenuation”. In the Shielding Thicknesses, remove all the values and add “0.0127 mm, 1 mm, 2 mm, ..., 10 mm”.

- The Computational Mode selected is CREES, due to it is the best model as it is explained in section 9.2.1.

- The Detector Type chosen is Silicon because, as it is mentioned in section 8.2, the solar panels are a silicon p-n multi-junction.

- The Detector Geometry selected is spherical due to it is a better approximation of the double CubeSat.

- The Nuclear Attenuation, including neutrons, is chosen in order to take into account all the possible factors in the simulation of the QB50 mission.

- The Shielding Thicknesses starts with 0.0127 mm because is the lower value that STK recognize.

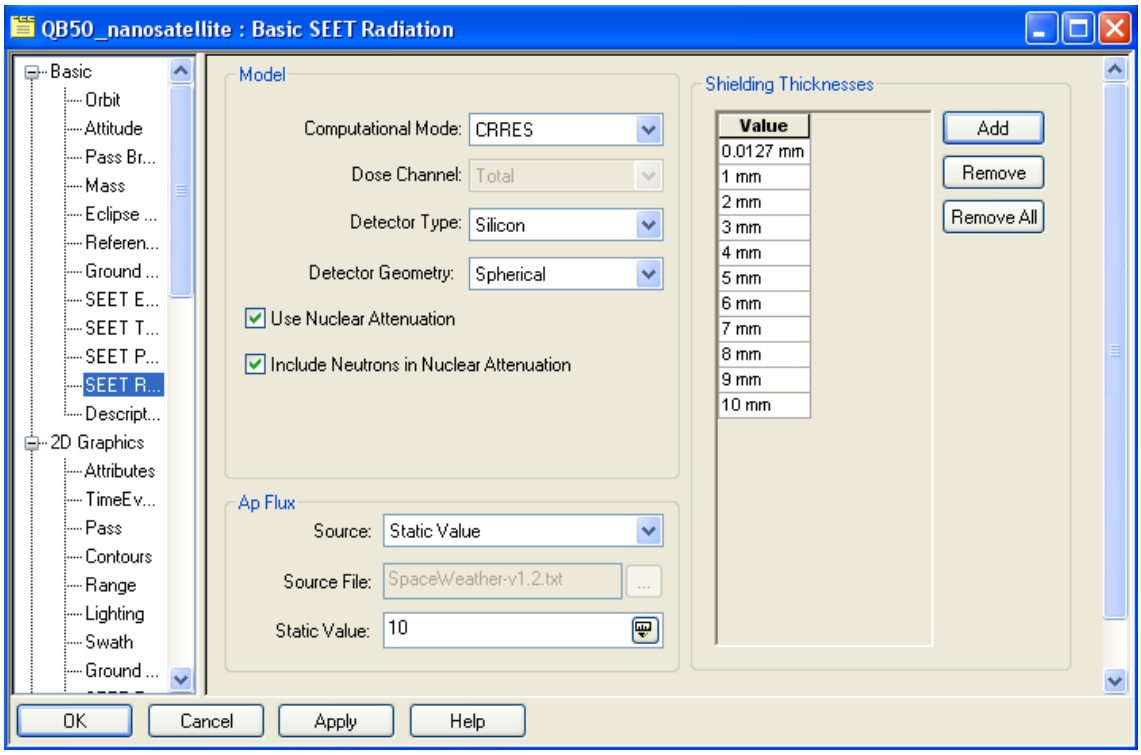

Figure 10.6: SEET Radiation panel

4. To compute and view the dose depth graph for this computational mode, bring up the Report and Graph Manager from the main menu.

5. Select in the Object Type the “Satellite”. In My Styles pane, select “New” and then “Graph”. Enter a name for the graph.

6. In the Graph Style dialog box, scroll down to the “SEET Radiation Dose Depth”. For the X-axis select “Shielding Thickness” and for the Y-axis select “Electron dose”, “Electron-Bremsstrahlung dose”, “Proton dose” and “Combined dose”.

7. Before generate the graph, in the Time Properties select “Specify properties”, select “Use step size” and introduce it for example 3600 sec, because it does not work with small step size, as 60 sec. The graph should look like as Figure 9.9.

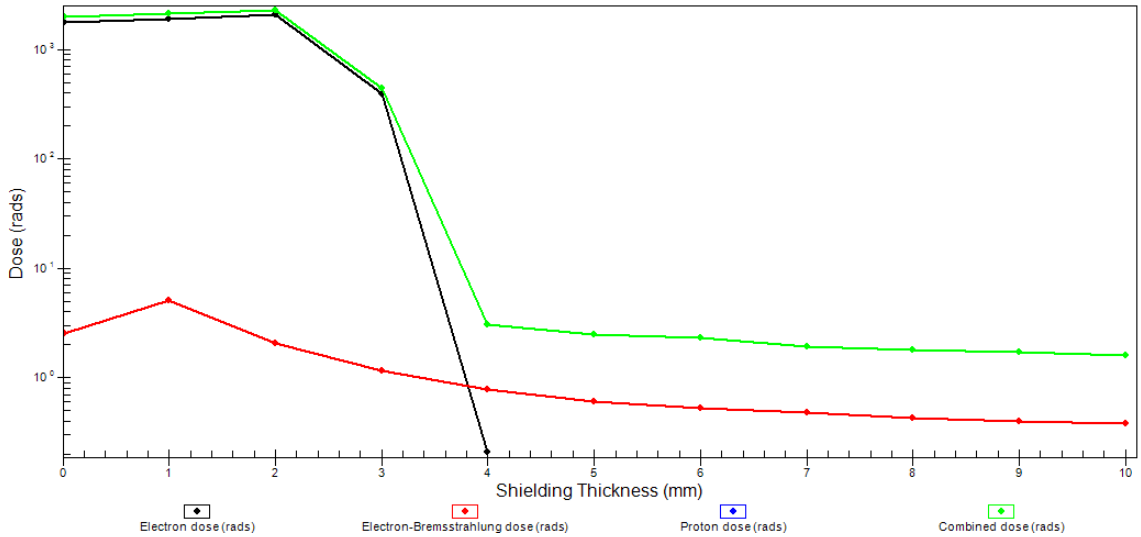

Figure 10.7: Radiation dose received for QB50

8. To obtain only the total radiation dose graph, it has to be followed the same steps than before, but just select "Combined dose". The graph should look like as Figure 9.10.

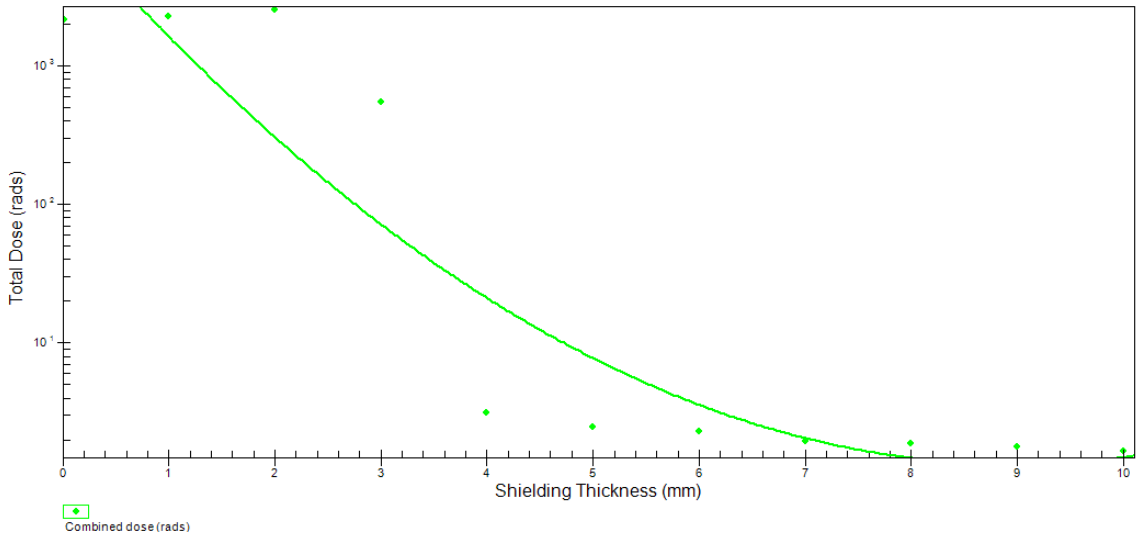

Figure 10.8: Regression curve of total radiation dose received for QB50

3. The vehicle temperature module

1. Select the "Satellite Properties". In the properties panel tree, under Basic, select "SEET Thermal". Those properties related to the calculation of satellite temperature will be displayed in the Thermal Model panel.

2. Use the default value for albedo. Set the Material Emissivity to "0.86" and the Material Absorptivity to "0.91". The Dissipation chosen is "0 W", the default value. Set the Cross-Sectional Area to "0.016667 m^2". And change the Shape Model property to "Sphere".

- The default value of albedo is used in this tutorial, because it is near the centre of the usual range of this value.

- The values of Material Emissivity and Absorptivity are the solar cells ones, defined in section 8.2.

- The Dissipation value represents the heat generated by the operation of internal components of a space vehicle. As this thesis is a first approximation of the QB50 mission and the heat dissipated for the internal components it is still unknown, the Dissipation value chosen is 0 W.

- The Cross-Sectional Area is 0.016667 m^2 following the QB50 parameters defined in section 4.3.

- A sphere is chosen as the Shape Model instead of a plate, due to it is the best approximation of the double CubeSat.

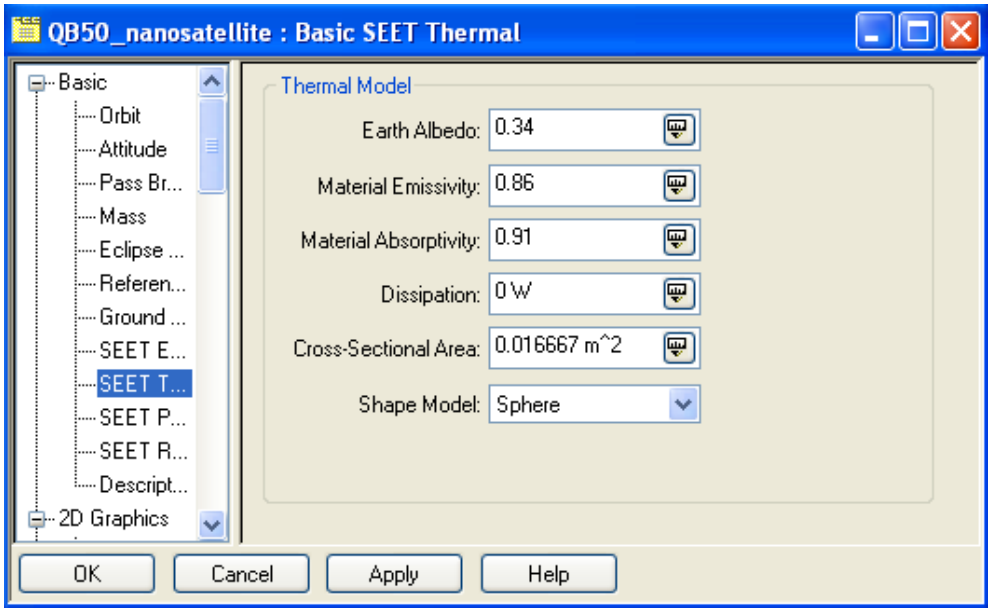

Figure 10.9: SEET Thermal panel

3. In the Report and Graph Manager dialog box, select “My Styles folder”. Select “New” and then “Graph”. Enter a name for the graph.

4. In the Graph Style dialog box, scroll through the Data Providers list to the “SEET Vehicle Temperature” set and expand the set by clicking the plus symbol. Choose “Temperature” from the expanded list into the Y-axis pane. Generate the graph. It should look like as Figure 9.11:

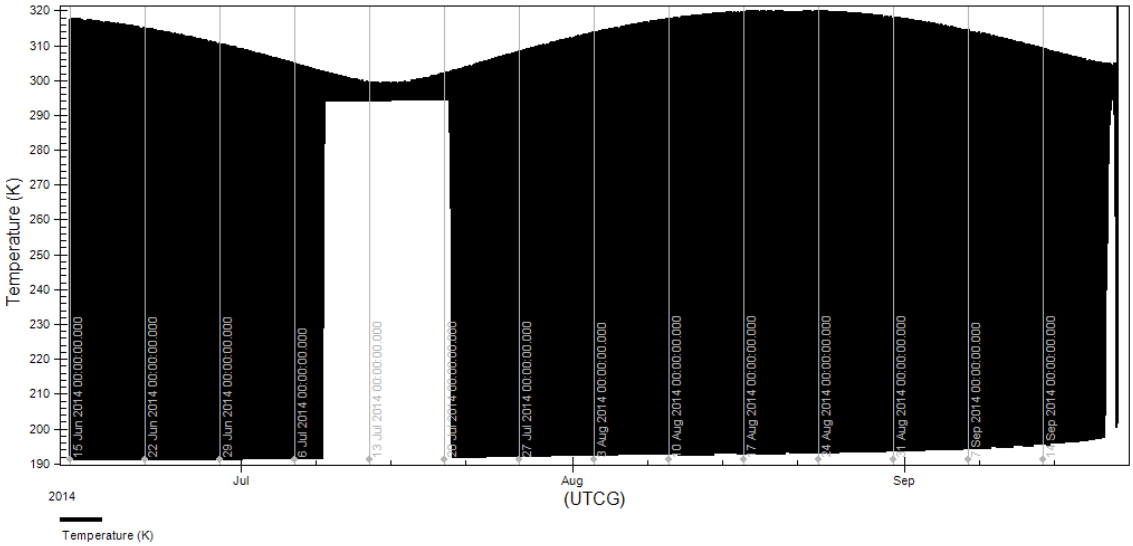

Figure 10.10: Temperature achieved for QB50 during its lifetime

10. To obtain a report, follow the same steps that for the graph, choosing "New report" instead of graph, and inside Data Providers list to the "SEET Vehicle Temperature Model" and choose "Definition".

4. The particle impacts module

1. Select "Satellite Properties". In the properties panel tree, under Basic, select "SEET Particle Flux". Those properties related to the calculation of impact information will be displayed in the Basic SEET Particle Flux panel. Then fill in the following values: For $F_{10.7}$ Source, use the "Flux File". Leave the $F_{10.7}$ Source File default. The Cross-Sectional Area is "0.016667 m^2". The Pit Depth is "1.5 mm". Select "User Defined" as the Material option, and the Density and Tensile Strength are respectively "5.7333 g/cm^3" and "0.6 MPa". Mark "Use Sporadic Meteors".

- Choosing the $F_{10.7}$ Source and the $F_{10.7}$ Source File default is the best approximation of the solar activity, due to STK uses its database to forecast it.

- The Cross-Sectional Area is 0.016667 m^2 following the QB50 parameters defined in section 4.3.

- The Pit Depth is 1.5 mm, the thickness of the solar panels without the aluminium structure of the nanosatellite. It has been considered just the solar panels, due to it is the surface material above the aluminium structure and it is weaker than aluminium.

- The material of the solar panels is not defined for STK software, hence it has to be determined its properties. The Density is 5.7333 g/cm^3[28], and the Tensile Strength is 0.6 MPa [44].

- It has been selected the option of Sporadic Meteors in order to take into account all the possible factors in the simulation of the QB50 mission.

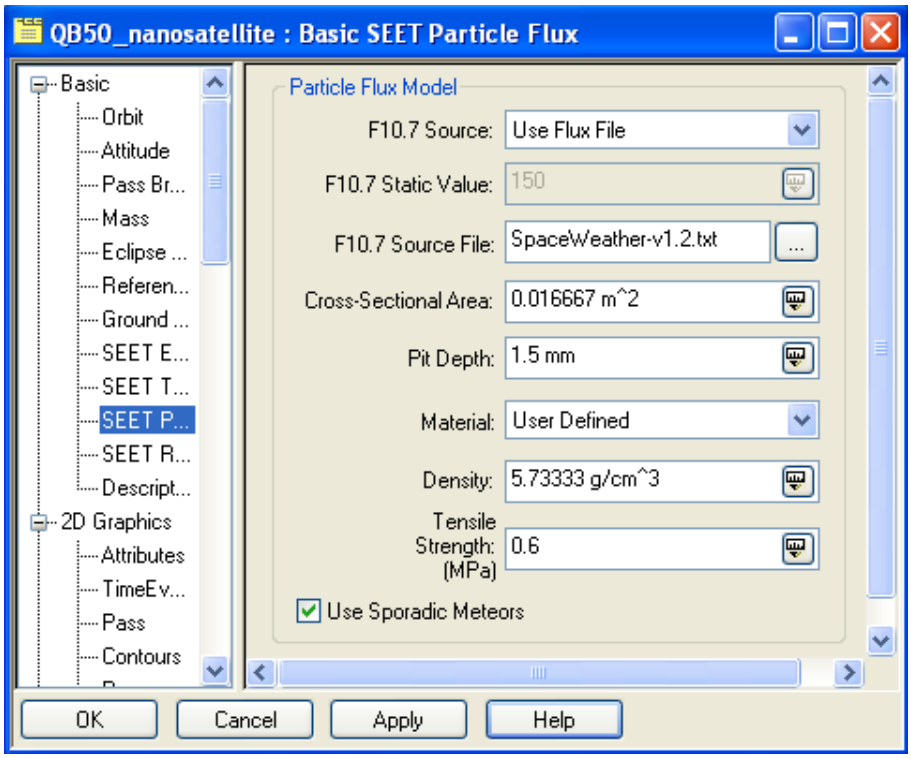

Figure 10.11: SEET Particle Flux panel

2. In the Report and Graph Manager dialog box, select “My Styles”. Select “New” and then “Graph”. Enter a name for the graph.

3. In the Graph Style dialog box, scroll through the Data Providers list to the “SEET Meteor Flux” data provider and expend the “Damaging Impacts” folder. Choose ‘Impact rate’ in the Y-Axis pane. Generate the graph. The graph should look like as Figure 9.14:

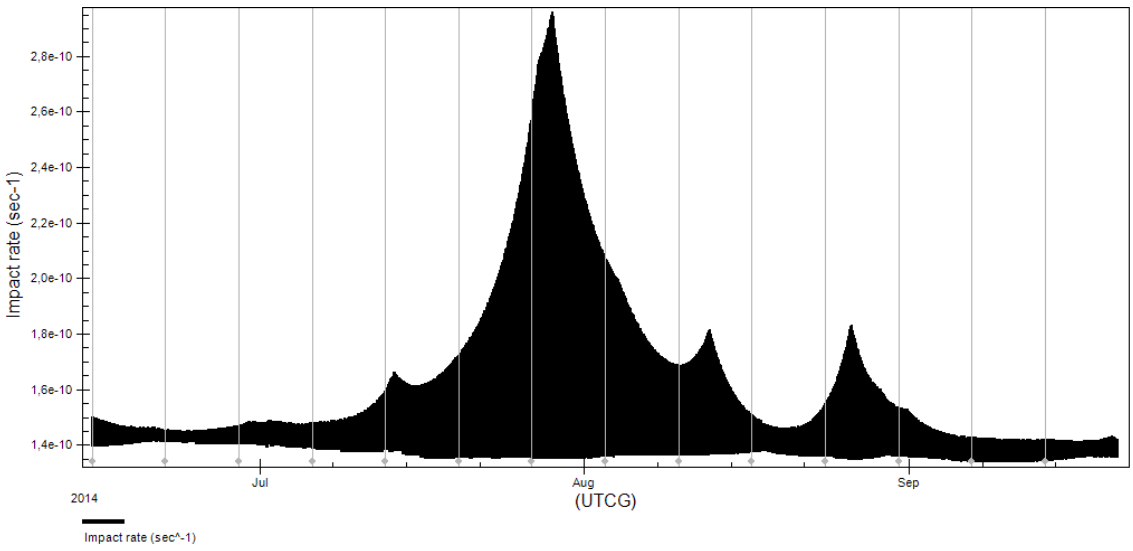

Figure 10.12: Particle impacts rate of QB50

References

[1] http://www.vki.ac.be/QB50/

[2] http://www.genso.org/

[3] http://mtech.dk/thomsen/space/cubesat.php

[4] California Polytechnic State University (CalPoly), *Cubesat design specification,* 2004.

[5] http://www.globalsecurity.org/space/world/russia/shtil.htm

[6] T. Logsdons, *Orbital Mechanics: Theory and applications*, 1998

[7] D.A. Vallado and W.D. McClain, *Fundamentals of astrodynamics and applications*, 2001.

[8] J. Naviaux, *QB50, an international network of 50 CubeSats for multi-point, in-situ measurements in the lower thermosphere and re-entry research*, 2010.

[9] G.E. Cook, *Satellite Drag Coefficients*, Planetary and Space Science Volume 13, 1965.

[10] R. Schamberg, *A new analytic representation of surface interaction for hyperthermal free molecule flow with application to neutral-particle drag estimates of satellites*, 1959.

[11] O. Montenbruck, E. Gill, *Satellite orbits: models, methods and applications*, Springer, 2000.

[12] C. Pardini, W.K. Tobiska and L. Anselmo, *Analysis of the orbital decay of spherical satellites using different solar flux proxies and atmospheric density models*, 35th COSPAR scientific assembly, Paris, France, 18-25 July.

[13] C.M. Cox, C.E. Doll, D.H. Oza and R.J. Feiertag, *Evaluation of semiempirical atmospheric density models for orbit determination applications*, NASA, Goddard Space Flight Centre (GSFC), Maryland, USA.

[14] L.G. Jacchia, *Static diffusion model of the upper atmosphere with empirical temperature profiles*, 1965.

[15] L.G. Jacchia, *New static model of the thermosphere and exosphere with empirical temperature profiles*, 1971.

[16] L.G. Jacchia, *Revised static model of the upper atmosphere with empirical*

temperature profiles, 1971.

[17] C.E. Roberts, *An analytic model for upper atmosphere densities based upon Jacchia's 1970 model*, 1971.

[18] A.E. Hedin, *MSIS-86 themospheric model*, J. Geophys. Res. 92, p. 4649-4662, 1987.

[19] A.E. Hedin, *Extension of the MSIS thermosphere model into the middle and lower atmosphere*, J. Geophys. Res. 96, p. 1159-1172, 1991.

[20] J.M. Picone, A.E. Hedin, D.P. Drob and A.C. Aikin, *NRLMSISE-00 Empirical model of the atmosphere: Statistical Comparisons and Scientific Issues*, Naval Research Laboratory, Washington DC, USA, December 2001.

[21] J.R. Wertz, *Spacecraft Attitude Determination and Control*, D. Reidel, Dordrecht, Holland, December 1978.

[22] P.P. Teodorescu, *Mechanical Systems, Classical Models*, 2007.

[23] P. Fortescue, J. Stark, G. Swinerd, *Spacecraft systems engineering*, 3rd Edition, 2003.

[24] http://www.ngdc.noaa.gov/ngdc.html

[25] J. B. Rutenbeck, *Tech Terms: What Every Telecommunications and Digital Professional Should Know*, 3rd Edition, 2006.

[26] A. Luque, S. Hegedus, *Handbook of photovoltaic science and engineering*, 2010.

[27] http://cubesat.wikidot.com/the-technology-of-solar-cells

[28] http://azurspace.de/index.php?mm=97

[29] Analytical Graphics Inc. (AGI), *STK tutorials*.

[30] N.A, Tsyganenko and M. I. Sitnov, *Magnetospheric configurations from a high-resolution data-based magnetic field model*, 2007.

[31] W.P. Olson and K. A. Pfitzer (1977), *Magnetospheric magnetic field modeling*, Annual Scientific Report, 1977.

[32] http://www.spenvis.oma.be

[33] A. Holmes-Siedle and L. Adams, *Handbook of radiation effects*, 2nd Edition, 2002.

[34] J.T. Bell and M.S. Gussenhoven, *APEXRAD Documentation*, 1997.

[35] K.J. Kearns and M.S. Gussenhoven, *CREESRAD Documentation*, 1992.

[36] D.H. Brautigam and J. Bell, *CREESELE Documentation*, 1995.

[37] J.D. Meffert and M.S. Gussenhoven, *CREESPRO Documentation*, 1994.

[38] S.M. Seltzer, *Updated Calculations for Routine Space-Shielding Radiation Dose Estimates: SHIELDOSE-2*, 1994.

[39] F.G. Cunningham, *Earth Reflected Solar Radiation Input to Spherical Satellites*, 1961.

[40] F.G. Cunningham, *Earth Reflected Solar Radiation Incident Upon an Arbitrarily Oriented Spinning Flat*, 1961.

[41] E. Grun, H.A. Zook, H. Fechtig and R.H. Geise, *Collisional Balance of the Meteoric Complex*, 1985.

[42] D.J. Kessler, A.J. Watts and J. Crowell, *Orbital Debris Environment for Spacecraft Designed to Operate in Low Earth Orbit*, 1989.

[43] http://skytour.homestead.com/met2011.html

[44] M.M.R. Howlader, T. Watanabe and T. Suga, *Investigation of the bonding strength and interface current of p-Si/n-GaAs wafers bonded by surface activated bonding at room temperature*, 2001.